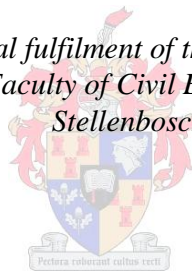


CHARACTERIZING LONG WAVE AGITATION IN THE PORT OF NGQURA USING A BOUSSINESQ WAVE MODEL

By
Duncan Charles Alistair Stuart

*Thesis presented in partial fulfilment of the requirements for the degree
Master of Science in the Faculty of Civil Engineering at the University of
Stellenbosch*



Supervisor: Mr Geoff Toms

December 2013

ABSTRACT

Characterizing long wave agitation in the port of Ngqura using a Boussinesq wave model

The port of Ngqura is situated on the east coast of South Africa. Since its first operational winter excessive vessel motions have interrupted container shipping operations and lead to mooring line failure. A major component contributing to the excessive motions is the presence of seiche in the port, resonating long waves. This study investigates the long wave generation, penetration into the port and subsequent resonance in the vicinity of the problem berths.

An extensive literature review identified two predominant types of long waves along the coast of South Africa. Long waves with periods over 12 min generated by resonant air-water coupling and then shorter long waves between 30 s and 6 min attributed to bound long wave energy and broadly speaking, surf beat. A review of the state of the art long wave modelling techniques was included and contributed to the methodology in this study.

Analysis of simultaneous measurements from the outside and inside of the port confirmed the generating mechanism of the long waves to be storm systems also responsible for generating short waves. Long waves outside the port were found to be on average 8% of the height of the short waves. On average 90% of the long wave height outside the port penetrated the port. The measurements further identified distinct resonating periods of the long wave energy inside the port.

Calibrated Boussinesq wave models allowed for identification of how long waves penetrated the port and subsequently resonated. Both surface elevation measurements and white noise spectra were used as inputs. The penetration mechanisms were attributed to direct diffraction around the main breakwater as well as reflection off the beach south of the port leading to refraction and reflection off the lee side of the main breakwater. Tests with both free and bound long waves proved that at least for some period intervals the long wave energy was indeed bound to short waves.

The excessive vessel motions are attributed to berths positioned in line with nodes created by the resonating long waves; nodes are characterized by strong horizontal currents which can induce surge motions in vessels. Various long waves between the period intervals of 45 s to 125 s resonate in the port to generate nodes at the berths of interest.

In conclusion, the port of Ngqura is susceptible to a range of long wave periods resulting in significant basin oscillations which present nodes at mooring places. As a result of the analyses in this study the mechanisms of interaction between the port, port basins and the long waves penetrating into the port directly, or via the surf zone as surf beats, have been modelled, documented and better understood. This provides the potential for better prediction of severe long wave events and for the investigation of feasible mitigation measures to prevent damage to moored ships in the port.

OPSOMMING

Die karakterisering van langgolf agitatie in die Ngqura hawe deur die gebruik van 'n Boussinq golfmodel

Die Ngqura hawe is aan die ooskus van Suid-Afrika geleë. Sedert die hawe se eerste operasionele winterseisoen, het oormatige skeepsbewegings operasies van behoueringskepe onderbreek en gelei tot faling van vasmeertoue. Die teenwoordigheid van langgolf resonansie is 'n groot bydraende faktor tot die oormatige skeepsbewegings. Hierdie studie ondersoek die opwekking, penetrasie en gevolglike resonansie van langgolwe in die areas aangrensend tot die problematiese kaaie.

'n Uitgebreide literatuurstudie het twee tipes langgolwe aan die Suid-Afrikaanse kus geïdentifiseer, naamlik langgolwe met periodes langer as 12 minute wat deur resonante lug-water koppeling opgewek word en korter langgolwe met periodes tussen 30 s en 6 min wat aan gebonde langgolfenergie of, meer algemeen, surf beat toegeskryf word. Verder is 'n studie rakende die jongste langgolfmodelleringstegnieke ook uitgevoer waaruit die metodiek van hierdie studie bepaal is.

'n Analise van gelyktydige opmetings binne en buite die hawe het bevestig dat kortgolwe wat deur stormsisteme gegenereer word, die opwekkingsmeganisme van lang golwe is. Daar is bevind dat langgolwe buite die hawe gemiddeld 8% so hoog soos kort golwe is. 'n Gemiddeld van 90% van die langgolfhoogte het die hawe penetreer. Die opmetings het ook verder duidelike resonansieperiodes van langgolfenergie binne die hawe aangedui.

Gekalibreerde Boussinq-golfmodelle is gebruik om te identifiseer hoe langgolwe die hawe binnedring en gevolglik resoneer. Beide oppervlakmetings en wit geraas spektra is as invoerwaardes vir die model gebruik. Die penetrasiemeganismes is toegeskryf aan diffraksie rondom die hoof hawemuur asook refleksie vanaf die strand, suid van die hawe, wat lei tot refraksie en refleksie teen die lykant van die hoof hawemuur. Toetse met vry langgolwe het bewys dat die langgolfenergie, vir ten minste sommige periode intervalle, aan die kort golwe vebonde is.

Die oormatige skeepsbewegings is toegeskryf aan die kaaie wat in lyn met nodes van die langgolfresonansie ge-positioneer is. Nodes word gekarakteriseer deur sterk horisontale strome wat surge bewegings in skepe kan veroorsaak. Verskeie langgolwe met periode intervalle tussen 45 s tot 125 s resoneer in die hawe en vorm nodes by die kaaie van belang.

Ten slotte, die Ngqura hawe is vatbaar vir 'n reeks langgolfperiodes wat ossillasies in die bekkens van die hawe veroorsaak en nodes naby kaaie vorm. As gevolg van die analyses in hierdie studie is die meganismes van interaksie tussen die hawe, sy bekkens en langgolwe wat die hawe direk of via die brandersone binnedring gemodelleer, gedokumenteer en beter verstaan. Hierdeur is die potensiaal

vir beter voorspelling van ernstige langgolftoestande verhoog en is dit moontlik gemaak om lewensvatbare oplossings vir skade aan vasgemeerde skepe te ondersoek.

ACKNOWLEDGEMENTS

I would like to thank those who have contributed to the completion of this thesis:

My employer PRDW for financing my studies and allowing me time off work to attend lectures and finish off my thesis report. In particular I would like to thank Stephen Luger for his efforts in training me in the fields of coastal processes, numerical modelling and problem solving. Rhydar Harris for many technical discussions and opening my eyes to programming. Allan Wijnberg and Anton Holtzhausen for their perspectives and general mentoring. The coffee club for good banter and laughs.

Geoff Toms my supervisor for his guidance and comments on this thesis.

The CSIR and in particular Marius Roussow and Ursula Von St Ange for providing me with all the data used in this thesis as well as some good ideas. The DHI for providing me with an academic licence and user friendly software. The South African Weather Service for supplying me with synoptic charts and meteorological data. Mauricio Wesson and Jan de Bont for sharing their knowledge with a stranger. InterOcean systems, inc. for the provision of the S4DW post-processing software and advice on its best application.

My parents for the support, love, encouragement and upbringing they have given me.

I would especially like to thank my wife Kathryn and daughter Charlotte. My wife for all her incredible support and both of them for all the joy they bring. I look forward to making up lost time.

God.

CHARACTERIZING LONG WAVE AGITATION IN THE PORT OF NGQURA USING A BOUSSINESQ MODEL

TABLE OF CONTENTS

DECLARATION.....	ii
ABSTRACT.....	iii
OPSOMMING.....	iv
ACKNOWLEDGEMENTS.....	vi
TABLE OF CONTENTS.....	vii
LIST OF FIGURES.....	x
LIST OF TABLES.....	
LIST OF SYMBOLS.....	
1. INTRODUCTION.....	1
1.1. Port Description.....	2
1.2. Thesis Objective.....	3
1.3. Outline of Thesis.....	3
2. DEFINITIONS AND LONG WAVE GENERATION.....	4
2.1. Wave Classification.....	4
2.2. Short Waves.....	5
2.3. Long Waves.....	5
2.3.1. Bound Long Waves – Set up and set down.....	6
2.3.2. Free Long Waves.....	6
2.4. Seiches – Harbour Oscillations.....	8
3. LITERATURE OVERVIEW AND PREVIOUS STUDIES.....	10
3.1. Introduction.....	10
3.2. Seiches and Long Waves on the Coast of South Africa.....	10
3.2.1. Studies by Wilson (1953 to 1959).....	10
3.2.2. Studies by Darbyshire & Darbyshire (1963).....	13
3.2.3. Studies by Wilson (1972).....	14
3.2.4. Studies by Botes et al., (1982 to 1984).....	14
3.2.5. Studies by Shillington (1984).....	18
3.3. Seiches and Long Waves Internationally.....	21
3.3.1. Generation of Seiche Events by Atmospheric Convection Cells – Rotterdam Harbour.....	21
3.3.2. Long Wave Numerical Model Studies.....	22
3.4. Conclusions and Summary.....	30
3.4.1. Long waves on the coast of South Africa.....	30
3.4.2. Long Wave Modelling.....	31
4. THEORETICAL CONSIDERATIONS.....	32
4.1. Introduction.....	32
4.2. Classic Description of Random Sea Waves.....	32

4.2.1.	The Amplitude and Variance Spectra	33
4.2.2.	Inherent Conditions for the Classic Description of Random Sea Waves.....	34
4.3.	Limitations of the Fourier analysis	35
4.4.	Long Wave Measurements	36
4.4.1.	Wave Record Length.....	36
4.4.2.	Sampling Interval	37
4.4.3.	Nyquist frequency.....	37
4.5.	Boussinesq Model.....	38
4.5.1.	Boussinesq Equations	38
5.	HYPOTHESIS – SIMPLIFIED ANALYSIS	40
5.1.	Introduction.....	40
5.2.	Hydrodynamic Theory	40
5.3.	Typical Moored Vessel Motions.....	43
5.4.	Typical Environmental Conditions and Long Wave Type	45
5.5.	Conclusions and Summary	47
6.	DATA DESCRIPTION	49
6.1.	Introduction.....	49
6.2.	Wave Data	49
6.2.1.	Historic S4DW Data.....	49
6.2.2.	Recent S4DW Data.....	50
6.2.3.	RBR 1 and RBR 2 Data	51
6.2.4.	Long Wave Recorder Data	51
6.3.	Log of Vessel Instabilities.....	51
7.	DATA ANALYSIS	55
7.1.	Introduction.....	55
7.2.	Outside the Port	55
7.2.1.	Short Waves.....	55
7.2.2.	Long Waves.....	56
7.3.	Measurement Correlations between the Outside and Inside of Port	58
7.3.1.	Available Data	58
7.3.2.	Long Wave Height Comparisons (Inside vs. Outside)	59
7.3.3.	Direct Time-series Comparison.....	60
7.4.	Direct Spectral Analysis Comparisons	62
7.4.1.	Individual Event Comparisons.....	62
7.4.2.	Temporal Spectral Variation	64
7.5.	Meteorological Data	71
7.6.	Summary and Discussion	75
8.	IDENTIFYING LONG WAVE PENETRATION MECHANISMS	77
8.1.	Introduction.....	77
8.2.	Modelling Approach	77
8.3.	Model Setup	78
8.3.1.	Bathymetry	78
8.3.2.	Waves	78
8.3.3.	Numerical Parameters	80
8.3.4.	Water Levels	81

8.3.5.	Sponge Layers	81
8.3.6.	Reflection Coefficients	82
8.3.7.	Bottom Friction	83
8.4.	Calibration	83
8.4.1.	Calibration Approach	83
8.4.2.	Summary of Calibration Progression	83
8.4.3.	Calibration Results	85
8.5.	Results	88
8.5.1.	Base Case	88
8.5.2.	Beach Reflection Test	89
8.5.3.	Free Long Wave Test.....	93
8.6.	Conclusions and Summary	95
9.	CHARACTERIZING PORT RESONANCE – WHITE NOISE SIMULATION	96
9.1.	Introduction.....	96
9.2.	Modelling Approach	97
9.2.1.	White Noise Simulation	97
9.2.2.	Band-pass Filtering.....	98
9.3.	Model Setup	98
9.4.	Results	99
9.4.1.	Base Case - White Noise Simulation	99
9.4.2.	Quasi-Validation	99
9.4.3.	Beach Reflection Test - White Noise Simulation.....	101
9.4.4.	Band-pass Filtering.....	104
9.4.5.	Conclusions and Summary	112
10.	CONCLUSIONS	114
10.1.	Introduction.....	114
10.2.	Long Wave Characteristics and Generation Mechanism	114
10.3.	Long wave Penetration Mechanisms	115
10.4.	Port Resonance.....	115
10.5.	Excessive Vessel Motions.....	116
11.	RECOMMENDATIONS	118
12.	REFERENCES.....	120
APPENDIX A: DRAWINGS OF VESSEL MOTION EVENT – APRIL 2010		125

LIST OF FIGURES

	Page
Figure 1-1: The port of Ngqura on the east coast of South Africa.....	2
Figure 2-1: Approximate distribution of ocean surface wave energy illustrating the classification of surface waves by wave band, primary disturbing force, and primary restoring force. Source: SPM after Kinsman (1965).	4
Figure 2-2: Example of bound long waves with generating short wave groups (Council for Science and Industrial Research, 2008).	6
Figure 2-3: Generation mechanisms for infragravity waves in the coastal zone (Rabinovich, 2009).....	7
Figure 2-4: Surface profiles for oscillating waves (USACE, 2006).	9
Figure 3-2: Approximate instantaneous form of 2-3/4-min seiche off Table Bay Harbour (graphical synthesis) (Wilson, 1953).....	12
Figure 3-3: Two-dimensional mode of resonant oscillation in Duncan Basin, Table Bay Harbour, Cape Town. Instantaneous water surface shapes contoured from model experiments (Wilson, 1957).	12
Figure 3-4: South Africa with approaching low-pressure systems, passing from west to east (Botes et al., 1984).	14
Figure 3-5: Normalised long and short period wave heights (April 1981) (Botes et al., 1982).	15
Figure 3-7: Spectral density exceedances for September 1981 inside the harbour (Botes et al., 1982).....	17
Figure 3-8: Tide gauge recordings for 11 May 1981 (Shillington, 1984).....	19
Figure 3-9: Agulhas Bank bathymetry and location of measuring stations. The hatched area shows the region of the generation of the waves for 11 May 1981 (Shillington, 1984).	19
Figure 3-10: S.A. Weather Bureau synoptic weather maps for 10 and 11 May 1981 (14h00 SAST) (Shillington, 1984).	20
Figure 3-11: Air pressure microbarograph recordings for 11 May 1981 (Shillington, 1984).	20
Figure 3-12: Sketch of convection cells in the area behind a cold front together with a theoretical surface elevation response (De Jong, 2004).	21
Figure 3-13: Natural long-period resonance modes for Layouts 1 and 2. Long wave energy intensity and surface elevation envelopes along the longitudinal lines of the basin. (Example from (Gierlevsen et al., 2001)).....	23
Figure 3-14: Instantaneous band-pass filtered surface elevation map (left) and map of relative long period wave energy between new and old layout (30-60 s) (Kofoed-Hansen et al., 2005).	24

Figure 3-15: Location of wave gages. The rectangle indicates the boundaries of the MIKE 21 BW model. Coordinates are UTM zone 11 (Kofoed-Hansen et al., 2005).	25
Figure 3-16: Wave spectrum of the white-noise simulation at the stations LB2, LB7, LB8 and LB9 (Pier J), see Figure 3-15 for location. For comparison the measured spectrum at LB9 (1 August 2000 20:00-23:00) is depicted (Kofoed-Hansen et al., 2005).	25
Figure 3-17: Port Geraldton, Western Australia- Bathymetry Image, showing extensive reef to the West of the dredged entrance channel (McComb et al., 2009).	26
Figure 3-18: Example of instantaneous surface elevation of the 0.0-0.04 Hz filtered surface elevation showing the long wave field within the port of Geraldton domain during Event 4. Areas of long wave generation can be seen across the reef platform to the west and north of the entrance. Units are in m (Johnson & McComb, 2011).	28
Figure 3-19: Long period significant wave height during event 4. The locations of the long period wave sensors (LW6 & LW34) within the basin are shown. Units are in m. (Johnson & McComb, 2011). .	29
Figure 3-20: Significant wave height of high frequency (0.015-0.04 Hz) and low frequency (0-0.015 Hz) components of the long wave field. A clear nodal structure is seen in the low frequency partition [right frame], contrasting to a more complex distribution of energy in the high frequency waves. Units are m. (Johnson & McComb, 2011).	29
Figure 3-21: Estimated spectra of the modelled surface elevation at location LW34. The well defined peaks correspond to the dominant seiche modes of the basin. (Johnson & McComb, 2011)	30
Figure 4-1: The random waves moving in time, i.e., the sum of a large number of harmonic wave components, travelling across the ocean surface with different periods, directions, amplitudes and phases cited by (Holthuijsen, 2007).	33
Figure 4-2: Wave record analysis and regeneration (Journée & Massie, 2001).	34
Figure 4-3: Resolution of linear and nonlinear spectral components for a recorded spectrum (Goda, 2000).	35
Figure 4-4: Effect of Wave Record Length (Journée & Massie, 2001).	36
Figure 4-5: Two harmonic waves with frequencies f_1 and f_2 that are given at discrete, constant time intervals $t = 1 / (f_1 + f_2)$ are indistinguishable at these discrete times (as indicated by the dots) (Holthuijsen, 2007).	37
Figure 4-6: Aliasing in the spectrum of a wave record with discrete time intervals Δt is equivalent to mirroring the spectrum around the Nyquist frequency $f_{Nyquist} = 1 / (2\Delta t)$ (Holthuijsen, 2007).	38
Figure 5-1: Ngqura, Short closed basin idealized resonating mode $n=1$ – Longitudinal.....	41
Figure 5-2: Ngqura, Short open basin idealized resonating mode $n=1$ – Longitudinal.....	41

Figure 5-3: Ngqura, Short open basin idealized resonating mode $n=2$ – Longitudinal.....	42
Figure 5-4: Ngqura, Short closed basin idealized resonating mode $n=2$ – Transverse.....	42
Figure 5-5: Ngqura, Long closed basin idealized resonating mode $n=1$ – Longitudinal.....	43
Figure 5-6: Definition of Ship Motions in Six Degrees of Freedom, modified from (Journée & Massie, 2001).....	44
Figure 5-7: Ship motions in standing waves.	44
Figure 5-8: Graphs showing the monthly frequencies of occurrence of weather types and sea storms in the different areas (MacHutchon, 2006).	46
Figure 6-1: Location of wave measurement devices (Google Earth, 2013).	49
Figure 6-2: Mooring Layout - Instability event on the 23 April 2010 (PRDW, 2010a).	52
Figure 6-3: Environmental Data - Instability event on the 23 April 2010 (PRDW, 2010b).....	54
Figure 7-1: Wave height rose at port entrance, approximately 5 years data (1-hourly data).....	55
Figure 7-4: Comparison of Short and Long period significant wave heights. Long period axis is correlated to short wave height by 8%. Short and Long period measurements are from the S4DW instrument outside the port.	58
Figure 7-5: Correlation of significant long wave heights between the outside and inside of the port. Data consists of three separate data sets.	59
Figure 7-6: Comparison of significant long wave heights (m) between the S4DW instrument (blue) and the Long Wave recorder (red). S4DW was stationed outside breakwater, Long Wave recorder inside the harbour basin.	60
Figure 7-7: Comparison of significant long and short wave heights, including effect of tidal modulation. RBR1 instrument (blue), RBR2 instrument (red) and the Long Wave recorder (green). RBR instruments were stationed outside the port, Long Wave recorder inside the harbour basin.....	61
Figure 7-8: Direct spectral analysis comparison between outside and inside of port – 2011/08/09 18h00 event.	63
Figure 7-9: Direct spectral analysis comparison between outside and inside of port – 2012/07/28 08h30 event.	63
Figure 7-11: 3D Temporal spectrogram (spectral energy-frequency-time) variation, long wave periods only – (2011/08/08 to 2011/08/18). Measured inside the port with the LWrec.	65
Figure 7-12: 2D Temporal spectrogram (spectral energy-frequency-time) variation, long wave periods only – (2011/08/08 to 2011/08/18). Measured outside the port with the S4DW.	66
Figure 7-13: 2D Temporal spectrogram (spectral energy-frequency-time) variation, long wave periods only – (2011/08/08 to 2011/08/18). Measured inside the port with the LWrec.	66

Figure 7-14: 3D Temporal spectrogram (spectral energy-frequency-time) variation, long wave periods only – (2012/07/27 to 2012/08/01). Measured outside the port with the RBR1. 67

Figure 7-15: 3D Temporal spectrogram (spectral energy-frequency-time) variation, long wave periods only – (2012/07/27 to 2012/08/01). Measured inside the port with the LWrec. 67

Figure 7-16: 2D Temporal spectrogram (spectral energy-frequency-time) variation, long wave periods only – (2012/07/27 to 2012/08/01). Measured outside the port with the RBR1. 68

Figure 7-17: 2D Temporal spectrogram (spectral energy-frequency-time) variation, long wave periods only – (2012/07/27 to 2012/08/01). Measured outside the port with the LWrec. 68

Figure 7-18: 2D spectral collation comparison between the outside and inside of the port, long wave periods only – (2011/08/08 to 2011/08/18)..... 69

Figure 7-19: 2D spectral collation comparison between the outside and inside of the port, long wave periods only – (2012/07/27 to 2012/08/01)..... 69

Figure 7-20: 2D spectral collation showing maximum spectra envelopes for 3 events inside the port from LWrec. 70

Figure 7-21: Comparison of significant long wave heights (m) with meteorological parameters from 2011-08-07 to 2011-08-16. Panels shown (top to bottom): Significant long wave height (outside port), Air pressure, Wind speed, Wind Direction and Temperature. 72

Figure 7-22: Comparison of significant long wave heights (m) with meteorological parameters from 2012-07-23 to 2012-08-01. Panels shown (top to bottom): Significant long wave height (outside port), Air pressure, Wind speed, Wind Direction and Temperature. 73

Figure 7-23: Daily synoptic charts, left pane: 2011-08-08, right pane: 27-07-2012. Red dot indicates the port of Ngqura (South African Weather Service, 2011 & 2012). 74

Figure 8-1: Ngqura model bathymetry. 78

Figure 8-2: Visualization of boundary input. Top pane: de-trended surface elevation data and corresponding $H_{m0:HF}$ and $H_{m0:LF}$ parameters. Bottom pane: zoom of validation event. 80

Figure 8-3: Example of filtered long wave signal – validation event 80

Figure 8-4: Sponge layers for base case (left) and beach reflection test (right)..... 82

Figure 8-5: Ngqura reflection coefficients. 82

Figure 8-6: Significant long wave height comparison between model results and measurements at Long Wave Recorder position inside the port basin..... 86

Figure 8-7: Long wave spectrum comparison, model vs. LWrec – Event; 2012/07/28 14h30. Model $H_{m0:LF} = 0.17$ m, LWrec $H_{m0:LF} = 0.17$ m. 86

Figure 8-8: Long wave spectrum comparison, model vs. LWrec – Event; 2012/07/29 08h30. Model $H_{m0:LF} = 0.18$ m, LWrec $H_{m0:LF} = 0.19$ m.	87
Figure 8-9: Example of modelled significant short wave height (left pane) and instantaneous surface elevation (right pane).	88
Figure 8-10: Long wave spectra comparison, Model vs. LWrec – 2012/07/28 08h30. Model $H_{m0:LF} = 0.18$ m, LWrec $H_{m0:LF} = 0.21$ m.	89
Figure 8-11: Long wave spectra comparison, base case vs. beach absorber test, also showing actual LWrec.	90
Figure 8-12: Reflected long wave components, showing increased wave diffraction, reflection and refraction for energy over 100 s. All panes show instantaneous surface elevation. Upper: Incident waves (no reflection), Centre: Incident and reflected waves, Lower: Isolated reflected waves. Left and right columns represent split in energy for 30 s to 100 s and 100 s to 1000 s.	92
Figure 8-13: Long wave spectra comparison, base case vs. free long wave test, also showing actual LWrec.	94
Figure 9-1: Construction Layout and Final Layout on left and right respectively.	97
Figure 9-2: Long wave spectrum from white noise simulation, positioned at Long Wave Recorder, inside the port basin.	99
Figure 9-3: Long wave white noise results spectrum vs. long wave maximum spectra envelopes for three events.	100
Figure 9-4: Long wave spectra comparison, normal white noise case vs. beach absorber white noise case, also white noise input spectra.	101
Figure 9-5: Out of phase resonance between reflected and normal wave components. All panes show instantaneous surface elevation. Left column: 85 s to 105 s. Right column 230 s to 270 s wave. Upper: Incident waves (no reflection), Centre: Incident and reflected waves, Lower: Isolated reflected waves.	103
Figure 9-6: ~820 s - Long Open Basin - Helmholtz –. Left: normalized long wave energy, Right: surface elevation, Lower: surface elevation profile envelope.	105
Figure 9-7: 230 s to 270 s - Short Open Basin coupled with Short Closed Basin – Fundamental Modes. Left: normalized long wave energy, Right: surface elevation, Lower: surface elevation profile envelope.	106
Figure 9-8: 155 s to 200 s - Long Open Basin - Mode 2. Left: normalized long wave energy, Right: surface elevation, Lower: surface elevation profile envelope.	107

Figure 9-9: 115 s to 125 s - Long Closed Basin – Mode 2. Left: normalized long wave energy, Right: surface elevation, Lower: surface elevation profile envelope.....	108
Figure 9-10: 85 s to 105 s - Long Closed Basin - Mode 3. Left: normalized long wave energy, Right: surface elevation, Lower: surface elevation profile envelope.....	109
Figure 9-11: 67 s to 71 s - Long Open Basin - Mode 4. Left: normalized long wave energy, Right: surface elevation, Lower: surface elevation profile envelope.....	110
Figure 9-12: 52 s to 58 s - Long Open Basin - Mode 5. Left: normalized long wave energy, Right: surface elevation, Lower: surface elevation profile envelope.....	110
Figure 9-13: Long Open Basin - Mode 6 – 42 s to 49 s. Left: normalized long wave energy, Right: surface elevation, Lower: surface elevation profile envelope.....	111
Figure 10-1: Conclusion annotation summary.....	117

LIST OF TABLES

	Page
Table 5-1: Summary of free oscillating periods	43
Table 5-2: Maximum significant surge motion amplitudes for an (un)loading efficiency of 95%, for large container vessels (PIANC, 2012).	45
Table 5-3: Maximum allowable significant motion amplitudes for an (un)loading efficiency of 95%, for smaller container vessels (PIANC, 2012).	45
Table 5-4: Grouped Weather Types and Synoptic Patterns effecting sea storms around the South African Coastline (MacHutchon, 2006).	46
Table 6-1: Summary of Recording Frequency, Record Length and Sampling Periods (PRDW, 2005).	50
Table 6-2: Log of vessel instabilities – partial coverage from 2010 to 2012.....	52
Table 7-1: Individual event parameters.....	62

LIST OF SYMBOLS**Roman Symbols**

Symbol	Designation
CD	Chart Datum
H_{mo}	Significant short wave height, calculated from the integral of the variance spectrum
$H_{mo:HF}$	Significant short wave height, calculated from the integral of the variance spectrum
$H_{mo:LF}$	Significant long wave height, calculated from the integral of the variance spectrum
$H_s/H_{1/3}$	Average of the highest 1/3 of the wave heights in a particular record, referring to short waves with periods < 30 s
H_{sl}	Average of the highest 1/3 of the wave heights in a particular record, referring to long waves with periods > 30 s
HF	High frequency waves with period < 30 s
LF	Low frequency waves with period > 30 s
L	Wave length/length
L_o	Deep water wave length
N	Total number of wave cycles
S	Spectral density
S(f)	Variance wave spectrum density
T	Wave period
T_p	Peak wave period
UTM	Universal Transverse Mercator, coordinate system
c	celerity
f	Frequency
f_N	Nyquist frequency

g	acceleration of gravity
h	Water depth
k	Wave number
l_b	Basin length
n	Resonating mode
t	Time interval
x, y and z	Space coordinates

Greek Symbols

Symbol	Designation
--------	-------------

α	Wave amplitude
ε	Phase angle
Δt	Time step
η	Surface elevation above mean water level
θ	Angle between the x -axis and the direction of wave propagation

1. INTRODUCTION

Long waves are present in all coastal regions experiencing swell and present a difficult challenge to port designers in terms of mitigating port downtime. They are characterized as waves with periods over 30 seconds, lengths between 0.4 km to 6 km and small amplitudes that are generally less than 0.5 m. Due to their physical properties they easily penetrate into harbours that are designed purely to reduce short wave energy. Furthermore they are typically ignored in generic coastal structure design and wave measurement campaigns leading to a lack of information on long waves at most sites.

The disruption of port activities by long waves is less intuitive than the disruptions that may be caused by short wave energy. A series of phenomena is required before long wave energy presents a disruption in a port; however, in many ports this series of phenomena occur frequently resulting in costly downtime, and can lead to dangerous accidents when mooring lines are forced to snapping point. Long wave disruptions are caused by the resonance of long waves in a port, which in turn, excite large vessels with flexible moorings. The prediction and mitigation of this problem is therefore multifaceted. The following factors need to be understood in the process of coming to a holistic solution:

- The occurrence and characteristics of long waves at the site and within the port.
- The correlation of the long wave frequencies with the natural frequencies of the port and port basins to identify resonance.
- The response characteristics of the typically moored vessels to the long wave resonance.

This thesis focuses on the first two aspects of the long wave disruption problem detailed above; hence, coupling the response of moored vessels with the long wave resonance is not dealt with and only a high level observation is made.

In particular this thesis focuses on the characteristics of long waves in the Port of Ngqura and how they enter and resonate within the port. The port is a relatively new port on the east coast of South Africa. A description of the port follows in Section 1.1. Vessels in the port experience loading downtime annually, and during extreme events mooring lines have snapped. The source of these events are attributed to long wave resonance in the port, coupled with the use of weak moorings.

While this thesis focuses specifically on the long wave agitation at one port it may also be used as reference to engineers and port planners in their design process. This thesis provides the reader with a collation of techniques to quantitatively assess long waves and predict how they will resonate in a port.

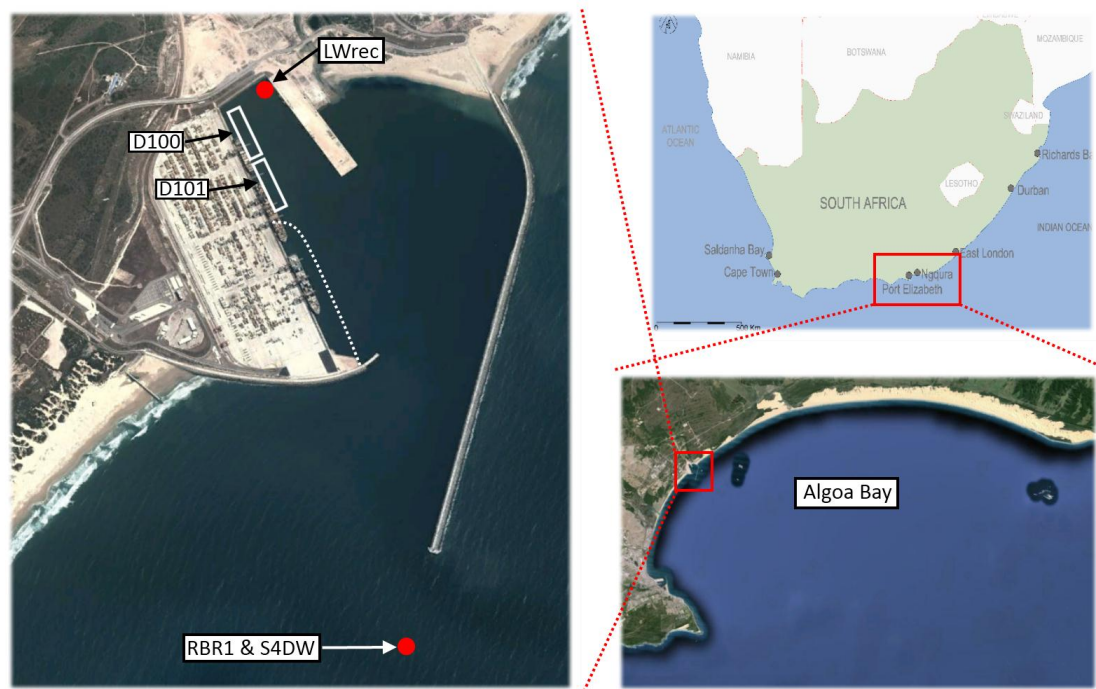
1.1. Port Description

Figure 1-1 shows the location of the port of Ngqura on the east coast of South Africa in Algoa Bay. Construction of the port began in 2002. Phase 1 of construction ended when the first two container berths became operational in October 2009. The two berths namely D100 and D101 are indicated on the figure. Phase 2 involved an extension of the container quay wall, allowing for a further 2 berths. Before the completion of phase 2 in 2012, a construction bund was used in order to allow for construction of the quay wall extension in the dry. The position of the historic construction bund is indicated by the white dotted line.

Berths D100 and D101 are the berths which have had excessive vessel motions, the first documented reports started in April 2010, the first winter (stormy) season in which the berths were operational. Excessive vessel motions are still reported up to the date of this study completion in August 2013.

Also shown in the figure are the positions of the wave recording instruments that supplied data to this study. The Long Wave Recorder (LWrec) is positioned opposite berth D100 and the RBR 1 and S4DW are positioned off the main breakwater.

Figure 1-1: The port of Ngqura on the east coast of South Africa.



1.2. Thesis Objective

The objective is to characterize the long wave agitation in the port of Ngqura. Characterization in this context refers to a holistic understanding of the long wave agitation in the port thus the objective may be broken down as the following sub-objectives:

1. Analyze and identify the long wave energy outside the port – from measurements
2. Investigate the excitation of the port of Ngqura due to the long wave energy
3. Identify how the long waves are entering the port
4. Identify the resonance frequencies of the port
5. Compare the resonance frequencies in the port during its construction phase and the final layout
6. Identify a high level link between reported ship motions and the long wave occurrence
7. Identify the optimal positioning of a long wave recorder in the port

1.3. Outline of Thesis

The remaining 10 Chapters in this report may be described briefly as follows: Chapter 2 defines long waves and their various generation and propagation theories; Chapter 3 chronologically reviews long waves and seiching in South African ports, this is followed by a review of the state of the art modeling techniques used to simulate long waves at ports; Chapter 4 describes some theoretical considerations and assumptions that have been made in the thesis; A simplified hypothesis, which gives a first pass at characterizing Ngqura long wave agitation is included in Chapter 5; Chapter 6 and 7 include a description of the data available for the study, the methodologies used to analyze it and the results; Chapter 8 and 9 include the use of a Boussinesq model in order to investigate long wave penetration mechanisms and then subsequently characterize the port resonance characteristics. Where necessary to aid the reader conclusions have been made at the end of individual chapters; Chapter 10 gives an overall conclusion to the study followed by; recommendations in Chapter 11.

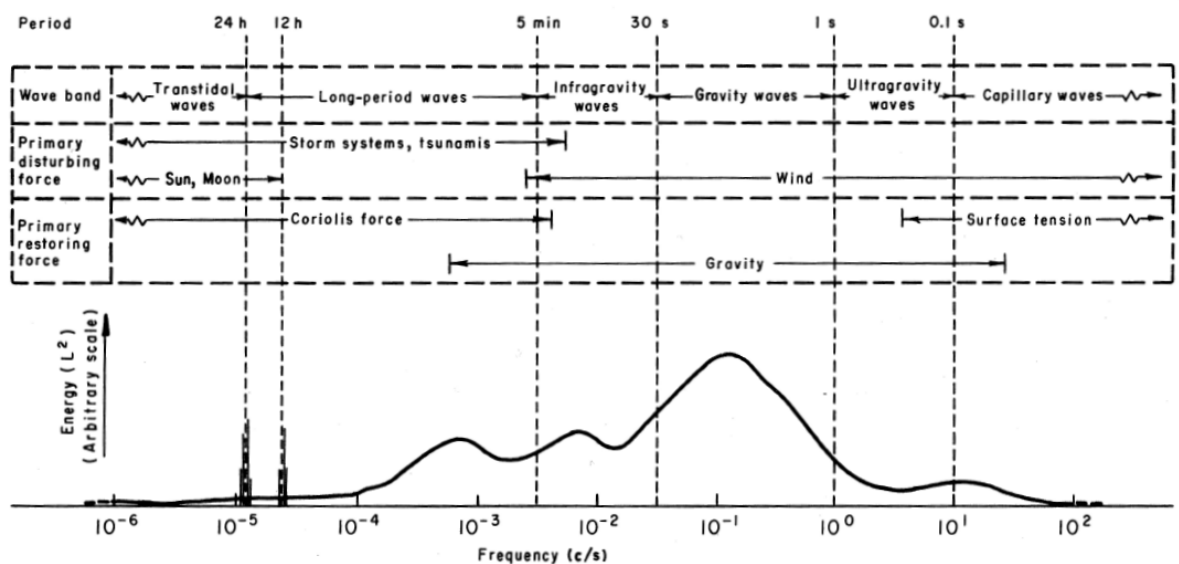
2. DEFINITIONS AND LONG WAVE GENERATION

2.1. Wave Classification

Surface waves may be classified by a number of properties including; period / frequency, the shape, the motion, the disturbing force and /or restoring force. Once the classification of waves is understood, the various wave types which are named after the classification properties are much easier to identify. Kinsman (1965) gives an elegant description of the classification of waves which is summarized here for relevance to this thesis.

Figure 2-1 below gives a visual aid to understanding the classification of waves. The energy of waves for various frequencies has been estimated, in addition, the general description of the waves and their disturbing and restoring forces are identified.

Figure 2-1: Approximate distribution of ocean surface wave energy illustrating the classification of surface waves by wave band, primary disturbing force, and primary restoring force. Source: SPM after Kinsman (1965).



Wave period describes the length of time for a wave length to pass a point; it is the reciprocal of frequency. Short waves and long waves are named after their periods; in this thesis short waves shall refer to any wave with a period below 30 seconds, while long waves shall refer to waves of a higher period (period > 30).

The disturbing force refers to the force that made the wave. Waves may be created by wind, ship movement, gravity forces etc.; however, a more fundamental use of this classification property is to distinguish between free and forced waves. Free waves refer to waves that are no longer being created by the disturbing force and obey the free wave dispersion relation, linking wave period to

wave celerity and wave length. For example the waves travelling across a pond created by a dropped stone. Forced waves describe waves where the disturbing force is applied continuously and the wave takes on the characteristics of the forcing function with modifications imposed by the liquid. The tide is an example of a forced wave that is disturbed by the periods of the sun and moon but is out of step with them due to properties of water and the shape of the ocean basins. Free long waves and Bound long waves (a particular type of forced wave) are described in more detail below in Section 2.3.

The alternative to using the disturbing force to describe waves is to use the restoring force. Principle restoring forces are surface tension, gravity and Coriolis force. Envisaging the water surface as a stretched membrane helps to understand how these forces are used to classify waves. A short wave stretches the membrane much more per unit of length than a long wave as part of the surface is too high and part too low. Thus short waves are often termed gravity waves because gravity is the dominant restoring force. Infra-gravity waves commonly also described as long waves seem to have attained their name due to the lesser degree of gravity as a restoring force. Using the restoring force as a classification is principally a wave classification by length and has overlap where two or more forces are equal (Kinsman, 1965).

The motion of a wave allows for another classification type; if the profile of a wave moves relative to the medium, it is a progressive wave. If the profile does not move but merely oscillates in one place relative to the medium, forming and disappearing, it is a standing wave. Standing waves are described in more detail in Section 2.4.

2.2. Short Waves

Short waves in this thesis are defined as waves with a period of between 1 and 30 seconds. These waves may either be in a sea state or a swell state, the former referring to short waves that are disturbed by wind and may be described as a balance of forced and free waves that are steeper and more rugged than swell. The swell state refers to waves that are mostly free from the disturbing force of the wind and are more orderly. The rough period definition between these two states is 1 to 10 seconds for sea and 10 to 30 seconds for swell (Kinsman, 1965).

2.3. Long Waves

Long waves in this thesis are defined as waves with a period of over 30 seconds, although these waves may be defined as a combination of long and infra-gravity waves depending on various authors. Various types of long waves are described below using the wave classification detailed in Section 2.1 above. Figure 2-3 below gives a good overview of the various forms and mechanisms that create long waves and can be used as reference to aid in understanding the descriptions.

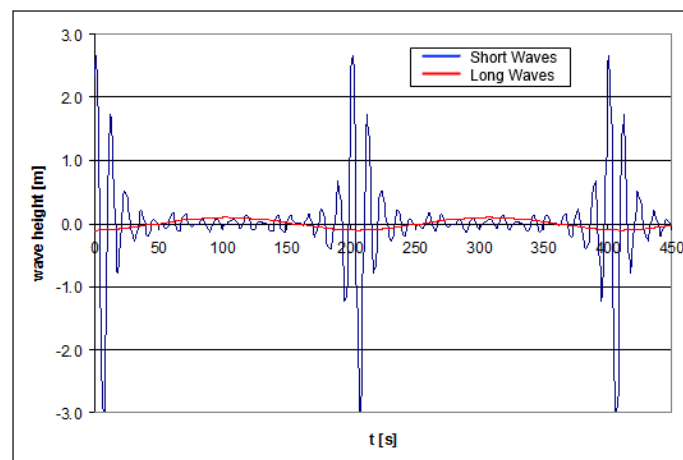
Well written reviews of long waves and their generation mechanisms may also be found in Van der Molen (2006), and Baldock & Huntley (2002).

2.3.1. Bound Long Waves – Set up and set down

Bound waves are associated with groups of wind generated waves. These waves are formed by the radiation stresses created by travelling groups of short waves; the wave groups essentially tilt the mean sea level creating set downs beneath groups of large waves, and peaks beneath the smaller waves. This is annotated in Figure 2-2. These bound long waves have a wave length equal to the spacing between successive wave groups and usually have a frequency above 30 seconds (Holthuijsen, 2007). The height of a bound long wave is larger under larger short waves, and vice versa, the bound long wave travels at the speed of its corresponding wave group until it is realised and becomes a free long wave (Baldock & Huntley, 2002).

Longuet-Higgins & Stewart (1964) mathematically described the effects of radiation stresses hence they have been attributed with identifying the mechanism for bound long waves which are also termed forced long waves.

Figure 2-2: Example of bound long waves with generating short wave groups (Council for Science and Industrial Research, 2008).

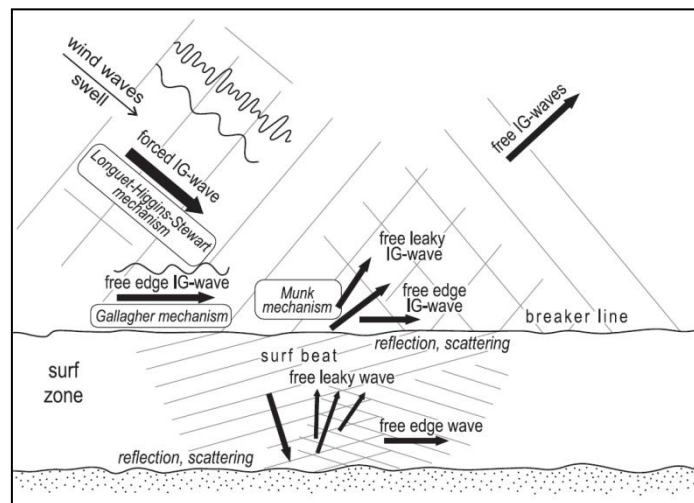


2.3.2. Free Long Waves

Once the short wave groups break in the surf zone their corresponding bound long waves are released and become free long waves. The free waves reflect off the shore line and travel seaward at the speed of a long wave rather than the speed of the wave group (Baldock & Huntley, 2002). The correlation of long waves shoreward of the surf zone with incoming groups of short waves was first observed by Munk, (1949) who named the process “surf beat”. The released long period waves may propagate cross-shore (leaky waves), be reflectively trapped (edge waves) or propagate as a mixture of both as described by Baldock & Huntely (2002). In the case of oblique incident waves the outgoing

long waves refract more strongly than the incident short waves. If the angle of incidence of the short waves is small, the outgoing long wave is likely to reflect back as a leaky wave in the cross-shore direction. When the angle of incidence is larger than a critical angle, the long wave refracts back to the shore creating a free edge wave; this process may occur in both alongshore directions due to interactions between wave components with different wave directions. At certain angles the edge waves may be amplified, resulting in a near-resonant edge wave. Due to directional spreading the long waves generally propagate as a combination of both leaky and edge waves (Van der Molen, 2006).

Figure 2-3: Generation mechanisms for infragravity waves in the coastal zone (Rabinovich, 2009).



Symonds, Huntley & Bowen (1982) state that in addition to the forcing of free long waves through bound wave release (as described above) there is another forcing mechanism in the vicinity of the surf zone; a breakpoint forcing mechanism. Baldock & Huntley (2002) later suggested that a time varying breakpoint may be the dominant long wave forcing mechanism during storms and times of incident steep short waves; while released and reflected bound long waves dominate in conditions with milder long-period swell waves. The breakpoint forcing mechanism is driven by the time varying breakpoint position (due to varying incident short wave heights) which radiates long waves both seawards and shoreward.

The precise periods of the long waves described above (both bound and free) are related to the particular site and generating mechanism. McComb et al. (2005), from analysis of measurements at port Taranaki, New Zealand, makes a period distinction of the long wave energy defining bound long waves as Far-infragravity waves (FIG waves); and long waves generated in the nearshore zone as Infragravity (IG) waves. He states FIG waves generally have periods between 2 min and 20 min and IG waves periods less than 120 s.

With regards to this study, all the long wave types described above have periods which to some extent fall within the vessel motion problem range between 30 s and 300 s (PIANC, 2012; Van der Molen, 2006; PAHRI, 1998). Furthermore, longer period wave energy ($t > 20$ min) is unlikely to resonate inside the port as the periods will exceed the Helmholtz mode (see Section 2.4) of the port, thus the long waves described above will be concentrated on for the study. Longer period long waves that are less likely to be relevant are described below.

Free long waves may also be generated by undersea earthquakes or landslides; this form of long wave is called a tsunami (Jacques et al., 2004). The tsunami wave is created by a large displacement of tectonic plates under the ocean which corresponds with an earthquake. The shift in plates creates a similar shift in the water column and a large free long wave is generated. The landslide tsunami is generated via a similar mechanism; however, the mass movement of the sea floor is due to a submarine landslide.

Long waves may also be created by meteorological phenomena. De Jong (2004) identified the seiche mechanism of Rotterdam harbour as originating from long waves created by variations in local wind speed and atmospheric pressure associated with the passage of a frontal system containing meso-scale convection cells. Seiche events or locally named rigassa events in Menorca, Spain, have been attributed to long waves called meteorological tsunamis. The meteorological tsunamis are created by an unusual pressure jump associated with a convective squall line (Jansa et al., 2007). In general, meteorological long waves have a longer period than released bound long waves; for example, the Rotterdam long waves have a period of ± 1 hour, and the Menorca long waves have a period of ± 10 minutes.

2.4. Seiches – Harbour Oscillations

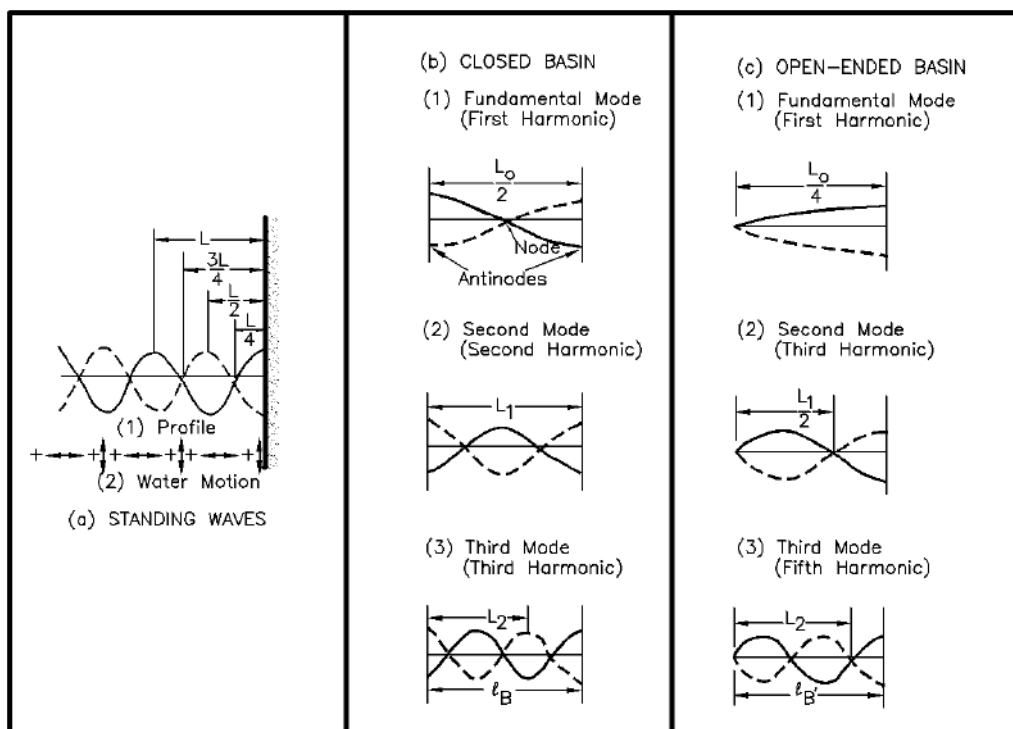
Seiches are long-period standing oscillations in an enclosed basin or in a locally isolated part of a basin (Rabinovich, 2009). Each harbour that experiences seiches has unique resonant periods that are a function of the basin geometry; if an external force matches the resonance periods, an oscillation will occur.

Thus the generation of a harbour seiche is commonly due to the excitation of the harbour by standing waves. A standing wave is created when an incident wave is reflected off a structure; the sum of the incident and reflected wave amplitudes creates a standing wave which does not propagate horizontally, but rather forms a fixed pattern of nodes and anti-nodes. Anti-nodes are characterized as positions of maximum amplitude resulting in a rise and fall of the water surface. At the nodes there is no vertical displacement however strong horizontal currents are created. Surface profiles for standing waves of various modes acting in theoretical open and closed basins are shown

in Figure 2-4. In practice, because of the scale of harbours and vessels, only long waves can create standing waves which can interrupt shipping operations.

The Helmholtz mode is a phenomena which creates seicheing but is not generated by standing waves. It is characterized as having a higher resonance period than the first mode of an open-ended basin as described in Figure 2-4. The Helmholtz essentially results in the water surface in the basin uniformly rising and falling while the inlet channel water oscillates in and out (USACE, 2006). It is described by the balance of potential energy from the rise and fall of the water surface with the kinetic energy of the water flowing in and out the channel. In Figure 2-4, L_x with various subscripts refers to the wave length for various modes of oscillation and l_b refers to the basin length.

Figure 2-4: Surface profiles for oscillating waves (USACE, 2006).



3. LITERATURE OVERVIEW AND PREVIOUS STUDIES

3.1. Introduction

South Africa has been the subject of a number of studies regarding long waves and seiching, in particular because the port of Cape Town in the 1950's was severely affected by seiching. Thus a chronological review of the studies performed for South African ports has been performed with the aim of identifying local long wave generation mechanisms, penetration mechanisms and study methodologies.

A more up-to-date review of seiches internationally, and in particular numerical modelling techniques used to investigate them, follows. This was aimed at identifying a suitable methodology for characterizing long waves at the port of Ngqura.

3.2. Seiches and Long Waves on the Coast of South Africa

3.2.1. Studies by Wilson (1953 to 1959)

Disruptive ship motions occurring during World War II in Table Bay Harbour, Cape Town, prompted extensive investigation during the 1940's and 1950's (Wilson, 1953, 1954 & 1957). Wilson concentrated on the characteristics of the seiches and their generation mechanisms. He identified resonant frequencies of the South Atlantic Ocean, Table Bay and Table Bay Harbour.

Wilson claimed that the oceanic basins were excited by meteorological pressure changes, the resulting oceanic seiches in turn excited Table Bay and then an area just outside the harbor; the so called breakwater-shore oscillating system. The standing wave acting between the breakwater and shore had the potential to create a difference in head between the outside and inside of the Harbour mouth; the alternating head difference provided the pulsation of energy to excite the main harbour basin. This series of seiches from large basins to smaller basins transformed the relatively long period ocean seiches to resonate the water mass inside Table Bay harbour at higher frequencies than the original ocean seiches (Wilson, 1953).

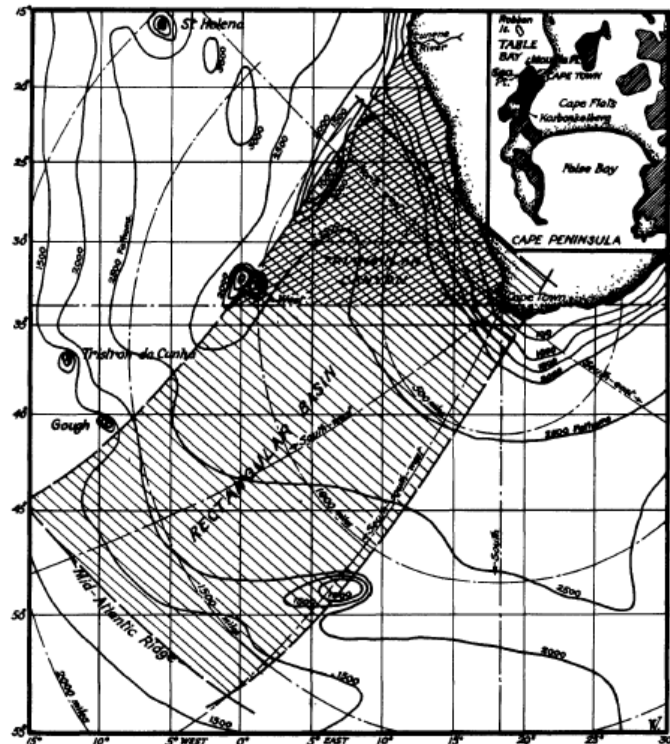
A brief description of each of the three oscillating systems that he identified follows:

1. Resonance of Oceanic Basins and Table Bay

A pseudo-rectangular trench and triangular canyon South of Cape Town permits oscillations of water masses when responding to the fluctuating pressure changes arising from the wave-like sequence of east bound frontal depressions. Table Bay is positioned on the boundary of both the oceanic basins (described above) and hence may be excited by the ocean oscillations. Wilson also suggested that Table Bay may resonate by excitation from

sources other than the oceanic seiches; he attributed possible wave or pressure disturbances as the generation mechanisms. Figure 3-1 illustrates the rectangular ocean basin and triangular canyon in different hatch patterns. Wilson identified the following oscillating periods in Table Bay by theoretical, observational and experimental methods: T - 71-66-57; 55-51; 43-36; 33-26; 23-17; 14-12; 11-10; 9.8-9.4; 8.3-7.3; 7.5-7.0; 6.8-6.5; 6.3-5.9; 5.7-5.4; 4.8-4.4; 4.3-4.1; 4.0-3.7; 3.6-3.4; 3.2-3.1; 2.9-2.7... in minutes.

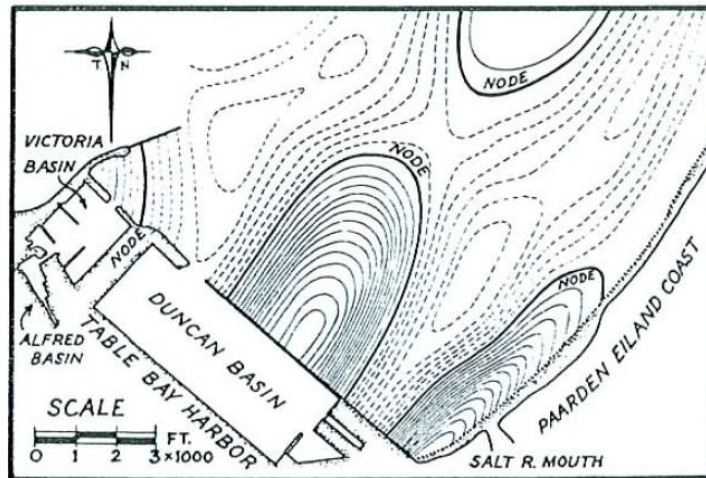
Figure 3-1: Configuration of South Atlantic Ocean (Wilson, 1954).



2. The Breakwater-Shore Oscillating System

Wilson suggested that seiches of particular frequencies resonating in Table Bay could in-turn resonate between the breakwater and shore. He termed this area a quasi-basin as illustrated in Figure 3-2. He claimed that the breakwater-shore oscillating system created higher frequency seiches than those occurring in Table Bay. The higher frequency seiches could thus reinforce the possible modes of oscillation in the Harbour Basin.

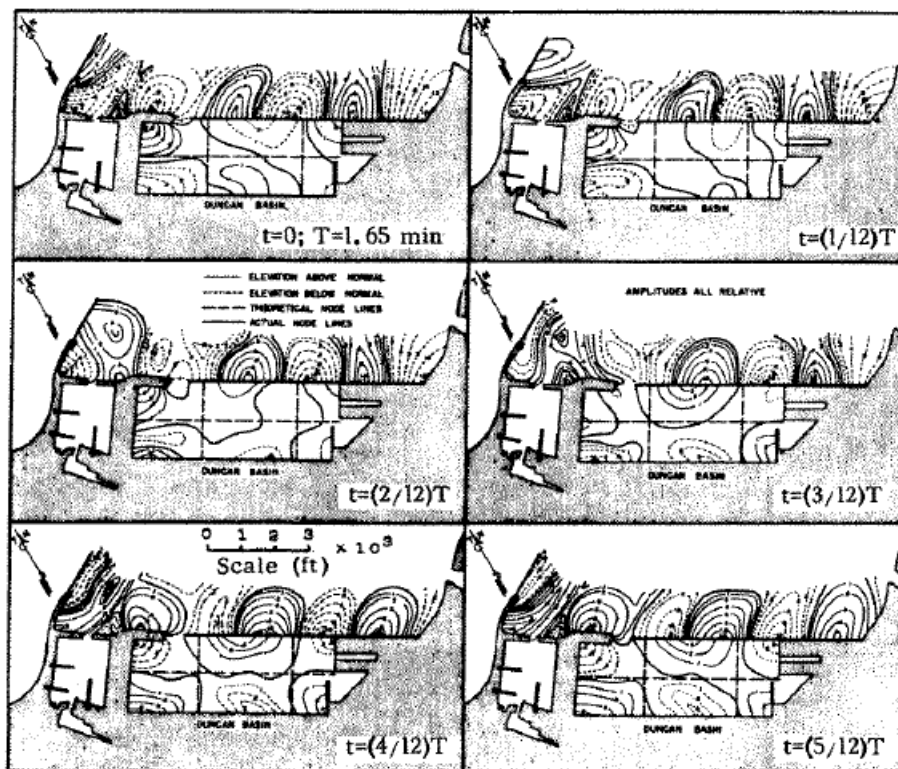
Figure 3-2: Approximate instantaneous form of 2-3/4-min seiche off Table Bay Harbour (graphical synthesis) (Wilson, 1953).



3. Duncan Basin

In 1957, Wilson used a physical model incorporating Table Bay and the Harbour to study the resonance of Duncan Basin, the largest basin of Table Bay Harbour. Figure 3-3 shows resonant modes of Duncan Basin from model experiments.

Figure 3-3: Two-dimensional mode of resonant oscillation in Duncan Basin, Table Bay Harbour, Cape Town. Instantaneous water surface shapes contoured from model experiments (Wilson, 1957).



Wilson used the analysis of tidal records, physical modelling and application of hydrodynamic theory equations to formulate his findings.

3.2.1.1. Commentary

Long wave theory was fairly new during this stage of Wilson's studies hence there is no reference to the resonance of Cape Town Harbour due to bound or released long wave energy. Rather the generating mechanism Wilson identified was atmospheric pressure fluctuations causing resonance in ocean basins which then shifted from very low frequency oscillations to higher frequencies through a series of smaller oscillating systems. This hypothesis is unlikely as it essentially equates to very large non-linear transfers of energy between waves of low frequencies to high frequencies. Darbyshire & Darbyshire (1964) in the following section suggest a more likely scenario in which surf beat is responsible for the higher frequency oscillations.

Wilson's identification of the Breakwater-shore oscillating system as a driver of Harbour basin resonance is interesting as it shows the importance in assessing the shore line and geometry of the coast outside of the port and not just the basin shape.

3.2.2. Studies by Darbyshire & Darbyshire (1963)

Darbyshire & Darbyshire (1964) revisited Table Bay Harbour resonance, referencing Wilson and using new long wave measurements to reinvestigate and elaborate on Wilson's conclusions. Darbyshire & Darbyshire (1964) summarized Wilson's descriptions for Table Bay Harbour oscillations as the following:

- Short frequency oscillations of frequent occurrence creating trouble for ships at the berth.
- A longer period oscillation that occasionally attains large amplitude and creates a dangerously strong current at the dock entrance.

Darbyshire & Darbyshire (1964) analysed long wave data recorded offshore of Witsands, south of Table Bay Harbour on the west coast of South Africa. They identified two types of long waves; long waves with periods between 30 seconds and 6 minutes and then longer period waves with periods over 15 minutes. The shorter period long waves were attributed to surf beat while the longer period waves were attributed to fluctuations in the atmosphere creating resonance of the water mass overlaying the continental shelf. Darbyshire & Darbyshire (1964) claimed that these generation mechanisms for long waves were also responsible for the resonance in Table Bay Harbour.

As mentioned these generation mechanisms although broadly described agree with current long wave theories.

3.2.3. Studies by Wilson (1972)

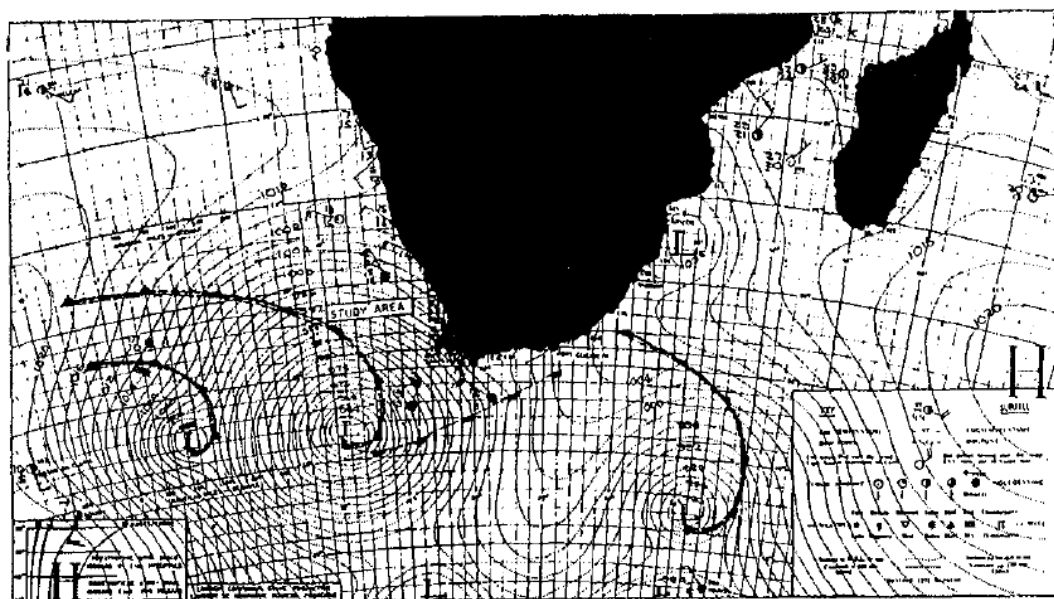
Wilson (1972) updated and summarized his investigations into Table Bay Harbour resonance. He states that in Table Bay there is an element of doubt as to the exact generation of the exciting long waves. He pointed out that while it is well recognized that higher period resonance (over 15 min) is correlated with frontal storms (Resonant air-water coupling) the lower period resonance (30 s to 6 min) generating mechanisms are unclear. He does however make a critical observation that the lower period resonance occurred during both stormy days and on clear days but only in the presence of high swell.

With our current understanding of long wave theory it can be speculated that the higher frequency seiches were a result of either surf beat or bound long wave energy entering into Table Bay harbour. It is also possible that a combination of both types of the long wave energy created the seiches.

3.2.4. Studies by Botes et al., (1982 to 1984)

Botes et al., investigated resonance in South African harbours from the late 70's to early 80's; two papers summarise this work; (Botes et al., 1982), and (Botes et al., 1984). In 1982 although resonance in SA harbours was recognized as a problem, they claimed that a better knowledge of the origin, occurrence and generation of long waves was in urgent need. In 1984 they identified, from experience, the relationship between approaching cyclonic weather systems and long wave occurrence on the West Coast of South Africa, giving the example shown in Figure 3-4 as a typical case.

Figure 3-4: South Africa with approaching low-pressure systems, passing from west to east (Botes et al., 1984).

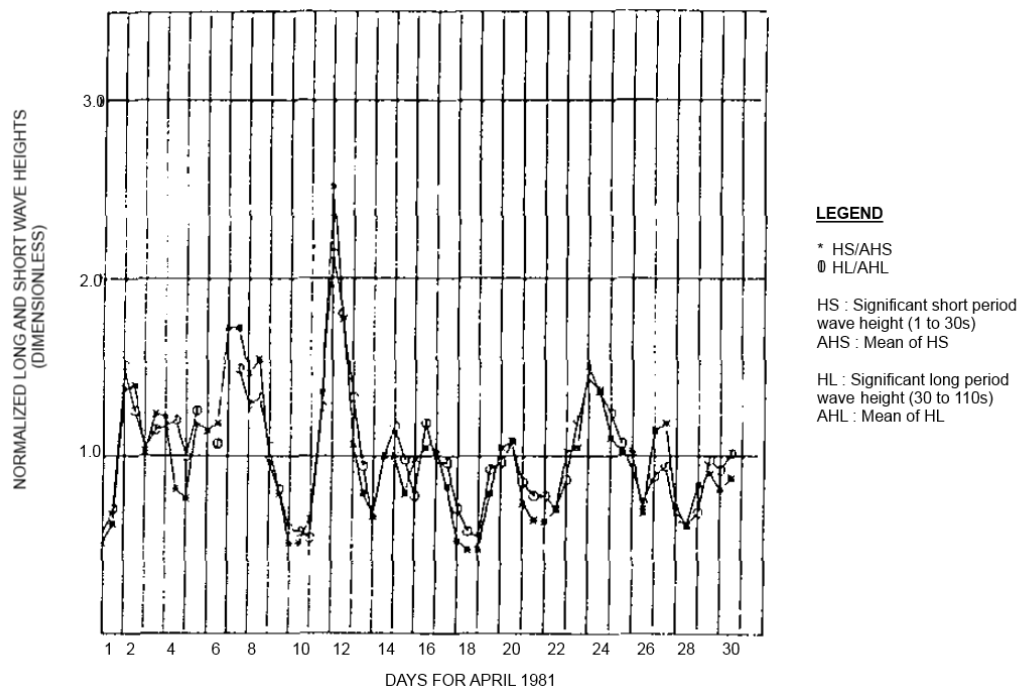


Their studies involved long wave data collection at two harbours (Koeberg and Cape Town), both in Table Bay, and with measurements both inside and at the entrance of the harbours. The data was collected in order to analyse the relationships between long and short waves and calibrate a numerical model for investigation into harbour resonance.

3.2.4.1. Analysis of Measurements

Correlation of an increase of long wave height with short wave height was displayed by plotting the normalised long (50 s to 110 s) and short (1 s to 30 s) wave heights together as shown in Figure 3-5. The wave heights were normalized by dividing the wave height record by the mean wave height over a month. The short waves and long waves were measured independently approximately 3 km from Koeberg on the West coast of South Africa.

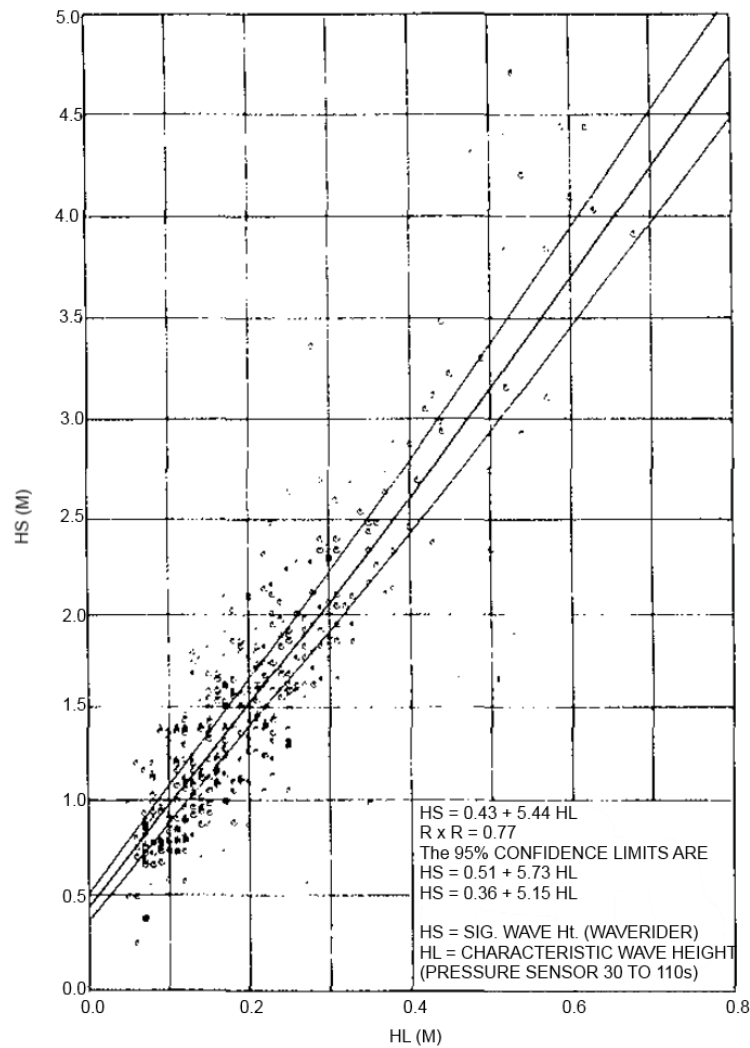
Figure 3-5: Normalised long and short period wave heights (April 1981) (Botes et al., 1982).



Further analysis of the long and short wave height correlation was made using Figure 3-6. The figure plots a linear trend line to the correlation of long and short wave energy. The grouping of the data scatter shows a fairly good correlation. In addition an exponential curve was fitted to the data which was defined as more realistic because the long wave heights will not increase indefinitely. The relationship is defined in Equation 3-1, with the parameters described in Figure 3-5 (Botes et al., 1982).

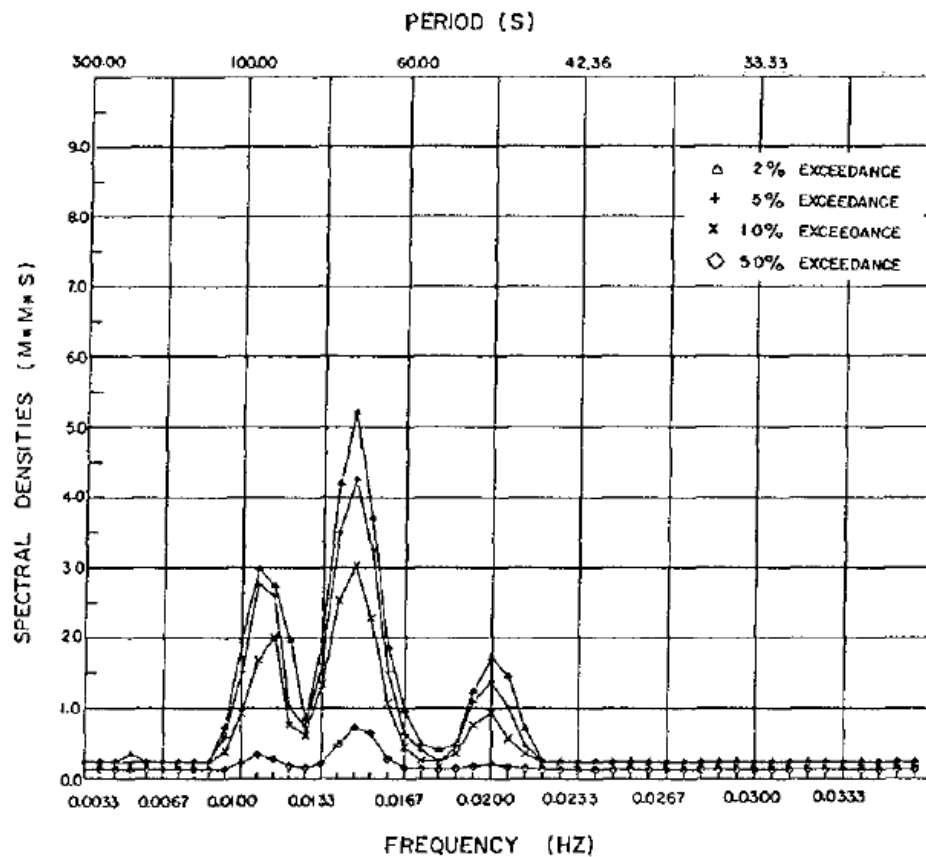
$$HS = 0.075e^{3.03 \cdot HL}$$

Equation 3-1

Figure 3-6: Correlation between long- and short-period wave heights (Botes et al., 1982).

Spectral density exceedance graphs were used to obtain an idea of the magnitude of the wave spectra and identify dominant frequencies. Figure 3-7 shows an example of a spectral density exceedance graph for inside Koeberg harbour (Botes et al., 1982). The figure essentially shows the percentage of time that the spectra, inside Koeberg harbour, will exceed spectral densities for specified percentages viz. 2%, 5%, 10% and 50%.

Figure 3-7: Spectral density exceedances for September 1981 inside the harbour (Botes et al., 1982).



3.2.4.2. Numerical Model

Botes et al. (1982) used a two-dimensional finite-difference numerical model, based on an approximation of the hydrodynamic equations, for the investigation of harbour resonance. They applied a technique of inputting a band-pass filtered white noise spectrum rather than individual sine wave conditions. This methodology was adopted in order to decrease computational time and incorporate a range of frequencies in the model. Frequencies that created high amplification were modelled by discrete sine wave conditions. Results of maximum water elevation and velocity fields were then extracted from the model. The authors used the numerical model to investigate the potential of long wave resonance for alterations of numerous South African harbours including:

- Table Bay Harbour
- Mossel Bay Harbour
- Granger Bay Harbour
- Koeberg

In (1984) Botes et al., further validated and tested their model using the data measured and presented in the 1982 study. The 1984 study used the Koeberg harbour to check the effects of varying the grid size and time steps on accuracy.

3.2.4.3. Commentary

Botes et al. presented ground breaking work on analysing seiching for South African Harbours. Since their studies very little published work has been presented for long waves and seiching in South Africa. Their methods of analysing the correlation between long and short wave measurements as shown in Figure 3-5 and Figure 3-6 is insightful and useful. The correlation of the increase of long wave height with short wave height clearly suggests the presence of bound long waves in the vicinity of Cape Town.

The numerical model that Botes et al. used in their studies is basic in terms of resolution and matching the actual physical processes. The modelling approach of using a band-pass filtered white noise spectrum for the input conditions is very similar to the state of the art white noise simulations performed currently using Boussinesq models as mentioned in Section 3.3.2 below.

3.2.5. Studies by Shillington (1984)

Shillington, (1984), investigated the occurrence of what he termed long period edge waves on the southern coast of South Africa. The waves were initially identified from tidal gauge measurements which revealed wave heights of up to 60 cm with periods between 12 min and 1 hour. Shillington analysed two typical cases (on 11 May and 16 April, 1981) when significant tidal gauge and air pressure oscillations occurred simultaneously. The investigation included pattern finding between synoptic charts, microbarograph air pressure readings and tidal measurements. Further investigation into identifying an amplification mechanism included use of a “resonant mode edge wave model”.

One of the cases Shillington reported on was the 11th of May 1981: Shillington identified a rectangular area on the edge of the Agulhas bank as the generation area for the waves travelling along the south coast, as shown in Figure 3-9. The area was defined by identifying the arrival time for the disturbance/edge waves from the tidal recordings as shown in Figure 3-8 and applying a celerity value. The waves were assumed to be freely propagating and hence celerity was defined as ($c = \sqrt{gh}$). From correlating the synoptic charts at the time of the event and the air pressure readings from the sites (Shown in Figure 3-10 and Figure 3-11) Shillington claimed that the long waves were created by atmospheric conditions. He further analysed this theory with a “resonant mode edge wave model”.

Figure 3-8: Tide gauge recordings for 11 May 1981 (Shillington, 1984).

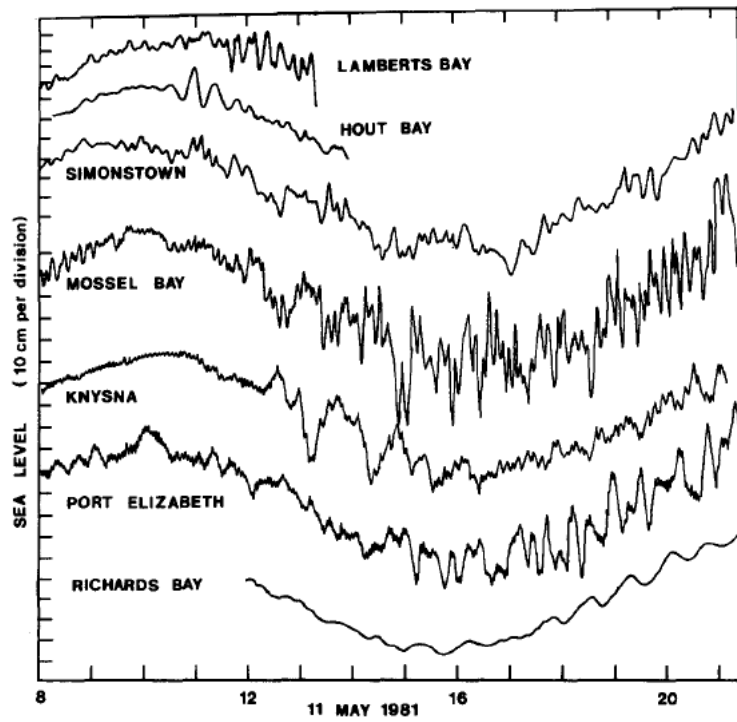


Figure 3-9: Agulhas Bank bathymetry and location of measuring stations. The hatched area shows the region of the generation of the waves for 11 May 1981 (Shillington, 1984).

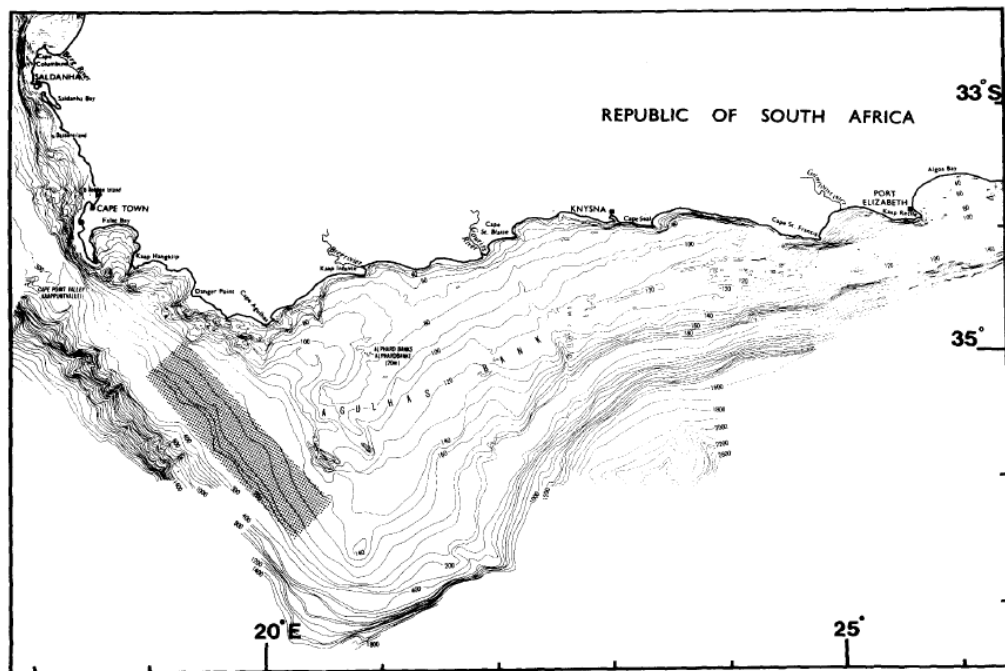


Figure 3-10: S.A. Weather Bureau synoptic weather maps for 10 and 11 May 1981 (14h00 SAST) (Shillington, 1984).

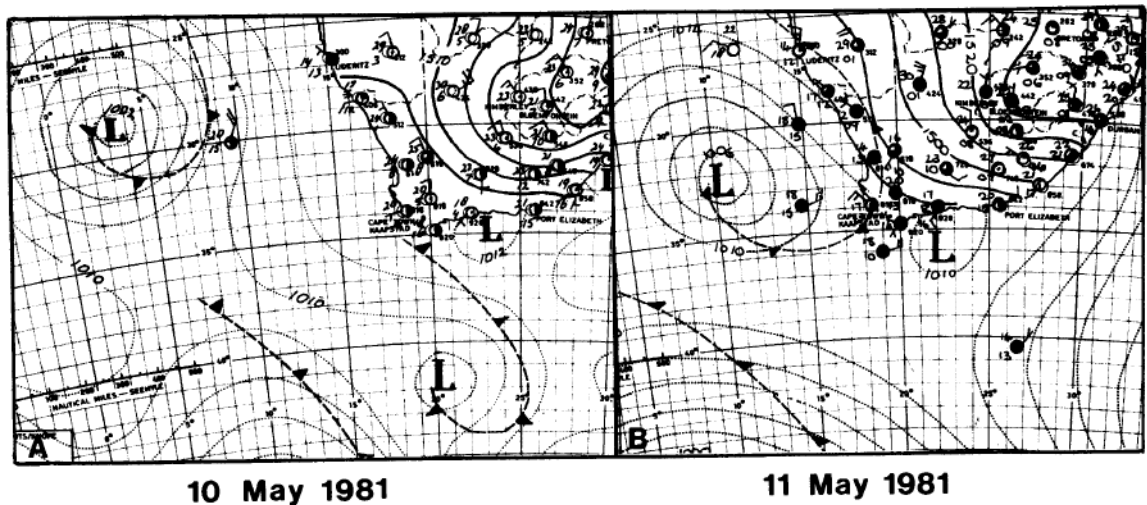
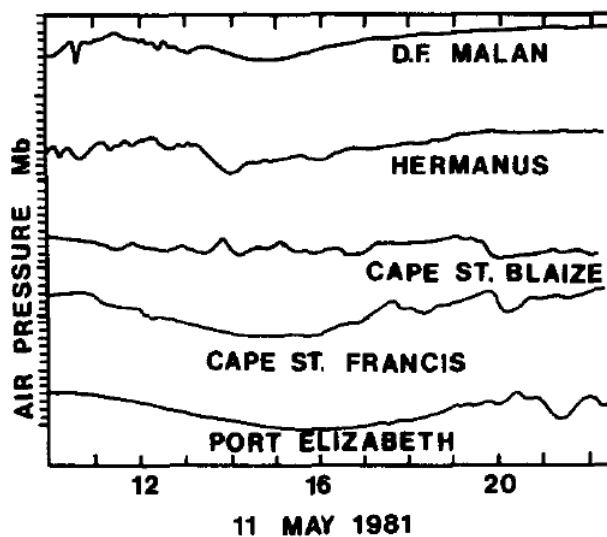


Figure 3-11: Air pressure microbarograph recordings for 11 May 1981 (Shillington, 1984).



Shillington (1984) concluded that the oscillations or long waves were created by a “**resonant forcing of the sea surface by atmospheric pressure fluctuations**”. He also identified the scenario for the long wave creation “**If such a forcing by the atmosphere is to be successful, there must be a matching of time and space scales between the atmospheric pulses and the resultant surface wave oscillations during the generation phase.**”

Shillington (1964) stated that after reviewing two years of tidal data only four or five events were identified at the same scale as the 11 May 1981 event. He states that all the events have similar synoptic scale air flow characteristics as the two cases he presented: however, the pressure pulse is what will govern the type of response of the sea surface. The two forcing mechanisms were stated as follows:

“The first event has a signal propagating through the atmosphere which can be closely linked to the propagation of a coastal low, while the second event shows a signal that is more harmonic, but travels more quickly than the coastal low or the frontal system associated with extra tropical cyclones.”

The months of April, May and September, October were identified as the most likely months that the waves would occur due to the atmospheric conditions.

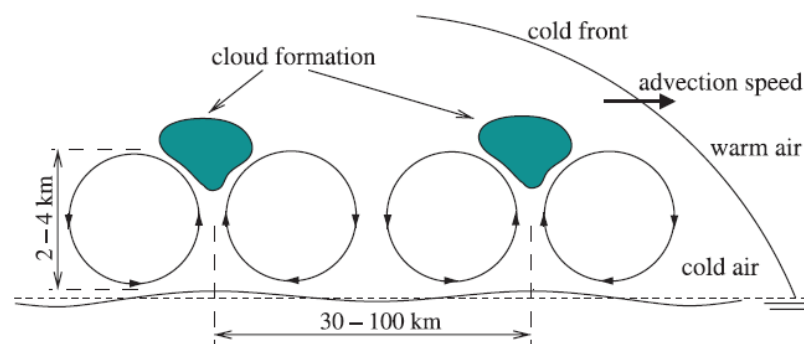
Shillington’s analysis was not comprehensive and his use of the term *edge waves* is ambiguous however just his analysis of the tidal measurements provides proof that there are relatively frequent events when longer period waves propagate past the port of Ngqura (17 km North of Port Elizabeth). As Shillington mentions he was not the first to identify this type of long wave generation mechanism as is mentioned above under Sections on Wilson and Darbyshire & Darbyshire’s work.

3.3. Seiches and Long Waves Internationally

3.3.1. Generation of Seiche Events by Atmospheric Convection Cells – Rotterdam Harbour

De Jong (2004) and De Jong & Battjes (2004) investigated the origin and prediction of seiches in Rotterdam harbour. The seiches in Rotterdam were attributed to long waves generated by fluctuations in wind speed and atmospheric pressure induced by meso-scale atmospheric convection cells. These events often arise following a cold front passing over the North Sea. A theoretical example is shown in Figure 3-12.

Figure 3-12: Sketch of convection cells in the area behind a cold front together with a theoretical surface elevation response (De Jong, 2004).



The seiches were identified by the analysis of surface elevation data both offshore and inside the harbour. The seiches were first characterized by visual inspection of Fourier filtered surface elevations; once a definition “seiche event” was identified, a wavelet analysis based on the *Morlet* wavelet (Morelet et al., 1982) was used to identify all the seiches occurring during the several years of recorded surface elevations. Meteorological measurements and visual inspection of the weather

charts helped identify the occurrence of the seiches with the passing of cold fronts and low pressure systems.

A 2D numerical model was also used, by De Jong (2004), in an attempt to identify the generation of the seiches; however, the model lacked the required detail to draw conclusive conclusions. It did however, help identify wind speed as a key factor in the generation process. Filtered wind speed measurements and surface elevations were analyzed, and a correlation of the wind speed with surface elevation was identified. The correlation of wind speed fluctuations and pressure fluctuations as a result of convection cells was then identified. The dynamics of the process were finally investigated using a 1D numerical model.

Although beyond the scope of this study, in light of De Jong's findings and methodology a reanalysis of the longer period waves (>300 s) identified in South Africa may identify the same generation mechanism.

3.3.2. Long Wave Numerical Model Studies

3.3.2.1. Wave Disturbance Modelling in the Port of Sines (2001)

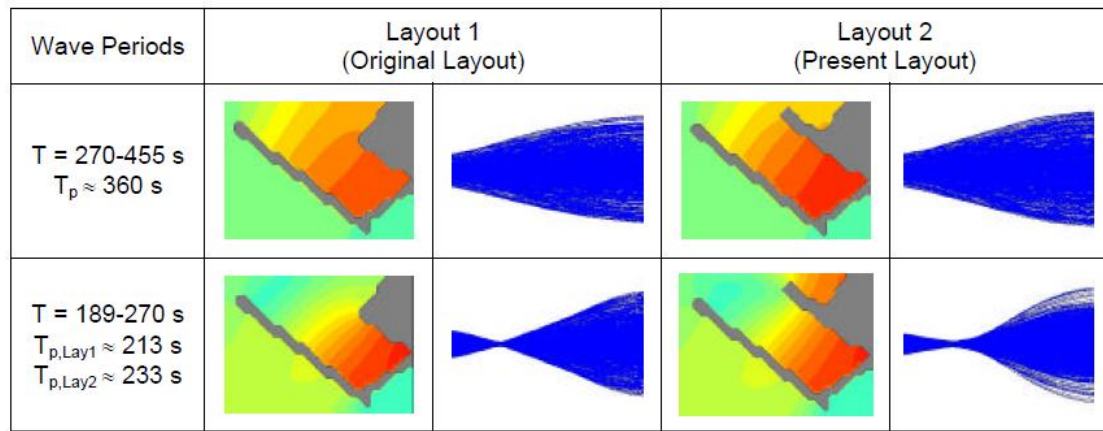
Gierlevsen et al. (2001) investigated severe mooring problems in the port of Sines, Portugal. Their study was performed with particular emphasis on numerical modeling techniques used to characterize long wave oscillations in the port.

The mooring problems started shortly after the completion of an extension of a quay in the port basin. The generation mechanisms of the long waves were not detailed because the objective of the study was to determine the role that the extended quay had in changing the oscillations in the port.

Gierlevsen, et al., used the Boussinesq Wave Module of DHI's MIKE 21 numerical model (Mike 21 BW) for the wave propagation into the port of Sines. A white noise simulation was used in order to identify the natural frequencies of the original layout. A "white noise" spectrum is defined as having equal amounts of energy at all frequencies. The white noise spectrum was applied at the boundary of the model as unidirectional waves from one direction (West). At points within the port basin surface elevations were extracted and spectral analysis was performed on this data. The spectra helped to identify the potential oscillating period ranges of the basin.

The period ranges were then further investigated using 2D band-pass filters of the surface elevation files which were in turn converted into 2D filtered energy level plots (shown in Figure 3-13). Envelope plots of the band-pass filtered surface elevations were also used to characterize the long wave oscillations (also shown in Figure 3-13).

Figure 3-13: Natural long-period resonance modes for Layouts 1 and 2. Long wave energy intensity and surface elevation envelopes along the longitudinal lines of the basin. (Example from (Gierlevsen et al., 2001)).



A comparison in intensity of long wave energy for the two (with and without quay extension) layouts was performed by extracting wave energy along a line through the position of berthed vessels. The extraction was performed on the 2D filtered band-pass energy files. The comparison of long wave intensity showed that for the majority of period ranges more energy was present with the quay extension and thus, it was concluded that for a natural sea state the new layout would have more long period wave energy.

A storm condition was modeled in order to further investigate the findings of the “white noise” simulation and to investigate the basin during natural wave conditions. The storm was modeled with a significant wave height of 1 m in order to avoid wave breaking in the model. Average short and long wave disturbance coefficients were extracted from the berth sites and compared for different layouts. These comparisons helped to identify two potential mitigation methods including reconstructing the demolished part of the western breakwater or extension of the eastern breakwater. It was noted that the long wave energy was only a relative value as the long wave energy was created within the model due to non-linear wave-wave interaction. As bound long wave energy increases with wave height, the long wave energy was obviously under estimated (Gierlevsen et al., 2001).

3.3.2.2. Torsminde Harbour and Port of Long Beach (2005)

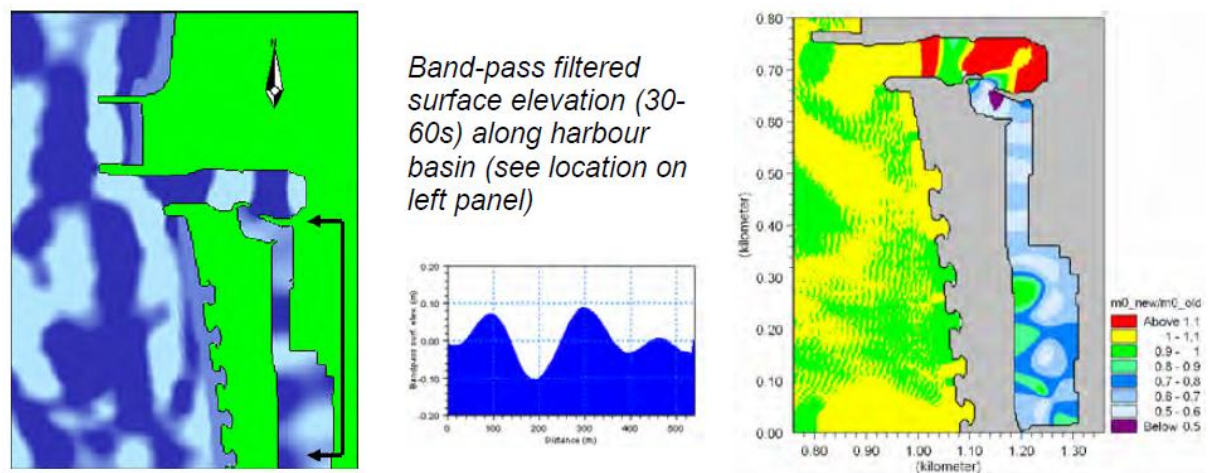
Kofoed-Hansen et al., (2005) also used the Mike 21 BW model and similar methods to those of Gierlevsen et al., (2001). The paper essentially shows the capability of the model by using two ports as case studies; Torsminde Harbour, and port of Long Beach.

Torsminde Harbour was modeled using a directional short wave event including breaking. The long wave energy is generated in the model simulation as a result of non-linearities and wave-wave

interactions. The grid dimensions were 1.5 km by 1.5 km at 2 m increments, a time step of 0.1 s was used and the model was run for 30 minutes. One short wave event was presented in the paper and detailed as follows: Directional wave $H_{m0} = 4$ m, $T_p = 9$ s Mean wave direction = 270° N, directional spreading – \cos^8 based on a standard Jonswap spectrum.

Using band-pass plots of relative long wave energy and instantaneous surface elevation the propagation of long wave energy was presented as shown in Figure 3-14.

Figure 3-14: Instantaneous band-pass filtered surface elevation map (left) and map of relative long period wave energy between new and old layout (30-60 s) (Kofloed-Hansen et al., 2005).



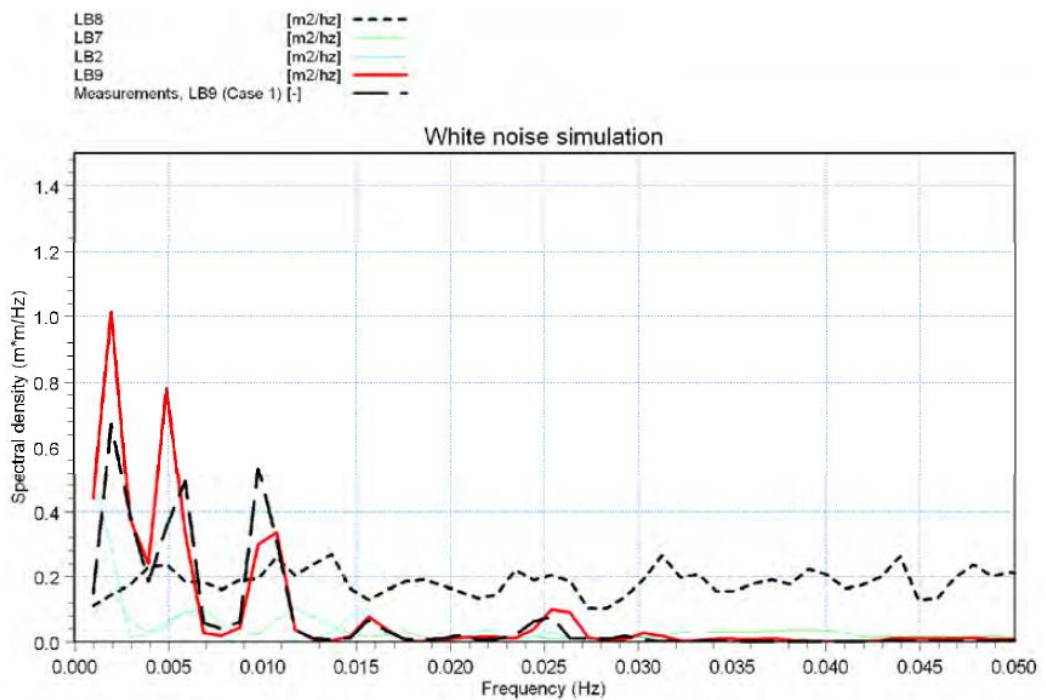
The paper unfortunately does not detail the result comparison with field measurements or the physical model of Torsminde Harbour but rather states that good agreement was found between the three.

The modeling of the port of Long Beach was included as an example of a large scale model. A model area of approximately 16 km x 21 km was used, as shown in Figure 3-15. The methodology involved a white noise simulation and spectral comparison excluding breaking, similar to Gierlevsen et al., (2001). The spectral comparison with field measurements taken within the harbour revealed a good match in frequency peaks as shown in Figure 3-16.

Figure 3-15: Location of wave gages. The rectangle indicates the boundaries of the MIKE 21 BW model. Co-ordinates are UTM zone 11 (Kofoed-Hansen et al., 2005).



Figure 3-16: Wave spectrum of the white-noise simulation at the stations LB2, LB7, LB8 and LB9 (Pier J), see Figure 3-15 for location. For comparison the measured spectrum at LB9 (1 August 2000 20:00-23:00) is depicted (Kofoed-Hansen et al., 2005).

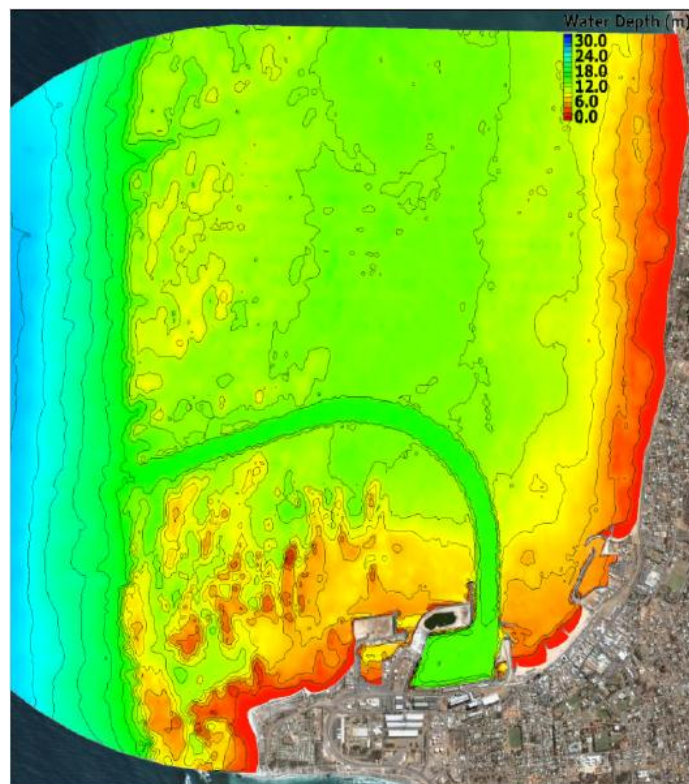


Secondly, two events were modeled in order to compare modeled results to existing field measurements. A sub-domain of the original model was used for this, the model boundary was forced with measured data and the comparisons presented showed a good match.

3.3.2.3. Wave Penetration at the Port of Geraldton (2009)

Various modeling techniques were used by McComb et al., (2009) to investigate (both short and long) wave penetration and reduction measures at the port of Geraldton in Western Australia. The presence of a broad shallow zone to the west of the port entrance channel provided a challenge to researchers in accurately quantifying the creation and propagation of long waves over the reefs. Figure 3-17 shows the bathymetry of the port.

Figure 3-17: Port Geraldton, Western Australia- Bathymetry Image, showing extensive reef to the West of the dredged entrance channel (McComb et al., 2009).



A combination of three numerical models was used in 2009 to provide insight into the waves entering the port and to test mitigation modifications to the port entrance. The mitigation tests included a range of structures (including detached options); the most effective option was a 350 m linear extension of the breakwater. A SWAN model was used for wave climate hindcasting and to generate the boundary conditions for a higher resolution CGWAVE nearshore model. The CGWAVE model was used to test the relative changes in harbor excitation due to various boundary conditions and mitigation modifications. A modified version of FUNWAVE 1.0 2D, which is based on the

Boussinesq equations, was used in order to investigate the creation of long waves over the reef system west of the port and help define the long wave boundary conditions for the CGWAVE model, specifically long wave direction at the port entrance. Due to the reef structure, wave breaking was included in the FUNWAVE model to account for the complexities of long wave creation and directionality. The port geometry was not included in the FUNWAVE model for the 2009 study; presumably due to the long computational time, hence the use of CGWAVE which lacks the complexity of FUNWAVE.

One offshore event was input at the FUNWAVE boundary, the offshore event corresponded with a time when there was noticeable long wave surging at the harbor. The event was input at a depth of 25 m as a directional spectrum which was extracted from the SWAN hindcast model. The model revealed to the authors that:

“long waves are generated on the outer reef structure and then propagate shoreward, essentially co linear with swell wave propagation over the reef platform.” (McComb et al., 2009)

Analysis of the long wave data at the entrance to the harbour revealed similar results to measured data at the port of Geraldton; hence, the authors concluded that the Boussinesq modelling was correctly modelling the main physical process of long wave generation. The 2009 study (McComb et al., 2009) identified that, of all the port modifications they tested for reduction of wave penetration, an extension of the main breakwater was the best option.

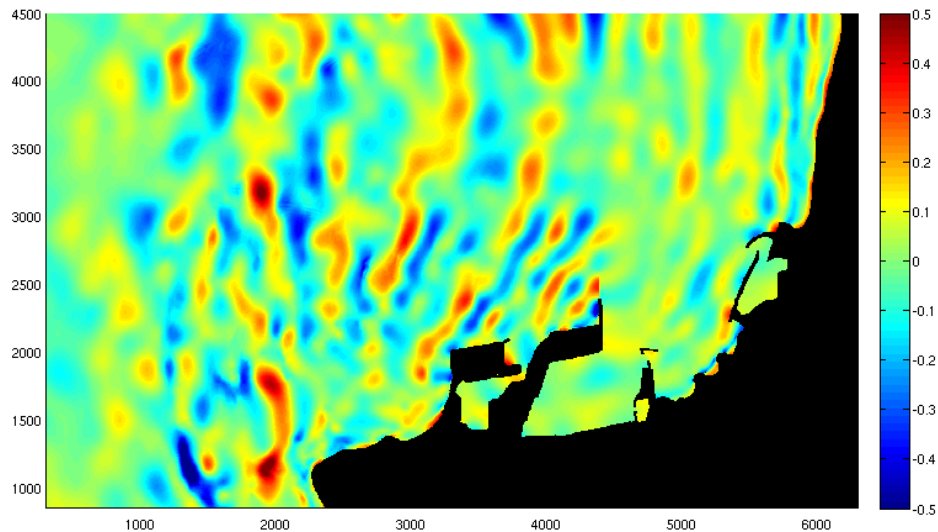
3.3.2.4. Wave Penetration at the Port of Geraldton (2011)

Two of the authors from the 2009 study continued their research of Geraldton Harbour as presented in Johnson & McComb (2011). The focus of the paper was on presenting a modeling approach that minimizes assumptions and measurements while investigating propagation of long waves into a port; the port of Geraldton was used as a case study. Commentary on their modeling approach is included in Section 3.4.2; this section summarizes their modeling approach and investigation of the port of Geraldton.

A modified version of FUNWAVE 2D was used to model the long and short waves penetration at the Port. As mentioned above FUNWAVE 2D is based on the Boussinesq equations. Four short wave events were input on the model boundary based on directional spectra extracted from a hindcast SWAN model. No long wave energy was input on the model boundaries; instead the ability of the Boussinesq equations to create long waves was relied on. Each event was run for 5000 seconds with the last 3600 seconds of data being used for the post processing. The model included breaking; the grid dimensions were 2101 by 1101 at a spacing of 3 m and 5 m in the x and y directions respectively.

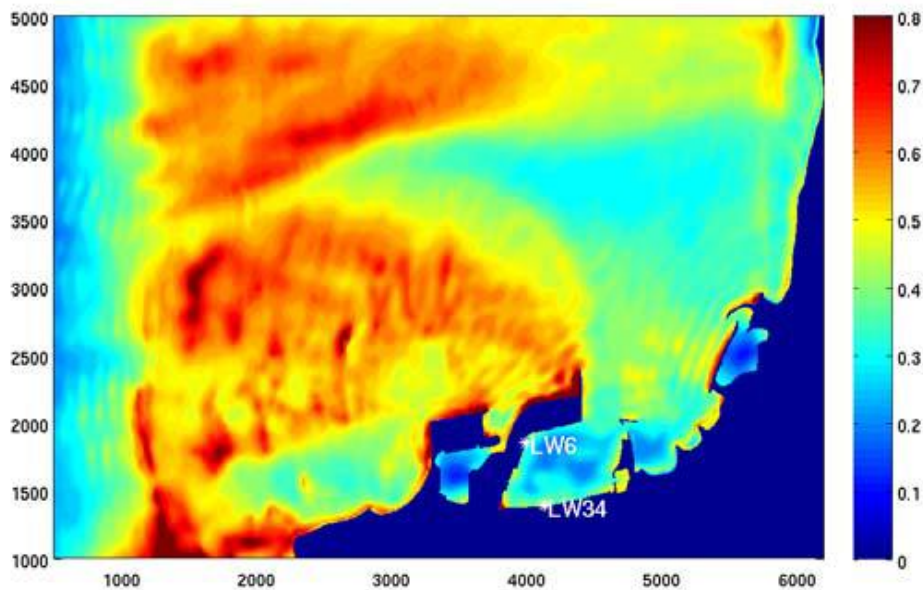
Post processing of the results included filtering the instantaneous surface elevation over the whole domain using a frequency domain filter; this gave visualizations of the instantaneous surface elevation of the long period waves (shown in Figure 3-18).

Figure 3-18: Example of instantaneous surface elevation of the 0.0-0.04 Hz filtered surface elevation showing the long wave field within the port of Geraldton domain during Event 4. Areas of long wave generation can be seen across the reef platform to the west and north of the entrance. Units are in m (Johnson & McComb, 2011).



The significant long wave heights were also calculated over the whole domain from the variance of the filtered long wave time series. This gave the spatial variation of the significant long wave heights over the whole domain, as shown in Figure 3-19. It is quite clear that a large amount of long wave energy is created or released over the reef structure to the west of the port which is visible in Figure 3-17.

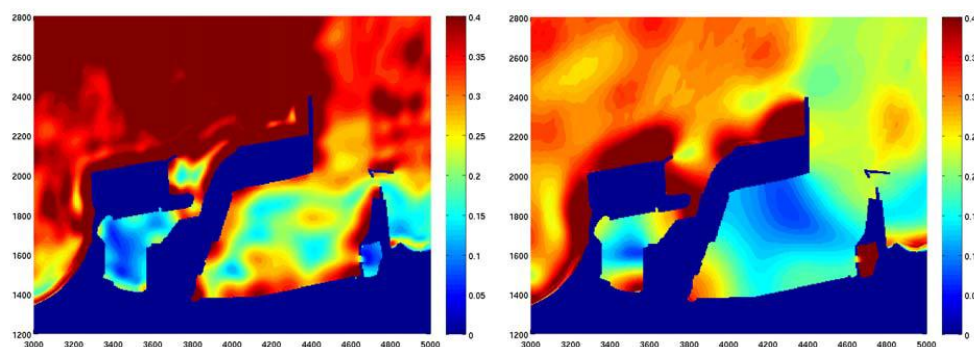
Figure 3-19: Long period significant wave height during event 4. The locations of the long period wave sensors (LW6 & LW34) within the basin are shown. Units are in m. (Johnson & McComb, 2011).



Using Figure 3-18 and Figure 3-19, Johnson and McComb (2011) identified direct refraction of the long waves into the port and partial reflection of the long waves off the marina east of the port as the main mechanisms of long wave penetration.

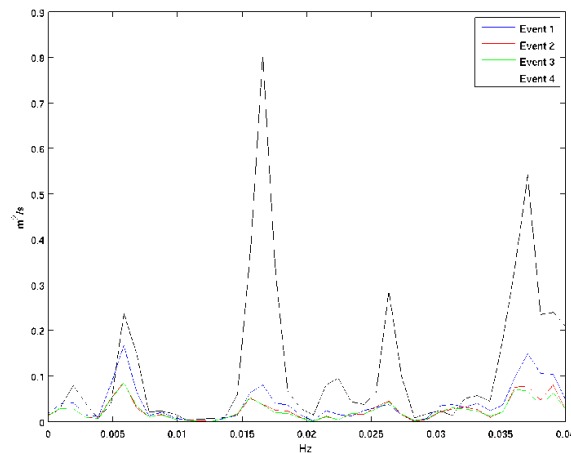
The 2011 study differed from the 2009 study in that the Port was included in the Boussinesq model domain. By using the long wave filtering technique it was possible to visualize modes of resonance in the port as shown in Figure 3-20.

Figure 3-20: Significant wave height of high frequency (0.015-0.04 Hz) and low frequency (0-0.015 Hz) components of the long wave field. A clear nodal structure is seen in the low frequency partition [right frame], contrasting to a more complex distribution of energy in the high frequency waves. Units are m. (Johnson & McComb, 2011).



Spectral analysis of the surface elevation inside the port also enabled the authors to identify the dominant seiche modes of the Harbour as shown in Figure 3-21.

Figure 3-21: Estimated spectra of the modelled surface elevation at location LW34. The well defined peaks correspond to the dominant seiche modes of the basin. (Johnson & McComb, 2011)



Each of the four events was compared with measurements in the harbor basin, the modeled long wave H_s values were within 15 % of the measured values, the long wave T_p values were within 25 % of the measured values.

Johnson and McComb (2011) concluded that the agreement between the modeled and measured data was very good, and that therefore the modeling technique may be applied with confidence.

3.4. Conclusions and Summary

3.4.1. Long waves on the coast of South Africa

The chronological review of long waves and seiching in South African ports, although mostly out of date, puts this study into context and ensures that no reported unexpected phenomena are overlooked. The literature has revealed that ports on the west coast of South Africa have historically been affected by seiching.

Two general long wave generation mechanisms were identified:

- The presence of very long period waves (Periods > 12 min) were linked to a resonant forcing of the sea surface by atmospheric pressure fluctuations (Resonant air-water coupling).
- Shorter period waves (30 s to 6 min) effecting vessel motions were attributed to the presence of high swell and termed surf-beat.

With relevance to Ngqura, the shorter period long waves are the focus of the study as they are most likely the cause of excessive vessel motions. The presence of the longer period long waves is noted but unlikely to be critical.

3.4.2. Long Wave Modelling

Gierlevsen et al., (2001) using a Boussinesq model and “white noise spectrum” demonstrates a powerful and efficient method for investigation of the natural frequencies of port. In particular the method lends itself to comparing port layouts and as a cursory analysis. Botes et al., (1982) also identified the benefits in using white noise type spectrum input with regards to decreasing computational time. Gierlevsen et al., (2001) make the valid point that as the white noise spectrum is a synthetic sea state, the results cannot conclude that the port will actually resonate at any of the resonance periods found. This is because the sea may not produce the energy required to force the resonance. The white noise simulation therefore is best for layout comparisons to check for any new Resonance periods or increased amplification.

As computer hardware has developed the modeling approaches have started to include more realistic processes, this is evident in comparing the techniques of Gierlevsen et al., (2001) and the latest approach by Johnson & McComb (2011). Where Gierlevsen et al. (2001) used a white noise approach and modeled a storm event with no wave breaking, Johnson & McComb (2011) model multiple short wave events with wave breaking letting the model develop the low frequency energy. Interestingly, Johnson & McComb (2011) and Kofoed-Hansen et al., (2005) reported good correlation to measurements even though their input had no control over the groupiness of the input wave train. This leads one to believe that in the cases they modelled the random generation of waves from the spectrum made a realistic allowance for the phasing of the wave components and hence: the groupiness was realistic and close to the real measured sea state. It also shows that bound and nearshore created long waves were the dominant source of long wave energy as there was no free long wave energy added into the models.

Johnson & McComb (2011) showed the power of post-processing techniques; their use of band-pass filtering on the domain (2D) result files show the low frequency waves propagating into the port. Simply by stepping through the time steps of a low frequency result file, it is possible to see how the long waves refract and diffract through the domain, and penetrate the port. These post processing techniques have been used in the analysis of wave penetration mechanisms for Ngqura.

4. THEORETICAL CONSIDERATIONS

4.1. Introduction

This Chapter includes some of the key theoretical concepts used in this study. An outline of the classic description of random sea waves is included in order to highlight the principles behind the conversion of wave measurements to processed wave spectra and parameters. This leads into a brief description of the inherent limitations of using the theory.

A section collating guidelines for measuring long waves is included; this section was used to ensure that the long wave data available for the study was in fact reliable. Finally a discussion of the Boussinesq equations is included because this is the basis of the models used in Chapters 8 and 9.

4.2. Classic Description of Random Sea Waves

The most common method of describing the random sea state is to describe the sea surface as a linear superposition of an infinite number of small amplitude waves having different frequencies and directions of propagation, these individual waves may be called wavelets. Under this assumption the profile of an individual wave is given by Goda (2000) as:

$$\eta = a \cos(kx \cos \theta + ky \sin \theta - 2\pi \cdot ft + \varepsilon)$$

Equation 4-1

Where η denotes the elevation of the water surface above the mean water level, a is the wave amplitude, and $k=2\pi/L$ is the wave number. The angle between the x -axis and the direction of wave propagation is θ , f is the wave frequency and ε is the phase angle. The space coordinates and time coordinates are defined by x , y and t .

This wave is assumed to propagate freely without interacting with other component waves. Equation 4-1 leads to the description of the random waves as a series expression shown in Equation 4-2. This expression describes random sea waves, where the profiles are changing from place to place and from time to time. The inherent assumption of this expression is that the random sea waves are a linear superposition of free progressive waves, this assumption has proven to give reliable results when the presence of non-linearity is low (Goda, 2000).

$$\eta = \eta(x, y, t) = \sum_{n=1}^{\infty} a_n \cos(k_n x \cos \theta_n + k_n y \sin \theta_n - 2\pi \cdot f_n t + \varepsilon_n)$$

Equation 4-2

This idea is illustrated using the Figure 4-1 which follows.

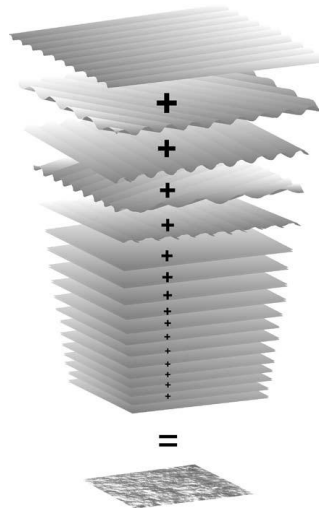


Figure 4-1: The random waves moving in time, i.e., the sum of a large number of harmonic wave components, travelling across the ocean surface with different periods, directions, amplitudes and phases sited by (Holthuijsen, 2007).

4.2.1. The Amplitude and Variance Spectra

Describing the random sea surface as described in Equation 4-2 is theoretically useful but in practice the sea surface elevation is most often measured in one location. Considering such a recording the wave profile may be expressed as a Fourier series as follows (Goda, 2000).

$$\eta = \eta(t) = \sum_{n=1}^{\infty} a_n \cos(2\pi \cdot f_n t + \varepsilon_n)$$

Equation 4-3

The component waves in Equation 4-3 now do not represent freely propagating independent waves like in Equation 4-2 but rather the sum of all waves of the same frequency. Equation 4-3 represents the amplitude spectrum however it is often more useful to use the variance density spectrum. The variance spectrum is represented by Equation 4-4. A more detailed description of the mathematics and benefits of the variance spectrum is available in (Goda, 2000).

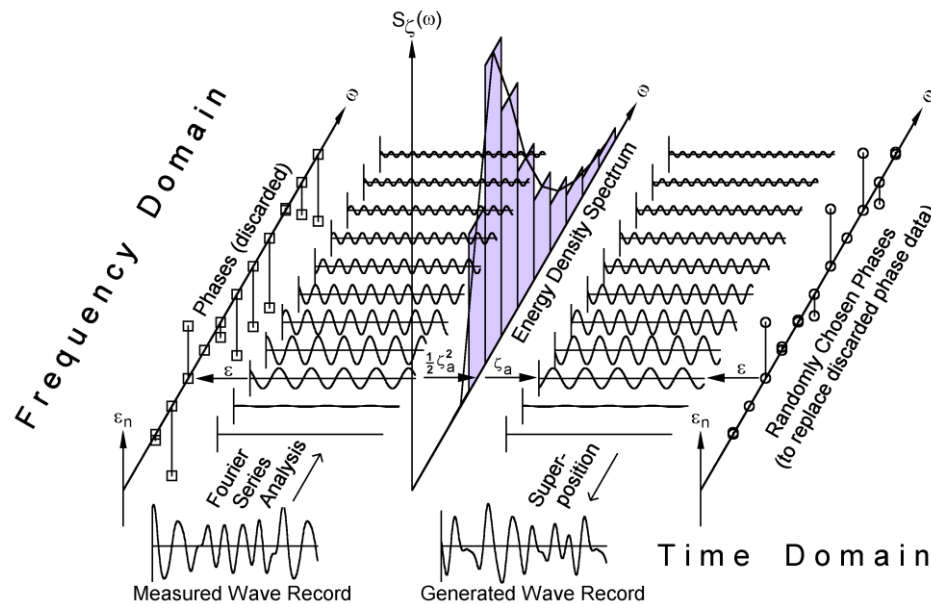
$$\sum_f^{f+df} \frac{1}{2} a_n^2 = S(f)df$$

Equation 4-4

Essentially the variance spectrum describes the sea surface as a stochastic process. By distributing the energy of each summed wavelet against frequency and direction one may obtain the directional wave spectrum. If direction is ignored the frequency spectrum may be generated. The process of

analysing the measured wave record, using a Fourier analysis, creating the frequency spectrum and regenerating a statistically similar surface elevation is represented by Figure 4-2 below.

Figure 4-2: Wave record analysis and regeneration (Journée & Massie, 2001).



The conversion of a measured wave record using a Fourier analysis, and subsequent representation of the sea state in the form of a spectrum, is used repeatedly in this study. The spectrum allows a simple visualization of the energy of a sea state in all the wave frequencies or periods.

4.2.2. Inherent Conditions for the Classic Description of Random Sea Waves

Representing the sea surface as described above implies that two conditions have been met; stationarity and a Gaussian process. The two conditions are briefly explained below; the reader is referred to (Goda, 2000) or (Holthuijsen, 2007) for more detail.

Stationarity implies that the sea state does not statistically change for the measurement duration. This leads to a trade-off in terms of measuring data as with more data retrieved a higher resolution spectrum may be attained; however, the longer the measurement period the less accurate the assumption of stationarity is (as the sea state will change).

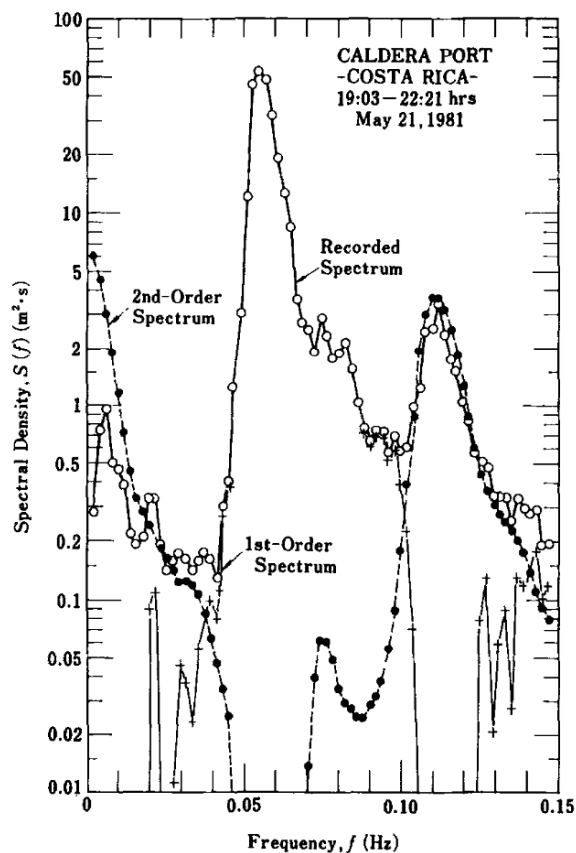
The Gaussian process refers to the assumption that the probability density function of the water surface elevation fits a Gaussian or normal probability distribution. This assumption has been proven to be incorrect, especially in shallow water cases (Goda, 2000). The deviation of the real wave probability density function away from the Gaussian distribution is due to wave non-linearity.

4.3. Limitations of the Fourier analysis

As discussed in Section 4.2, the Fourier analysis decomposes a signal into linear sinusoidal harmonics. When a Fourier analysis is performed on a non-linear wave signal, the wave energy is spread into its base frequency and higher harmonics. This results in a variance spectrum that underestimates the low frequency impact of wave motion (Hwang et al., 2003). Furthermore, in using the Fourier analysis the inherent conditions of stationarity and a Gaussian process, as discussed above, have to be assumed for the sea state.

Hwang et al., (2003), using alternative spectral analysis methods, estimated that the mean frequency of the ocean wave spectrum is about 1.2 times lower than that given by Fourier analysis. Goda, (2000) also identified the limitations of the Fourier analysis as shown in Figure 4-3. Goda (2000) resolved a recorded spectrum of long-travelled waves, at the Caldera port in Costa Rica, into both linear and secondary interaction components, using secondary interaction theory that ignored directional spreading. The spectra show energy in the lower frequencies which was not identified when using typical Fourier analysis.

Figure 4-3: Resolution of linear and nonlinear spectral components for a recorded spectrum (Goda, 2000).



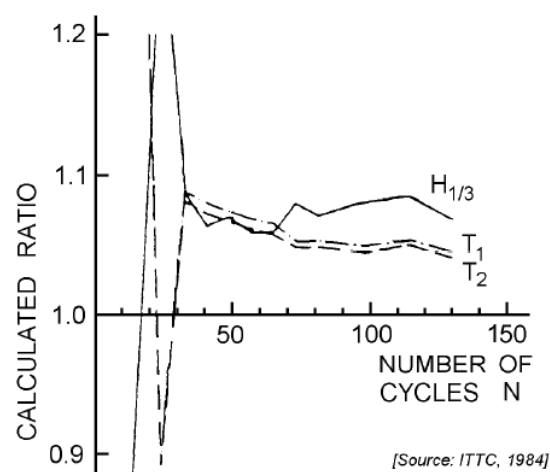
It is therefore clear that use of the Fourier analysis has limitations, especially with regard to representing lower frequency energy in the variance spectrum. Alternative methods of describing the sea surface state include wavelet analysis and using the Huang–Hilbert Transformation. These methods are not without their own limitations however. For this study the sea state will be assumed to behave as detailed in Section 4.2 and will be analysed with the use of Fourier analysis, which is the standard method.

4.4. Long Wave Measurements

4.4.1. Wave Record Length

In order to obtain proper spectral shapes and statistical values, the duration of the wave record needs to be of sufficient length. This duration may be presented by the total number of wave cycles, N . Figure 4-4 below provides a rough indication of the number of cycles required for calculation of accurate characteristic values (Journée & Massie, 2001). The ratios of the calculated characteristics for N cycles and the characteristics calculated for a very large N value are presented. Hence a value of 1 would be ideal but practical restraints make this level of accuracy unrealistic. According to Journée & Massie (2001) a minimum value of $N = 50$ should be the lower limit, while $N = 100$ is considered excellent (this is evident from the figure where convergence is reached at approximately $N = 40$). In practice assuming long waves with a 120 s period this equates to a wave record length of at least 1 hour and 40 min for the lower limit. If longer period waves are required this obviously increases. Another practical consideration is that, in order to obtain the statistical values, an assumption is being made that the sea state is constant for the duration of the measurement. This assumption becomes less accurate the longer the measurement duration is.

Figure 4-4: Effect of Wave Record Length (Journée & Massie, 2001).



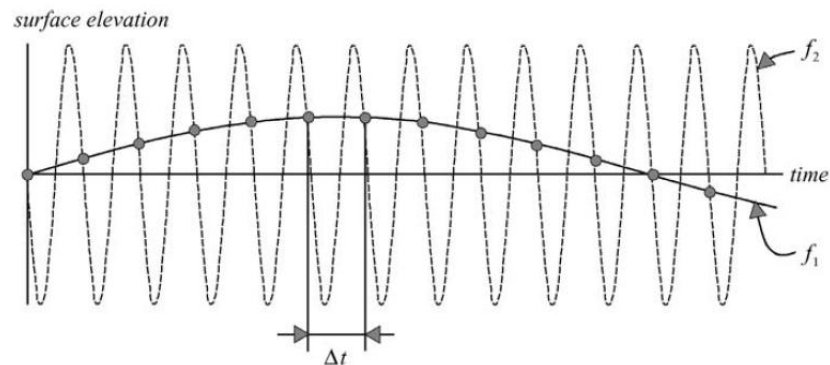
4.4.2. Sampling Interval

The sampling interval for the wave profile is recommended to be at least one tenth of the significant wave period, preferably a twentieth. A coarser sampling leads to missing small waves and underestimation of wave parameters. Finer sampling increases data however, as there is not a corresponding increase in accuracy, it is generally not required (Goda, 2000). Practically for long waves this means that for a significant period of 30 seconds a sampling frequency of approximately 3 seconds is required. When setting the sampling interval care needs to be taken to avoid the Aliasing phenomenon, as discussed in the next section.

4.4.3. Nyquist frequency

As wave measurements are recorded at a specific sampling frequency the surface elevation that is analysed, typically with a Fourier analysis, is actually a discrete wave record. As a result there are wave combinations that the sampling frequency cannot distinguish between. This is best illustrated by Figure 4-5.

Figure 4-5: Two harmonic waves with frequencies f_1 and f_2 that are given at discrete, constant time intervals $t = 1 / (f_1 + f_2)$ are indistinguishable at these discrete times (as indicated by the dots) (Holthuijsen, 2007).



The highest frequency that can be analysed for a specific sampling interval is given by the Nyquist frequency f_N (Equation 4-5).

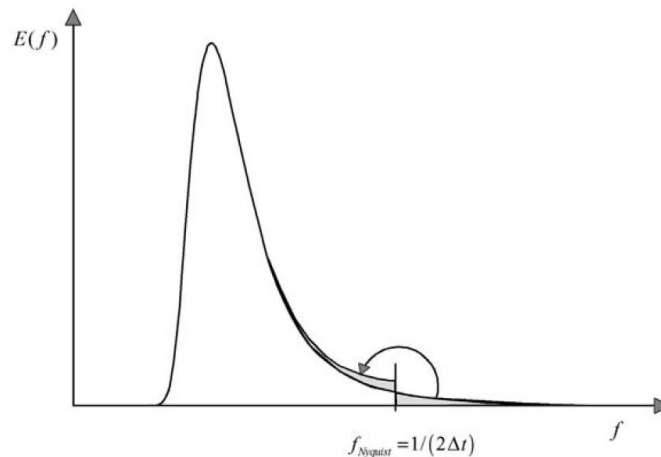
$$f_{Nyquist} = f_N = \frac{1}{2\Delta t}$$

Equation 4-5

Where Δt is the sampling interval.

The Nyquist frequency is also termed the folding frequency as any energy higher than the Nyquist frequency is redistributed to the energy between $0 < f < f_N$, this is termed Aliasing. Figure 4-6 shows an example of the aliasing effect.

Figure 4-6: Aliasing in the spectrum of a wave record with discrete time intervals Δt is equivalent to mirroring the spectrum around the Nyquist frequency $f_{Nyquist} = 1 / (2\Delta t)$ (Holthuijsen, 2007).



Practically, the Nyquist frequency is avoided by ensuring the sampling interval is high enough that aliasing only occurs at the tail of the wave energy spectrum.

4.5. Boussinesq Model

4.5.1. Boussinesq Equations

In order to investigate the propagation of long waves into a port, a number of complex wave phenomena need to be accurately modelled. These include shoaling, refraction, diffraction and partial reflection of irregular, finite amplitude waves propagating over complex bathymetries (Gierlefsen, et al., 2001). The Boussinesq Wave Module of MIKE 21 by DHI (MIKE 21 BW) incorporates enhanced Boussinesq equations that adequately model the phenomena mentioned above.

The Boussinesq Equations reduce the description of the three dimensional flow problem into a two dimensional problem (Madsen & Hemming, 1999). This is required as calculating a three dimensional flow problem with the Navier-Stokes equations over any significant domain is currently impractical (Kennedy et al., 2000). The Boussinesq Equations may be simply described as the shallow water equations supplemented with corrections for vertical accelerations (Holthuijsen, 2007).

The original Boussinesq Equations were derived by Joseph Valentin Boussinesq in 1871; however, these equations were limited to constant depth conditions and weakly represented both non-linearity and dispersion. Since then Boussinesq type equations have been enhanced in a number of ways in order to better replicate reality. Two sets of equations are available for use in the Mike BW program, the so called Classic Boussinesq equations (Peregrine, 1967), and a more enhanced set of equations developed by Madsen et al. (1991) and Madsen & Sørensen (1992). The classic equations are valid for a maximum depth to deep-water wave length ratio of $h/L_0 = 0.22$. The enhanced

equations allow for so called deep water terms and are valid for a maximum depth to deep-water wave length ratio of $h/L_o = 0.5$. The enhanced equations are further extended to incorporate wave breaking and a moving shoreline by Madsen et al. (1997b), Sørensen et al. (1998), and Sørensen et al. (2004).

A more in depth review of Boussinesq type equations and their evolution is given by Madsen & Hemming (1999), Kennedy et al., (2000) and (DHI, 2012).

The enhanced Boussinesq Equations incorporated into MIKE 21 BW can reproduce the following processes:

- Shoaling
- Refraction
- Diffraction
- Wave Breaking
- Bottom Friction
- Moving Shoreline
- Partial Reflection and Transmission
- Non-linear Wave-Wave Interaction
- Frequency Spreading
- Directional Spreading

A detailed description of the numerical methods used for solving them is included in DHI, (2012).

5. HYPOTHESIS – SIMPLIFIED ANALYSIS

5.1. Introduction

This Chapter details a high level investigation into identifying the long wave energy creating vessel instabilities within the port. The hypothesis is based on what has been learnt from the literature review and use of basic theory. The hypothesis was used to guide the more detailed investigation using numerical models and in depth data analysis, in Chapters 7, 8 and 9 .

It should be noted that the identification of geometric resonance mechanisms using hydrodynamic theory included in this chapter was performed before the use of the white noise simulation in Chapter 9 or the data analysis in Chapter 7. The results therefore are an example of the use of hydrodynamic theory.

5.2. Hydrodynamic Theory

The container basin in Ngqura, particularly the area in front of berths D100 and D101, may be subject to a number of potential resonating modes. When using linear wave theory idealized modes need to be assumed. In reality the mechanism is more complex and will be a variant of the idealization.

The following resonating mechanisms have been assumed, based on assessing the geometry of the port, for the berths:

- Short closed basin – Longitudinal, closed due to presence of berm, Figure 5-1
- Short open basin – Longitudinal, open due to removal of berm, Figure 5-2
- Short closed basin – Transverse, Figure 5-4
- Long closed basin – Longitudinal, Figure 5-5

Figure 5-1: Ngqura, Short closed basin idealized resonating mode n=1 – Longitudinal.

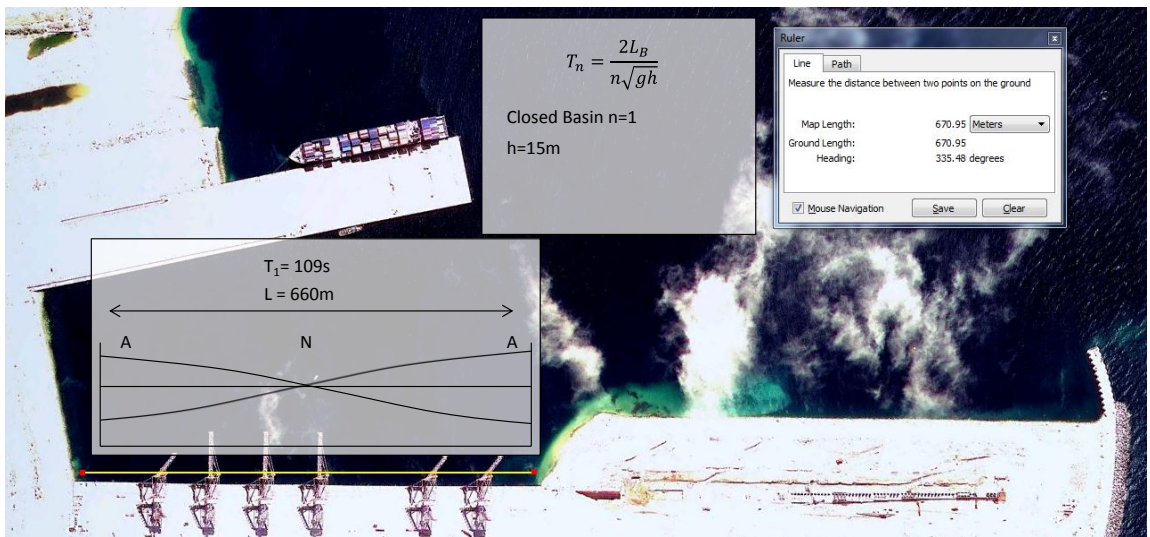


Figure 5-2: Ngqura, Short open basin idealized resonating mode n=1 – Longitudinal.

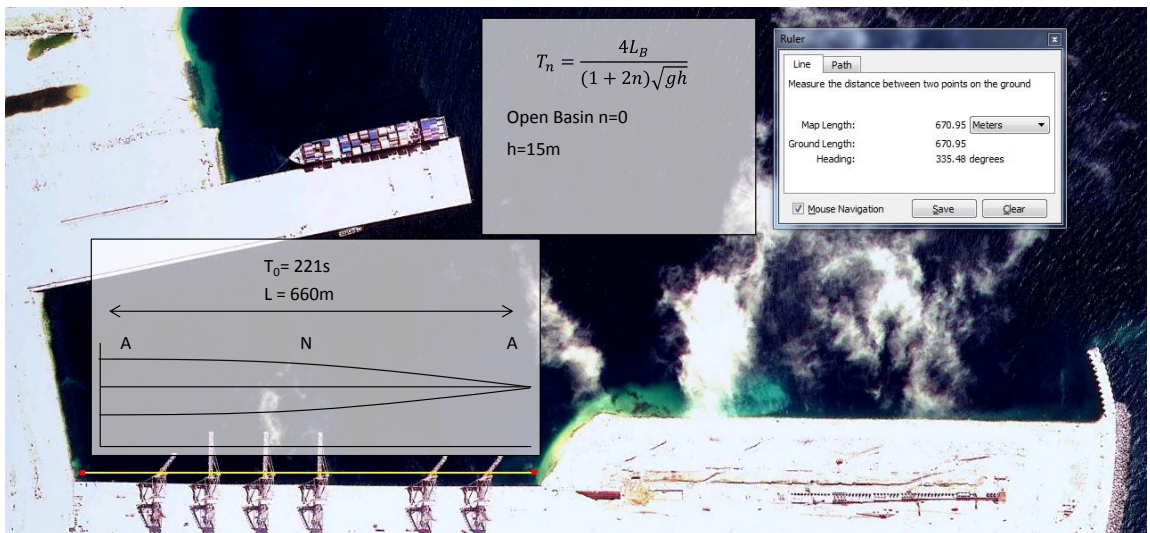


Figure 5-3: Ngqura, Short open basin idealized resonating mode n=2 – Longitudinal.

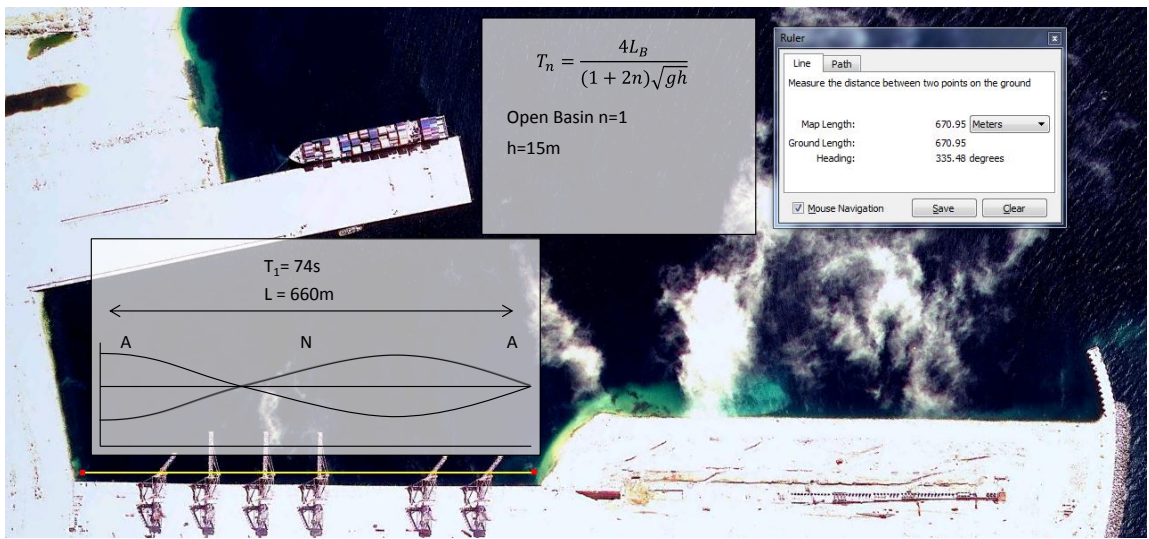


Figure 5-4: Ngqura, Short closed basin idealized resonating mode n=2 – Transverse.

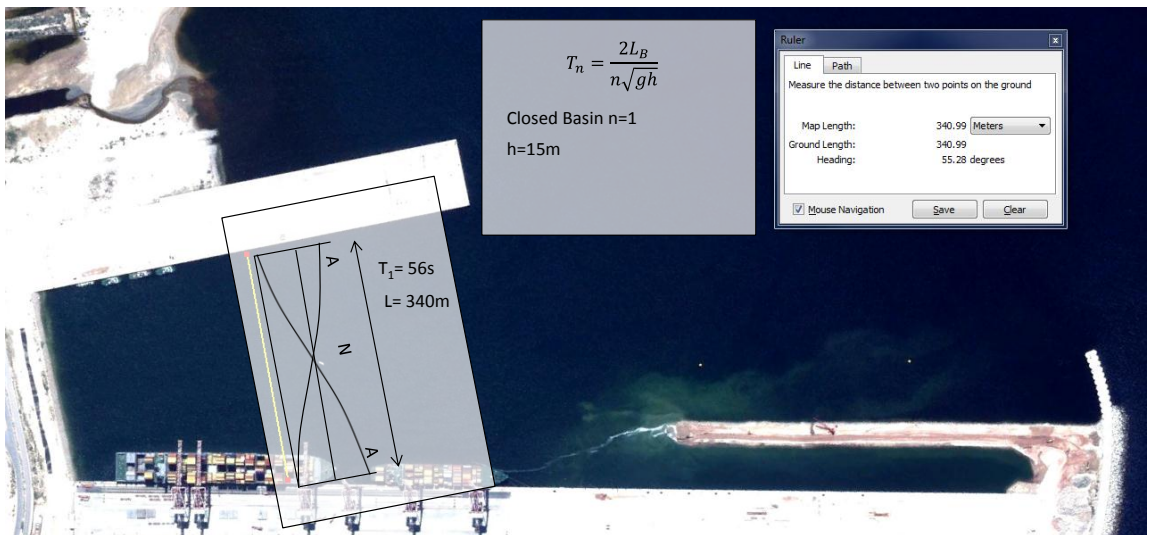


Figure 5-5: Ngqura, Long closed basin idealized resonating mode n=1 – Longitudinal.

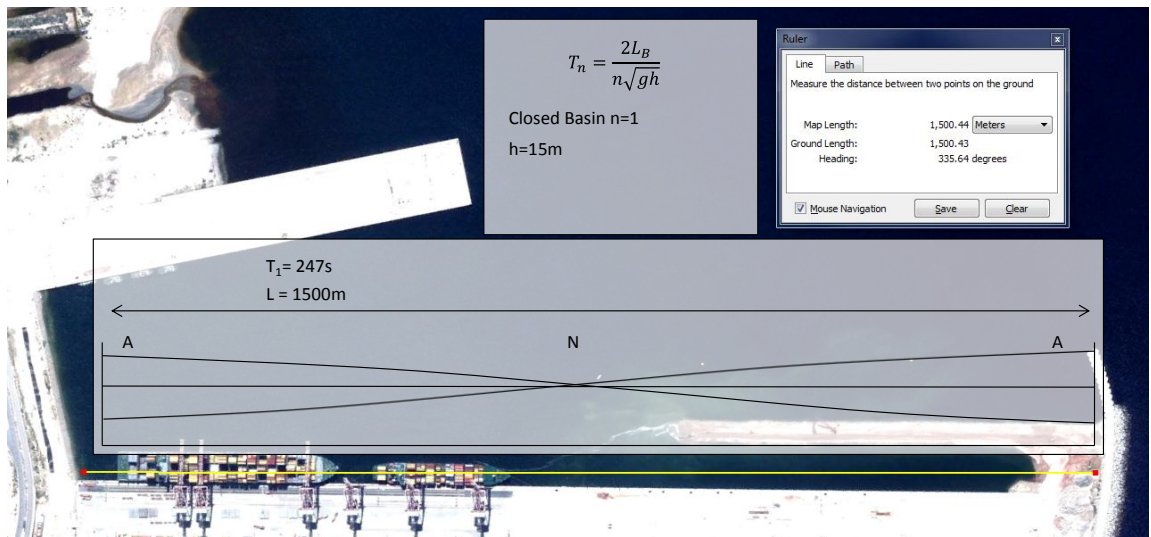


Table 5-1 shows the resulting resonating periods for various modes of the resonating mechanisms visualized in the figures above. All the mechanisms investigated result in resonance within the vessel motion problem range of between 30 s and 300 s (see next section), for at least the first 2 modes. It is noted that without any measurements showing long wave energy in the port vicinity at these periods (even if the right mechanisms have been identified) it cannot be concluded that the port will resonate.

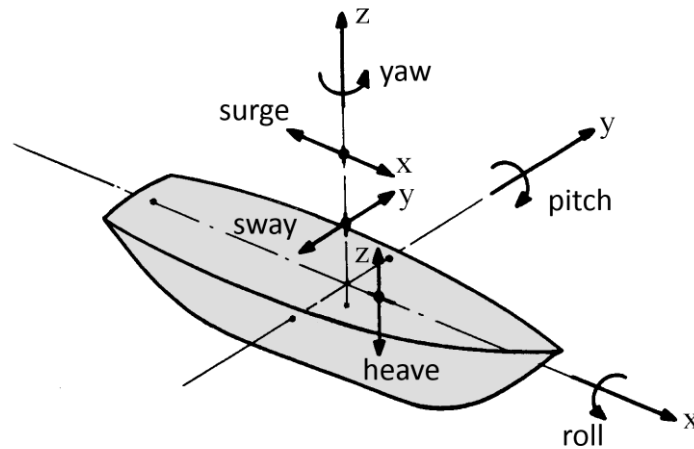
Table 5-1: Summary of free oscillating periods

Idealized Resonance Mechanism	Free Oscillating Period (s)				
	T ₀	T ₁	T ₂	T ₃	T ₄
Short closed basin – Longitudinal	-	110	55	37	28
Short open basin – Longitudinal	221	74	44	32	25
Short closed basin – Transverse	-	56	28	19	14
Long closed basin – Longitudinal	-	247	124	82	62

5.3. Typical Moored Vessel Motions

Vessels may move in six degrees of freedom as shown in Figure 5-6. The most critical in terms of (un)loading efficiency for container vessels is surge, this is partly due to the fact that container cranes cannot adapt to this motion (PIANC, 2012).

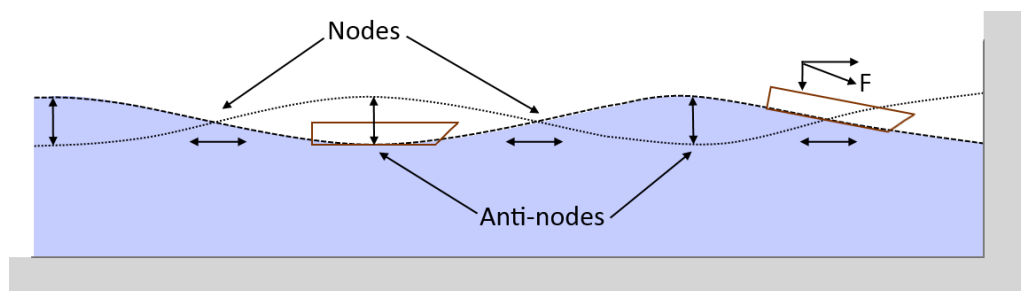
Figure 5-6: Definition of Ship Motions in Six Degrees of Freedom, modified from (Journée & Massie, 2001).



The vertical motions of moored vessels (heave, roll and pitch) have typical resonance periods of 10 to 15 seconds and are therefore most often induced by short waves at a berth (PIANC, 2012). Another mechanism driving vertical motions occurs when a vessel is moored on an anti-node of a standing wave as shown in Figure 5-7. The orbital velocities of a standing wave, at an anti-node, are vertical and hence the vessel will move vertically in a heave motion. The movements will be of a similar period to the standing wave which in ports is normally in the long wave period range; hence, there will be no resonance in the mooring system and the “slow” vertical movements are unlikely to create a problem.

On the other hand, horizontal moored vessel motions (surge, yaw and sway) typically resonate at higher periods with ranges from 30 s to 300 s depending on vessel type and mooring setup (PIANC, 2012), (Van der Molen, 2006) and (PAHRI, 1998). Surge motions may be strongly affected when a vessel is placed on a node, also shown in Figure 5-7. Nodes are characterized by horizontal orbital velocities and no change in the surface elevation. In addition to these horizontal currents the slope (angle) of the water surface may also induce surge motions. The resulting force on the mooring system, induced by the slope, may be described as $F = \sin(\text{angle}) \cdot \text{mass ship} \cdot \text{gravity}$.

Figure 5-7: Ship motions in standing waves.



The combination of vessel size and mooring system define the resonance periods of the moored vessel; in general a stiffer mooring system results in higher response frequencies (PIANC, 2012). Mitigation of vessel motions will often start by stiffening the mooring system in order to decrease the resonance periods below the long wave periods present in the port. Large vessels typically have a lower natural frequency compared to smaller vessels (PIANC, 2012); this often results in a small vessel being the critical vessel for mooring design.

PIANC, (2012) identifies surge as the critical criteria for large container vessel motions which are not exposed to broad-side waves, as shown Table 5-2. In the case of smaller container vessels each degree of motion should be checked criteria are given in Table 5-3.

Table 5-2: Maximum significant surge motion amplitudes for an (un)loading efficiency of 95%, for large container vessels (PIANC, 2012).

Container placing criterion	Basis for placing criterion	Maximum allowable significant surge motion amplitude ($T_{\text{surge}} = 30 \text{ s} - 100 \text{ s}$)
0.1 m	Twist-lock pins	0.2 m
0.2 m	Spreader flaps	0.4 m

Table 5-3: Maximum allowable significant motion amplitudes for an (un)loading efficiency of 95%, for smaller container vessels (PIANC, 2012).

Principal motion	Maximum allowable significant motion amplitude
Surge	0.2 m to 0.4 m
Sway	0.4 m
Heave	0.3 m
Roll	1.0°
Pitch	0.3°
Yaw	0.3°

5.4. Typical Environmental Conditions and Long Wave Type

Ligteringen & Moes, (2001) found from measurements that the long wave and short wave heights in front of the port of Ngqura (17 m water depth) were well correlated and well represented by the relationship represented in Equation 5-1.

$$H_{sl} = 0.08 \left(\frac{H_s T_p}{h} \right)^2$$

Equation 5-1

Where:

H_{sl} = long-period significant wave height (m)

H_s = short-period significant wave height (m)

T_p = peak period of the spectrum (s)

h = water depth (m)

The occurrence of the larger long waves will therefore occur with large swell, storms and their driving mechanisms. The occurrence of storms in the vicinity of the port and the relevant synoptic patterns driving the storms are shown in Figure 5-8; the port of Ngqura falls within the Agulhas bank area. Table 5-4 lists the typical synoptic patterns associated with sea storms in the area. A brief description of the relevant patterns follows.

Figure 5-8: Graphs showing the monthly frequencies of occurrence of weather types and sea storms in the different areas (MacHutchon, 2006).

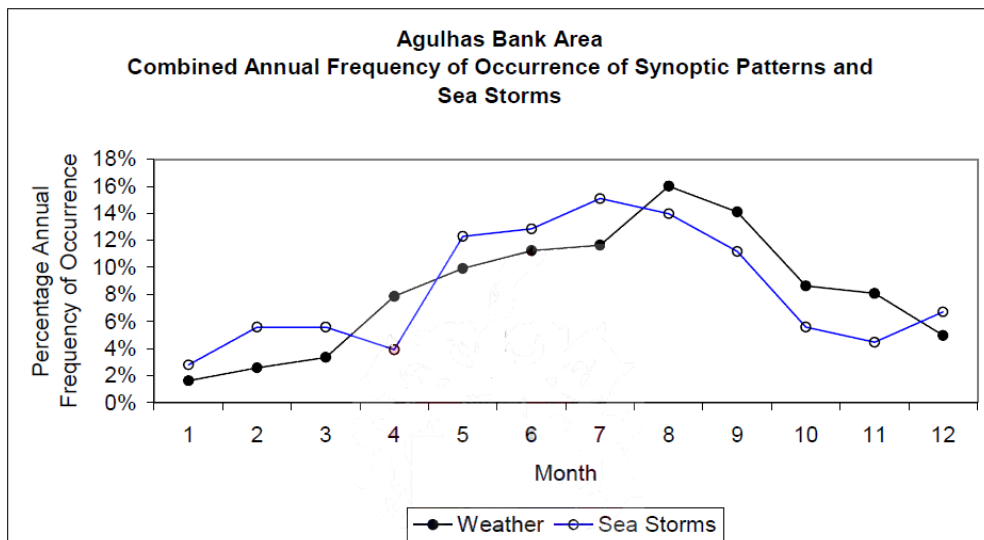


Table 5-4: Grouped Weather Types and Synoptic Patterns effecting sea storms around the South African Coastline (MacHutchon, 2006).

Part of South African Coastline	Type of Weather and/or Synoptic Patterns which could influence Sea Storms in the Area
Port Nolloth Area	Westerly Low (WL), Westerly Wave and Cold Snap (WW & CS) Cut Off Low (CoL)
Agulhas Bank Area, including the Cape Coast.	Continental High (CH) Westerly Wave and Cold Snap (WW & CS), Cut-off Low (CoL)
Durban Area	Westerly Wave and Cold Snap (WW & CS) Cut-off Lows (CoL), Easterly Wave (EW)

The continental high condition is characterized by large subtropical anti-cyclones centered over the sub-continent and surrounding sea areas. Continental highs over South Africa generally move north during the winter months allowing the southerly storm wave climate region to move closer to the South African shoreline (MacHutchon, 2006).

Westerly Atmospheric Waves, Rossby waves, describe the westward movement of ridges and troughs in the upper wind patterns circling the earth. They may occur independently or in conjunction with cold fronts, depressions and cut-off lows. MacHutchon generally refers to cold fronts when mentioning cold snaps in Table 5-4. Cold fronts are described as the leading edge of an advancing cold air mass. Generally with the passing of a cold front temperature and humidity drops, pressure rises and the wind direction shifts. Precipitation generally occurs at or behind the front (The Weather Channel, 2012). The passage of low pressure systems and their associated cold fronts are the main source of large waves on the South African coast line (Rossouw, 1989).

Cut-off lows are identified in South African synoptic charts as closed, cold-cored, low pressure systems occurring over the north eastern coastline. They are synonymous with heavy rainfall and floods (Ndarana & Waugh, 2010).

5.5. Conclusions and Summary

It is hypothesized that long waves enter the port of Ngqura and resonate in the vicinity of berths D100 and D101. The correlation of the periods of the resonating long waves and the resonance periods of the mooring systems leads to the vessel instabilities reported by port users and authorities. Specifically problematic vessel motions for container vessels are typically characterized by excessive surge motions and this is presumed to be the case for Ngqura. This is confirmed by the log of vessel instabilities (Section 6.3). Due to the protected position of berths D100 and D101, and the fact that only surge motions have been reported, it is hypothesized that only long waves excite the vessels.

Basic hydrodynamic theory shows that depending on the bathymetry and presence of the construction bund, standing waves are created that fall into the typical frequency range that excites moored vessels. The most likely mechanism creating vessel motions is the case where the bund is still present creating a "closed" basin. This results in resonance at 110 s along the length of the problem berths (Figure 5-1). The likelihood of the standing wave resonating along the length of the basin is high, as this would produce a node in the vicinity of the vessels which would amplify the surge (horizontal) motions.

Although there is evidence of free or trapped edge long waves passing the entrance of Ngqura (Shillington, 1984) these waves are generally of too high a period to affect moored vessels. It is hypothesized that the long wave energy that resonates in the port is a result of bound long wave

energy entering the port. This is based on Ligteringen & Moes (2001) who stated that there is a close relationship between the short and long wave height. It is expected that the long waves are entering the harbour via two predominant mechanisms:

- Freed bound waves released on the beach south of the port and long waves created due to the breaking process will reflect off the beach and further reflect off the main breakwater into the port.
- Diffraction of bound long waves around the north breakwater leading to a release of the bound long waves from the short wave groups.

The problem events are likely to occur during times of high swell (storms) when the short waves and hence bound long waves are larger. According to MacHutchon (2006) storms near Ngqura occur from May to September with the occurrence of the following synoptic patterns:

1. Continental high
2. Westerly Wave and Cold Snap
3. Cut-off low

The majority of the vessel motion complaints have occurred during this time as detailed in Section 6.3.

6. DATA DESCRIPTION

6.1. Introduction

This Chapter includes a description of the data available for this study; the subsequent analysis of the data is included in the following Chapter 7.

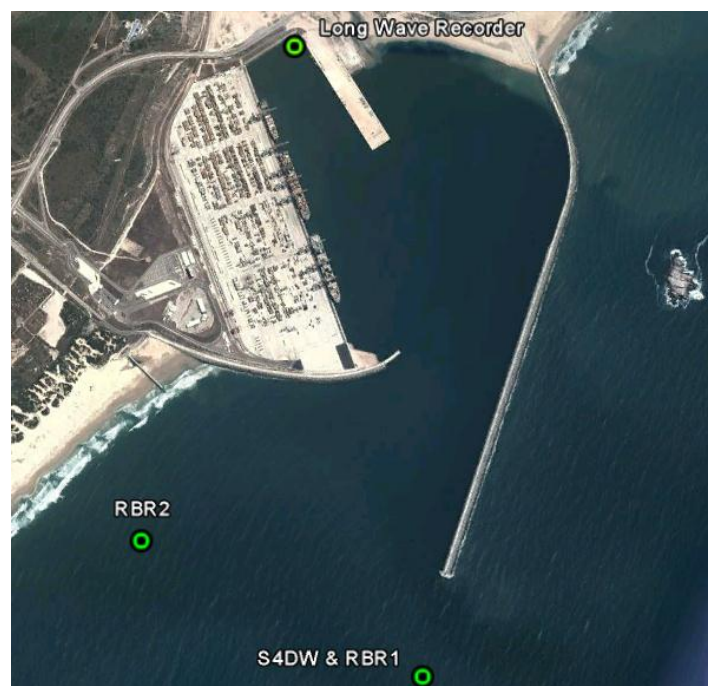
6.2. Wave Data

A large amount of historical wave data was available for this study, the majority of which had already been analysed and reported on (PRDW, 2005). Some of this historical data has been reanalyzed in the subsequent sections. In addition, more recent wave measurement records were available which included simultaneous measurements from outside and inside the port; a detailed analysis was performed, as part of this thesis, on this data to gain insight into the effect of the port on long wave energy. The data sets are described below:

6.2.1. Historic S4DW Data

The historic S4DW data set was collected over a period of approximately 12 years from the 14th Nov 1997 until the 23rd July 2008. The data measurement campaign was initiated to inform design parameters for the port of Ngqura. The data has been well documented, analysed and reported on. A series of six internal PRDW reports covers the first 82 deployments of the total 116 deployments (PRDW, 2005).

Figure 6-1: Location of wave measurement devices (Google Earth, 2013).



A S4DW p-u-v (pressure and current velocity vectors u , v) directional wave-current meter (Model S4DW of InterOcean Systems of San Diego USA) was used in dual mode in order to record both long and short waves simultaneously. Short and long waves were defined in periods between 5 s to 30 s and 30 s and 600 s respectively. The S4DW was installed near the entrance of the port of Ngqura, 1.7 m above the seabed in a depth of ~ 16.5 m below chart datum as shown in Figure 6-1.

Table 6-1 below shows a summary of the deployments, recording frequency, record length and sampling periods. Long waves were recorded for a sampling time (also known as record length and burst length) of 1 hour and 26 minutes, which allows for an adequate duration in which to gain sufficient accuracy in the statistics for resolving long waves below ~ 100 s (see Section 4.4.1.). The sampling time for this record thus has limitations in accuracy when considering longer waves than 100 s. Another limitation of the short sampling time was apparent when attempting to use the surface elevation time series for input to the Boussinesq model (Chapter 8). As the model takes time to warm up it was impossible to get adequate statistical convergence for the long waves of interest.

Table 6-1: Summary of Recording Frequency, Record Length and Sampling Periods (PRDW, 2005).

Deployment	1 to 12	13 to 21	22 to 56	57 to 82
Short wave data				
Frequency of measurements	3 hours	2 hours	3 hours	2 hours
Sampling time	18 min	36 min	18 min	1 hour 26 min
Samples averaged	1	1	1	1
Sampling frequency	2 Hz (0.5s)	2 Hz (0.5s)	2 Hz (0.5s)	2 Hz (0.5s)
No. sample points	2160	4320	2160	10320
Long wave data				
Frequency of measurements	3 hours	No data recorded	3 hours	2 hours
Sampling time	1 hr 26 min		1 hr 26 min	1 hour 26 min
Samples averaged	10		10	1 *
Sampling frequency	0.2 Hz (5s)		0.2 Hz (5s)	2 Hz (0.5s)
No. sample points	1032		1032	10320

For long wave measurements the S4DW was set to record long waves at a frequency of 0.2 Hz or $\Delta t = 5$ s; this corresponds to aliasing for waves with a period up to 10 seconds (see Section 4.4.3). This did initially raise concern that the S4DW long wave measurements may have false energy in the lower period range; however, upon inspection of the spectra there is little to no energy between 30 s to 40 s (see Figure 7-10). The measurements were therefore deemed acceptable because of the absence of low period energy in the spectra and because the long waves of interest were processed by cutting-off wave energy under 30 seconds.

6.2.2. Recent S4DW Data

The recent S4DW data measurements cover a period of two months, July and September of 2011. The measurements were performed on a similar instrument to the S4DW mentioned above. Additionally, the instrument was placed in the same position and set up in an identical manner to the

instrument mentioned in Section 6.2.1 above. Thus the same limitations were apparent as with the historic S4DW data; however, this data set was measured simultaneously with long wave measurements inside the port.

6.2.3. RBR 1 and RBR 2 Data

Two RBR submersible wave recorders provided pressure measurements from the 23rd July 2012 until the 4th of August 2012. Both instruments measured for 4.5 hour bursts at a sampling interval of 2 Hz. RBR 1 was deployed in the same position as the S4DW instrument in a depth of approximately 18 m, 0.6 m above the seabed. RBR 2 was positioned closer to shore in a depth of 14 m, 0.6 m above the seabed. The positions of each of the instruments are shown in Figure 6-1. This data set was measured simultaneously with long wave measurements inside the port.

6.2.4. Long Wave Recorder Data

The long wave recorder data set includes continuous water level measurements that were measured at the same time as the RBR instruments and the recent S4DW measurements detailed in Section 6.2.2 and 6.2.3 above. A LOG_aLevel ultrasound instrument from General Acoustics was used. The instrument is mounted on the quay wall and measures the water level by ultrasound methods from a position above the water. Water level was measured at 3 second intervals continuously at a position in the port as shown in Figure 6-1 (Long Wave Recorder).

6.3. Log of Vessel Instabilities

Table 6-2 shows a compilation of reported vessel instabilities. Although the log is not comprehensive, it does highlight some of the extreme events, and the fact that there are frequently loading difficulties on the quay side.

Table 6-2: Log of vessel instabilities – partial coverage from 2010 to 2012.

Date	Time - Vessel Instability	Berth	Vessel Name & Description	Description	Mooring arrangement	Reported Conditions	Port layout
08 August 2012	-	D100	MSC Natalia	Broke mooring line.	Not available	Long waves measured outside port. Over 0.3m.	No berm
02 August 2011	At night	D berths	MSC Adriatic	Disruption of loading.	Not available	-	Partial Berm present
01 August 2011	-	D berths	-	Excessive vessel motion, no line breaking but difficult conditions to load. Main movement was surge of up about 1 m and at times there were other vertical and horizontal movements as well.	Mooring arrangement was reasonable but with polyprop lines	-	Partial Berm present
07 July 2011	At night	D berths	MSC Zambia	Experienced surge in a 5 knt wind, Port claims fender damage.	A 5+3 configuration both ends. Out of the 5 stern lines, 3 were new, 1 brand new, and 1 with about 50% life. 4 lines had a good lead of 50m aft and 1 with a short lead of 20m. 3 spring lines had a lead of 30m ford. The layout on the bow was the same pattern. polypropylene lines	Long waves measured in port 110s to 230s range. above 25cm, Little wind.	Partial Berm present
07 July 2011	General complaint	D berths	General complaint	Excessive vessel motion.	Not available	-	Partial Berm present
23 April 2010	From 10h00 on 23rd to 15h00 24th	D101	Mol Destiny (LOA 260 m, GRT 39 906)	Broke 6 lines.	Not available	Hs over 3m, Tp over 12s	Berm present
23 April 2010	01h00 to 15h00	D100	MSC Mariner (LOA 304m GRT 73 819)	Broke 6 lines aft (stern lines and aft springs) and 2 fwd springs whilst working on berth. During unberthing, snapped 1 spring. Berhard Murphy estimated a surge of about 8 m at time of sailing.	FWD 4 headlines, 1 breast line 7 3 springs Aft 4 sternlines, 2 breast lines & 3 springs	Hs over 3m, Tp over 12s	Berm present

The most extreme event occurred on 23 April 2010; during the event two vessels, the MOL Destiny and MSC Marina, snapped 6 and 9 mooring lines respectively. A workshop was held where the event was detailed and discussed between Port Authorities and Consultants; the event was attributed to the presence of long waves, the temporary revetment bund, and the mooring setup. The temporary bund was attributed with exacerbating the effect of the long waves in the vicinity of the berths. The mooring line characteristics were identified as “soft”. Due to the cramped berthing space, the angles of the mooring lines were also acute, and these factors led to higher mooring line stress. One of the engineering consultants, PRDW, summarized the event in two drawings; these are included in Appendix A with extracts shown in Figure 6-2 and Figure 6-3.

Figure 6-2 shows the close vicinity of the two relatively large vessels which lead to the cramped mooring line setup.

Figure 6-2: Mooring Layout - Instability event on the 23 April 2010 (PRDW, 2010a).

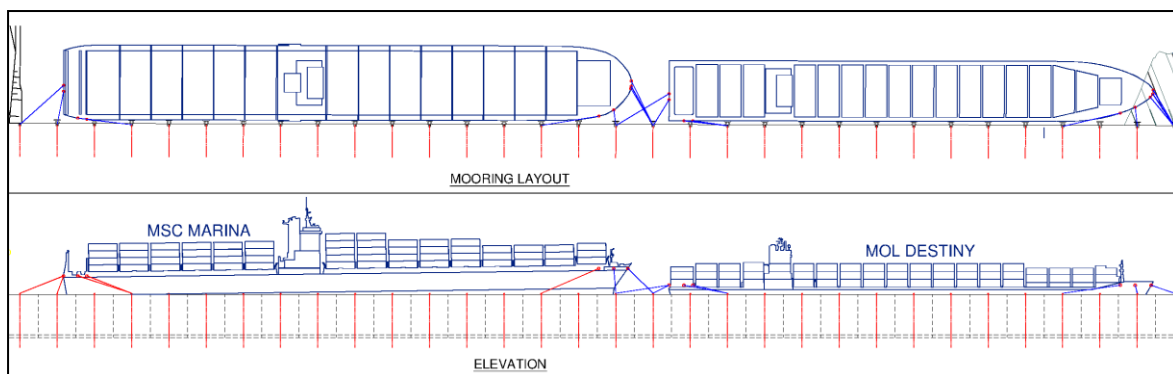
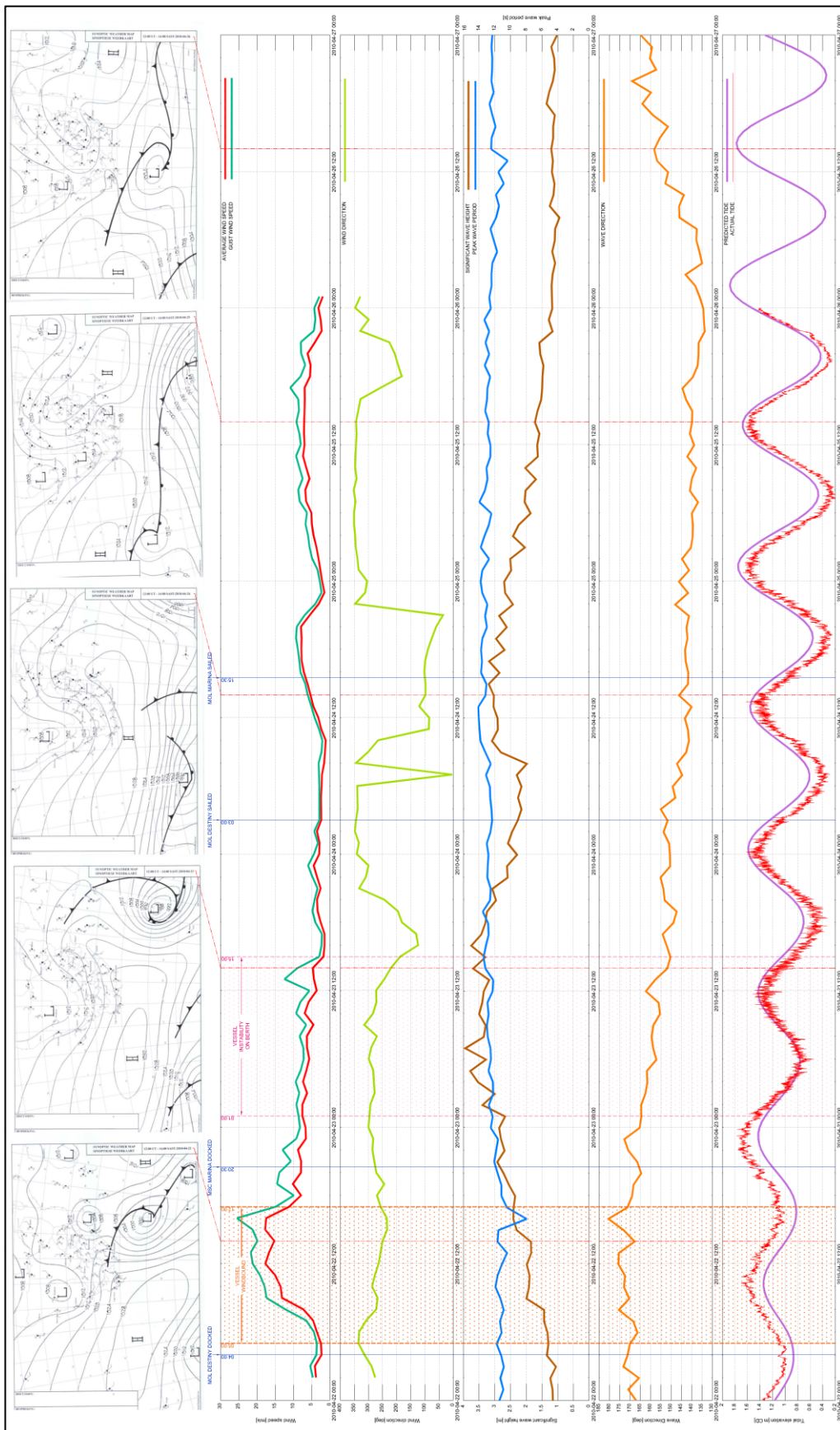


Figure 6-3 provides a summary of the environmental conditions during the event. The second red highlight from the left shows the time when the vessels were experiencing mooring line failure. The MOL Destiny and MSC Marina were docked on the 22nd of April at 04:00 and 20:30 hours respectively. Interestingly the instabilities only started to occur once the low pressure system had passed over the port and the wind speeds and storm surge had dissipated. The event seems to have occurred when the short wave peak period was at its highest over 12 s and the significant wave height was over 3 m.

Figure 6-3: Environmental Data - Instability event on the 23 April 2010 (PRDW, 2010b).



7. DATA ANALYSIS

7.1. Introduction

Several years of the historical S4DW data was analysed during design studies for the port of Ngqura. This analysis is trusted and covers a long data set making it statistically reliable. Nonetheless the historical data has been reanalysed in this section for the specific purposes of this study.

New data that includes simultaneous measurements both outside and inside the port has been used for validating the Boussinesq model and for quantifying the correlation of energy outside and inside the port. The analysis of the new data also allowed for a cursory but sufficient check of the historic data analysis.

7.2. Outside the Port

7.2.1. Short Waves

Figure 7-1: Wave height rose at port entrance, approximately 5 years data (1-hourly data).

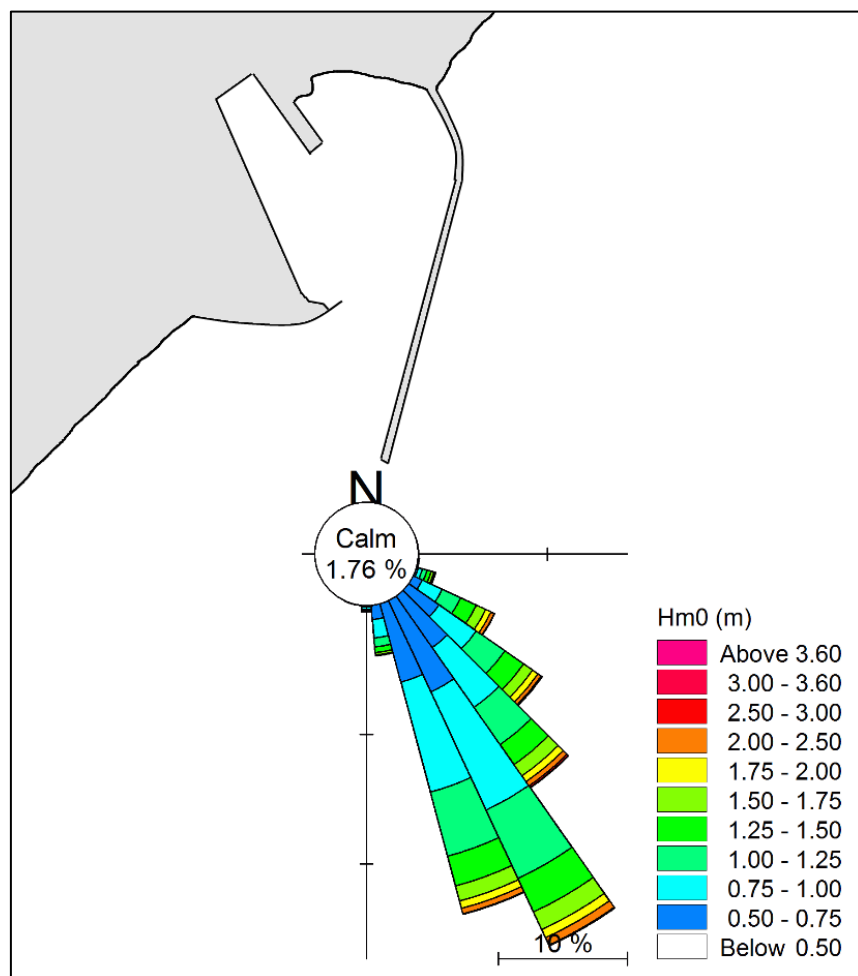
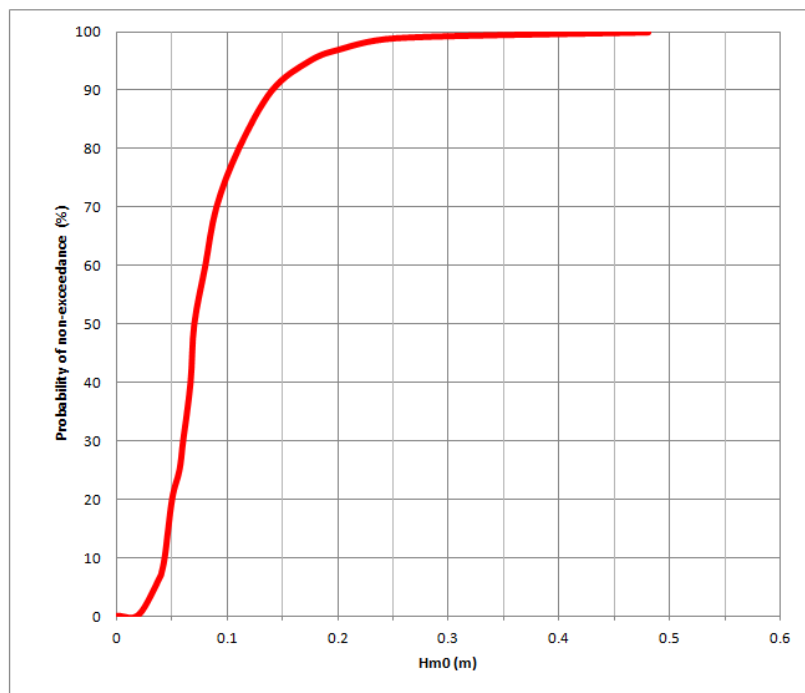


Figure 7-1 shows a short wave height rose in front of the port. The dominant wave direction is identified as approximately 150° with significant wave heights approaching 4 m. The waves are confined to the south-east sector as the port is positioned within a bay and protected from the typical swells propagating from the south west directions. The south westerly swell thus has to diffract around the headland south-west of the port. The figure was produced from a subset of the historic S4DW data detailed in Section 6.2.1. The data covers a period from November 1997 to April 2004, however due to gaps in the data the coverage is 5 years.

7.2.2. Long Waves

Figure 7-2 shows the non-exceedance of significant long wave heights outside the port of Ngqura. The figure shows that 10% of the time the significant long wave height is larger than 0.14 m. The data set presented in the figure is described in Section 7.2.1.

Figure 7-2: Non-exceedance of significant long wave height, approximately 5 years data (1-hourly data).



Probability of non-exceedance (%)	H _{m0} (m)
0	0
30	0.06
60	0.08
90	0.14
97	0.20
99	0.25
100	0.48

Figure 7-3 shows the correlation of significant long wave heights with short wave heights. The gradient of the linear trend line fitted to the data is 0.082 showing that on average the significant long wave height is 8% of the significant short wave height. The data scatter fits well between the 0.15 and 0.5 gradient lines giving a good indication of the extremities of the correlation i.e. the correlation of short to long wave height is most often between 5% and 15%. Figure 7-3 is based on the historic S4DW data set described in Section 7.2.1.

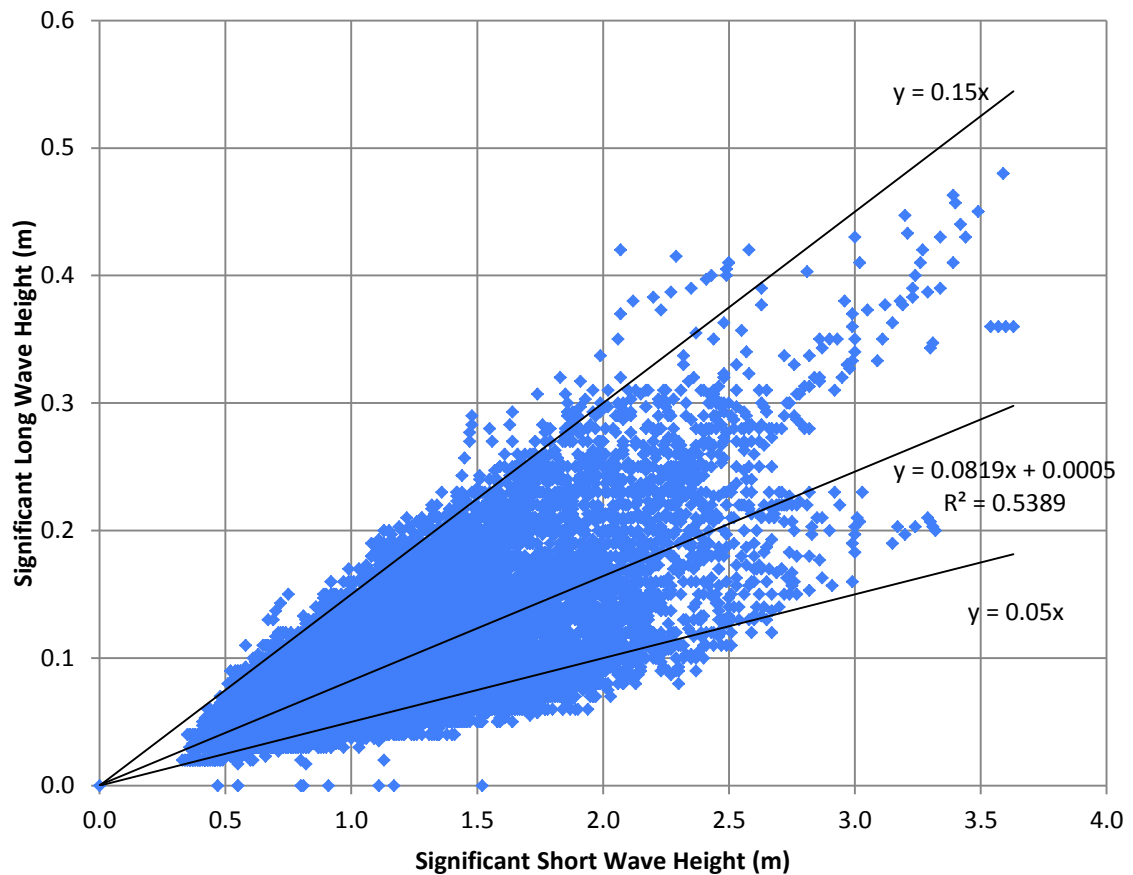
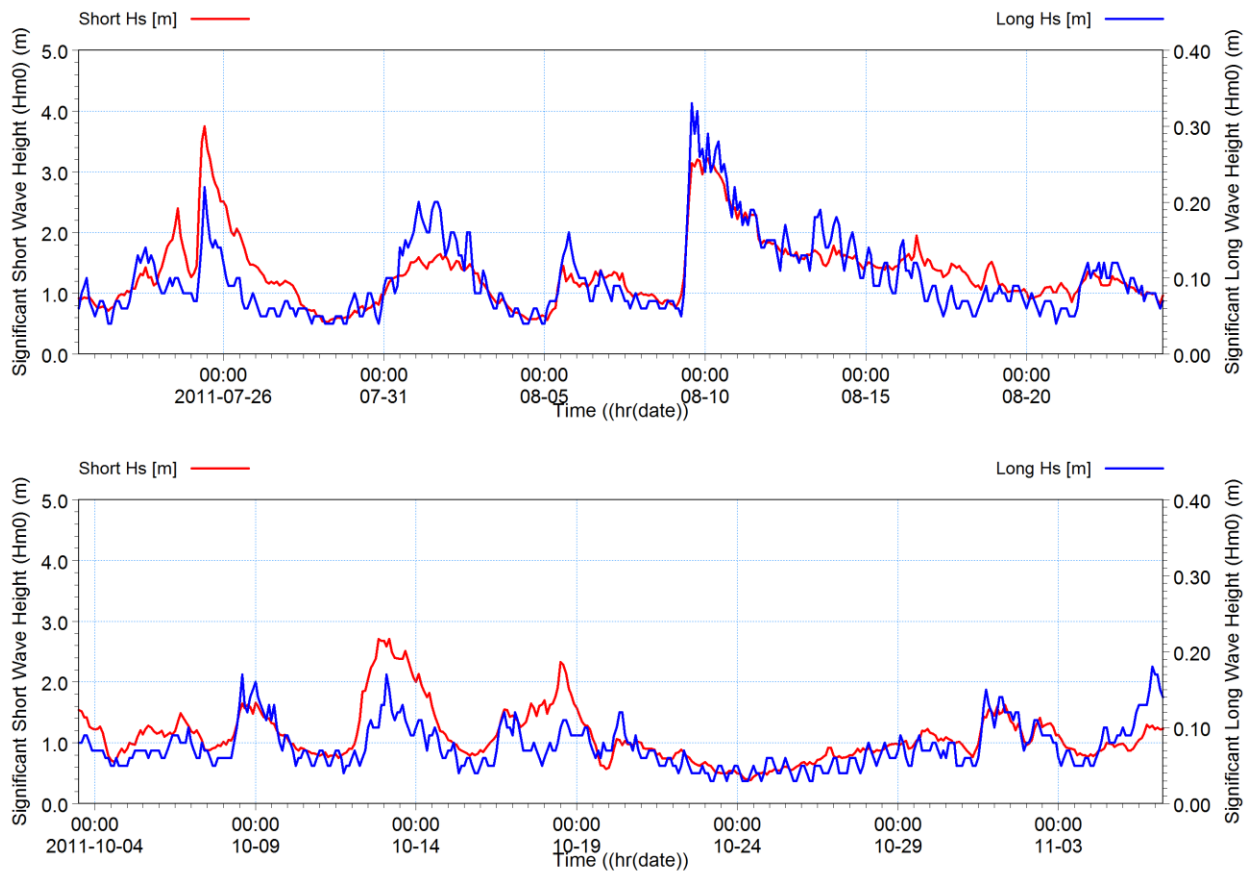
Figure 7-3: Correlation of long wave with short wave heights.

Figure 7-4 shows the correlation of significant long wave height to short wave height in time series format. The long wave and short wave curves are from the recent S4DW data set and are measured by the same instrument. The axis of the long wave height data series, shown on the right hand side, is 8% of the short wave axis; this ratio is based on the correlation figure above (Figure 7-3). The obvious trend is the correlation of the short and long wave heights; the two series match each other closely over the entire duration. This type of figure was presented for the historic S4DW data in the Ngqura Port Coastal Processes report (PRDW, 2001) with very similar trends.

An important observation concluded from Figure 7-3 and Figure 7-4 is that all the long wave energy corresponds to the short wave energy; hence it is concluded that the long wave energy at the port of Ngqura is predominantly generated from short waves, either through set down or nearshore breaking processes. Furthermore, on average, based purely on wave height correlation, the significant long wave heights appear to be 8% of the significant short wave heights.

Figure 7-4: Comparison of Short and Long period significant wave heights. Long period axis is correlated to short wave height by 8%. Short and Long period measurements are from the S4DW instrument outside the port.



7.3. Measurement Correlations between the Outside and Inside of Port

7.3.1. Available Data

Three simultaneous data sets have been used in the data correlations detailed in the sections below; the data sets are described below:

- RBR1 & RBR2 vs. LWrec – 2012-07-23 to 2012-07-31 (8 days)
- S4DWdep1 (co2dep1) vs. LWrec - 2011-07-27 to 2011-08-24 (28 days)
- S4DWdep2 (co2dep2) vs. LWrec - 2011-10-03 to 2011-11-06 (34 days)

All the internal port measurements were performed with the Long Wave recorder (LWrec) opposite berth D100. All the external port measurements were performed in the same position (400m off the main breakwater); however two sets of the data were recorded on the S4DW device as detailed in Section 6.2.2. The other data sets were recorded on the RBR instruments detailed in 6.2.3. The data sets described above were the only simultaneous data sets available at the time of study.

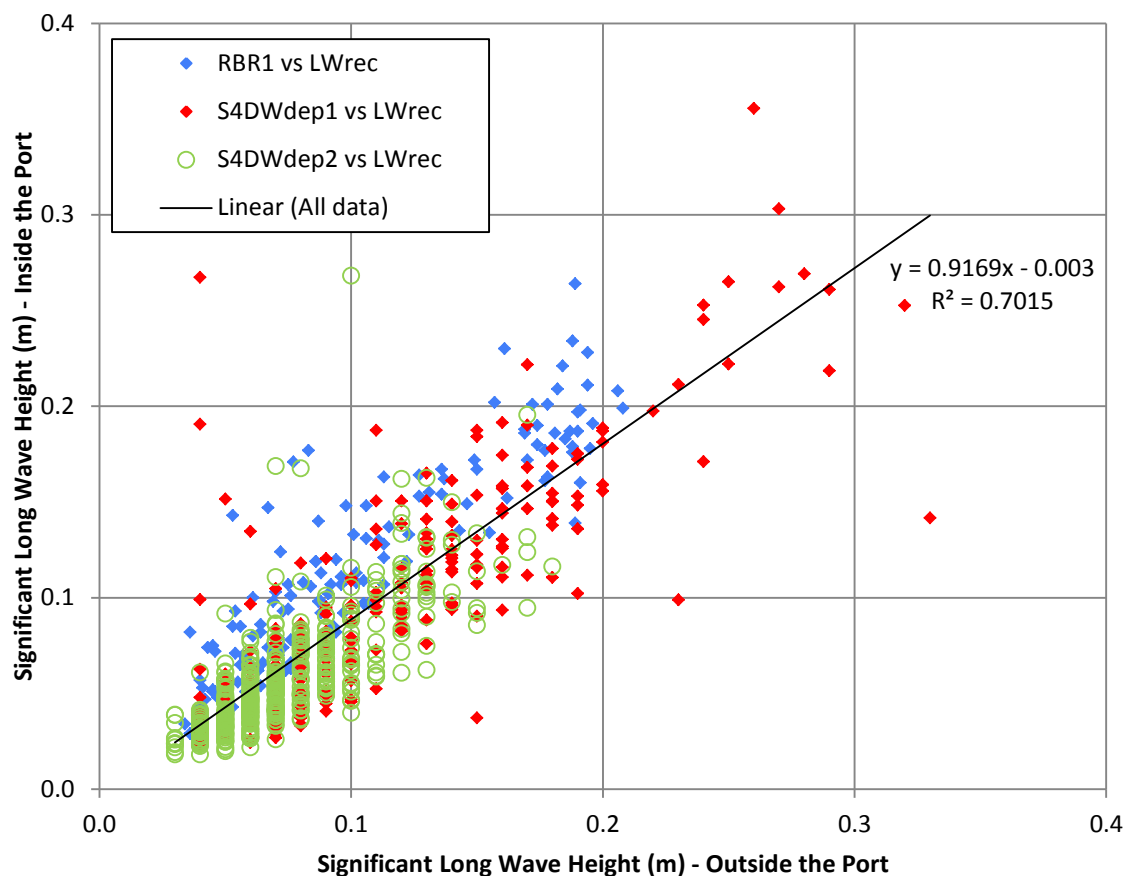
7.3.2. Long Wave Height Comparisons (Inside vs. Outside)

Figure 7-5 shows the correlation of significant long wave height measurements between the outside and inside of the port. All three simultaneous data sets as mentioned above were used.

The plot (Figure 7-5) shows a linear trend between the significant long wave heights outside and inside of the port. The linear trendline fitted to the data has an R^2 value of 0.7 showing the line has a fairly good fit to the data. The equation of the line shows that on average the significant long wave height outside the port is reduced by only 10% once it reaches the inside of the port. In other terms the average long wave agitation coefficient for the port of Ngqura is 0.9. In comparison the short wave agitation coefficient for Ngqura is approximately 0.15.

The significant difference between the ability of the port to reduce long wave energy and short wave energy highlights the difficulty in port design in reducing long wave penetration.

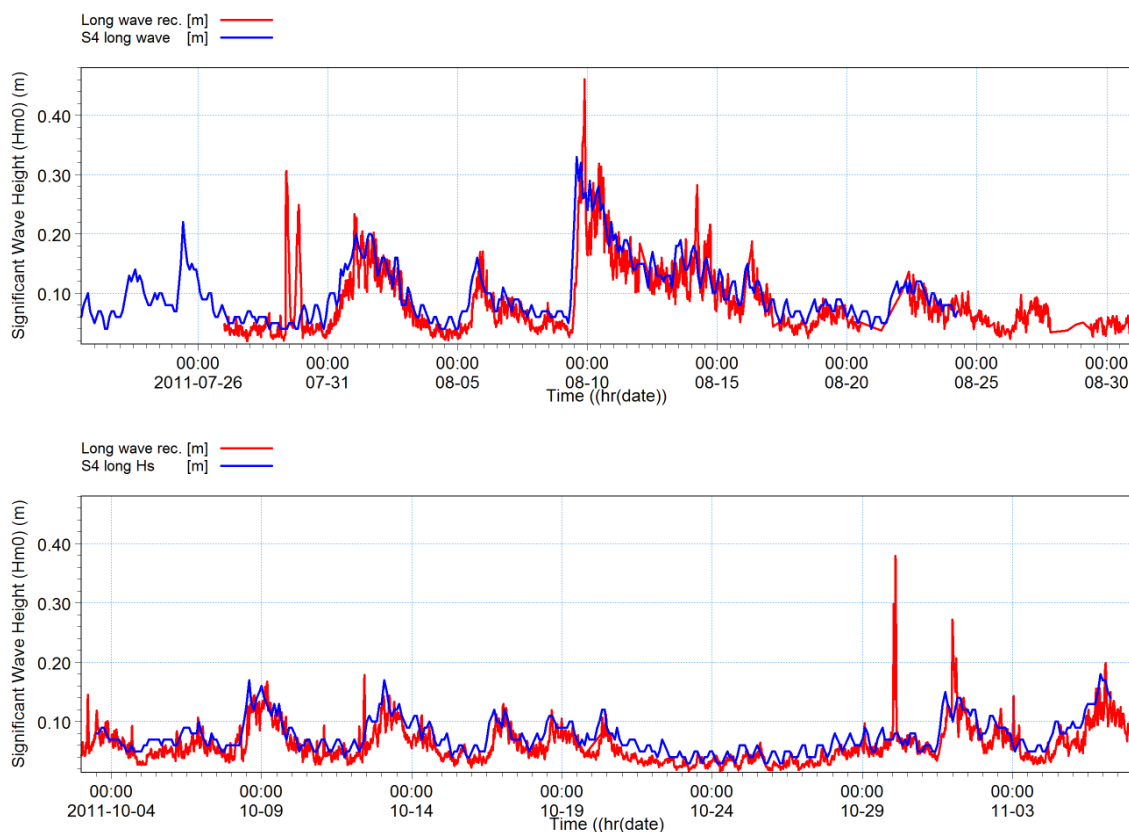
Figure 7-5: Correlation of significant long wave heights between the outside and inside of the port. Data consists of three separate data sets.



7.3.3. Direct Time-series Comparison

Figure 7-6 shows a direct time series comparison between the significant long wave height outside and inside the port. The data is sourced from the 2nd and 3rd data set as listed above. The figure shows a remarkable correlation in significant long wave height between the outside and inside of the port. This result was expected due to the 90% correlation found in Figure 7-5 above. The presence of apparent spikes are visible in the long wave recorder data (red) because the spikes consist of multiple data points they were not removed the data set.

Figure 7-6: Comparison of significant long wave heights (m) between the S4DW instrument (blue) and the Long Wave recorder (red). S4DW was stationed outside breakwater, Long Wave recorder inside the harbour basin.



7.3.3.1. Tidal Modulation of Long Waves

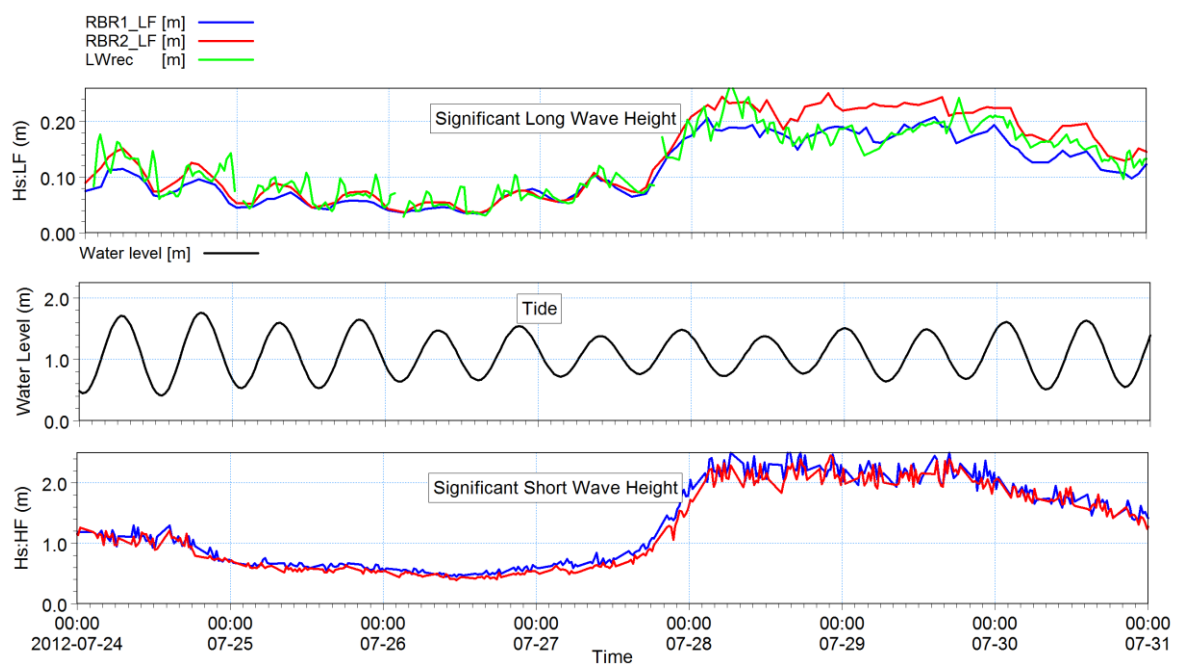
Figure 7-7 shows another direct comparison of significant long wave heights between the inside and outside of the port. Three instruments; the two RBR instruments (detailed in Section 6.1.4) positioned outside the port and the Long Wave recorder (Section 6.1.3) inside the port provided the data. As with Figure 7-6 above, the long wave heights between the outside and inside of the port track each other closely. Additionally, the significant long wave height is amplified once it gets closer to shore; this is evident when comparing the wave heights between the two RBR instruments. RBR 2 is closer to shore and almost always higher than the RBR 1 wave heights.

Figure 7-7 also shows a variation of the significant long wave heights that correlates with the tide (compare undulations between upper pane and middle pane), otherwise known as tidal modulation. Thomson (2006) studied a similar modulation of the long wave heights on the southern Californian shelf. Thomson explains the process as follows:

Observations and numerical model simulations of ocean surface-gravity waves between 15-m water depth and the shoreline show that in the surfzone nonlinear wave-wave interactions transfer energy from low-frequency (infragravity), long waves to higher frequency motions. The energy transfer is enhanced over the relatively flatter inner-surfzone bottom profile at low tide, explaining the tidal modulation of infragravity energy observed in bottom-pressure records on the southern California continental shelf. Similar tidal changes in beach profiles are common worldwide and thus tidal modulation of infragravity energy in the surfzone may affect nearshore processes and regional seismic activity in many areas.

Although profiles of the Ngqura beach are not available to check the theory stated above, it is assumed because of the wave height undulations that this is the cause of the tidal modulation. An implication of the tidal modulation in the measurements both outside and inside the port is that the measurements include a component of reflected wave energy and that some of the long wave energy inside the port has originated from the reflected energy off the beach south of the port. It should be noted that the tidal modulation observed in Figure 7-7 was also observed in the other data sets.

Figure 7-7: Comparison of significant long and short wave heights, including effect of tidal modulation. RBR1 instrument (blue), RBR2 instrument (red) and the Long Wave recorder (green). RBR instruments were stationed outside the port, Long Wave recorder inside the harbour basin.



7.4. Direct Spectral Analysis Comparisons

7.4.1. Individual Event Comparisons

Figure 7-5 above shows that the significant long wave height is on average only reduced by 10% when entering the port.

Figure 7-8 and Figure 7-9 below show in more detail how the long wave energy responds once entering the port. In particular, by comparing the spectra from inside and outside the port it is possible to see how energy may be amplified at specific frequencies once entering the port. It is the resonance at frequencies corresponding to the natural frequencies of the moored vessels that is typically more critical for vessel motion than just the significant long wave height. Figure 7-8 and Figure 7-9 show direct spectral comparisons for two selected events from two data sets which contain simultaneous measurements for the inside and outside of the port. The conversion of the raw data pressure measurements is reported in more detail in Section 8.3.2.

The 2011/08/09 event was captured outside the port by the S4DW instrument and inside by the Long Wave recorder. The 2012/07/28 event was captured outside the port by the RBR1 and RBR2 instruments and inside by the Long Wave Recorder. The two event parameters are given in Table 7-1.

Table 7-1: Individual event parameters.

Event Date & Time	Hm0:HF (m)	Hm0:LF (m)	Tp:HF (s)	Wave record length (min)
2011/08/09 18h00	3.2	0.29	12	86
2012/07/28 08h30	2.2	0.18	12	270

For both events the data from the Long Wave Recorder and the instrument outside the port, although covering the same time span, was captured at a different sampling rate. Hence, during the spectral analysis it was impossible to repeat the same size spectral analysis and degrees of freedom for the outside and inside data. Instead, where possible, the same degrees of freedom for the comparable spectral analysis were used. Again this was not always possible and hence the closest match that could be attained was used. Furthermore, the wave record length differed between the two events as the instrument outside the port differed and hence limited the available record length for the spectral analysis.

Figure 7-8 shows the LWrec spectrum calculated with 10 degrees of freedom compared with the S4DW spectrum with 8 degrees of freedom. Where the S4DW spectrum outside the port looks fairly

uniform with no significant spikes the internal spectrum shows that significant amplification of energy occurs at approximately 260 s and 160 s.

Figure 7-8: Direct spectral analysis comparison between outside and inside of port – 2011/08/09 18h00 event.

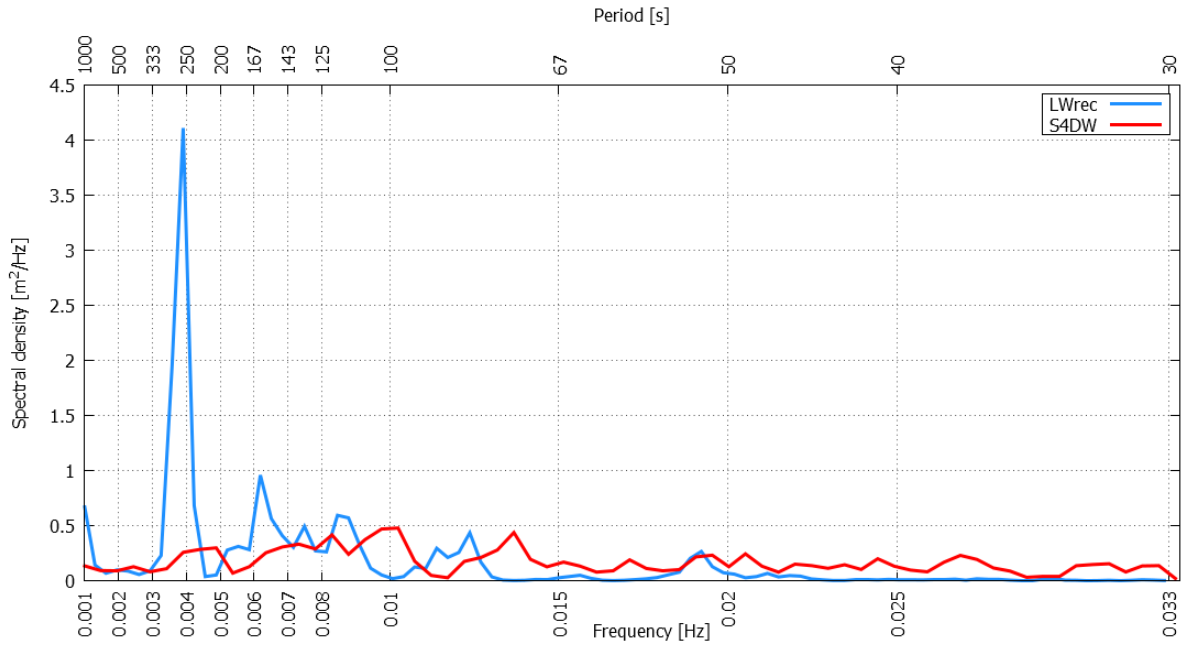


Figure 7-9: Direct spectral analysis comparison between outside and inside of port – 2012/07/28 08h30 event.

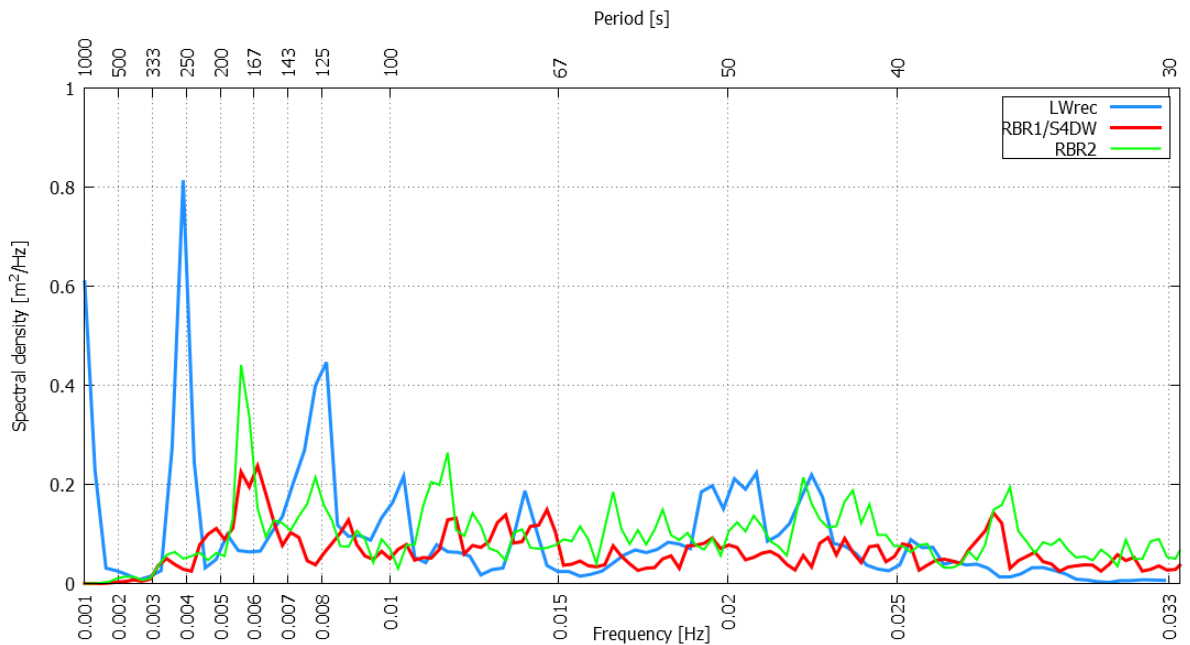


Figure 7-9 shows the LWrec spectrum calculated with 26 degrees of freedom compared with the RBR spectra which were both calculated with 18 degrees of freedom. The RBR1 spectrum which is in the same position as the S4DW outside the port is fairly flat with a slight spike of energy between 150 s

and 180 s. The RBR2 spectrum, positioned closer to the beach, has a similar spike and 2 more energy spikes at 130 s and 85 s. The LWrec spectrum is similar to the 2011 spectrum although of a different magnitude due to the higher energy in the 2011 event (note the difference in y-axis magnitude).

7.4.2. Temporal Spectral Variation

To gain more insight and increase confidence in the direct spectral analyses performed above, temporal spectrograms were plotted. A temporal spectrogram essentially adds a third axis to the standard 2D spectra as shown above, a time axis. The temporal spectrogram therefore shows how the sea state, in spectral form, develops over the duration of an event rather than the spectrum at just the peak of an event.

As a temporal spectrogram typically includes dozens of individual spectra and the associated raw data processing, the process should be automated. In this case, the process was automated using programmes written in the Python language for the data management and processing. The actual spectral analyses were performed, in batch mode, using the Mike Zero WS linear spectral analysis tool by DHI.

Figure 7-10 and Figure 7-11 show 3D temporal spectrograms over the duration of the 2011 event from 2011/08/08 to 2012/08/18. By comparing the spectrograms, the effect of the port on long wave energy is evident. In Figure 7-10, showing the long wave spectra outside the port, the long wave spectra over the entire event duration are fairly flat without prominent peaks at any specific periods. By comparison, in Figure 7-11, which shows the long wave spectra inside the port, there are clearly defined peaks of spectral density in certain period bands. Note that the spectral density and time axis are the same scale and are therefore directly comparable, however, the period axes differ.

Figure 7-12 and Figure 7-13 show 2D versions of Figure 7-10 and Figure 7-11, the 2D plots allow for more accurate identification of the peak periods. Figure 7-13 shows peaks of spectral density, inside the port, at the following periods: 45 s to 55 s, 59 s to 70 s, 75 s to 90 s, 100 s to 160 s, 250 s to 260 s, 1000 s¹. Although these peaks are related to only one event, because the spectra outside the port are fairly uniform it is fair to hypothesise that the periods identified coincide with the characteristic resonance periods of the port. Essentially, it can be said that these peaks of spectral density are a result of long wave resonance in the port due to the geometric shape of the port.

¹ It is noted that the wave record length is not of sufficient length to accurately define the 1000 s resonance period (see Section 4.4.1) however subsequent white noise simulations in Chapter 9 identified the Helmholtz frequency of the port at ~820 s thus it has been included here.

Figure 7-10: 3D Temporal spectrogram (spectral energy-frequency-time) variation, long wave periods only – (2011/08/08 to 2011/08/18). Measured outside the port with the S4DW.

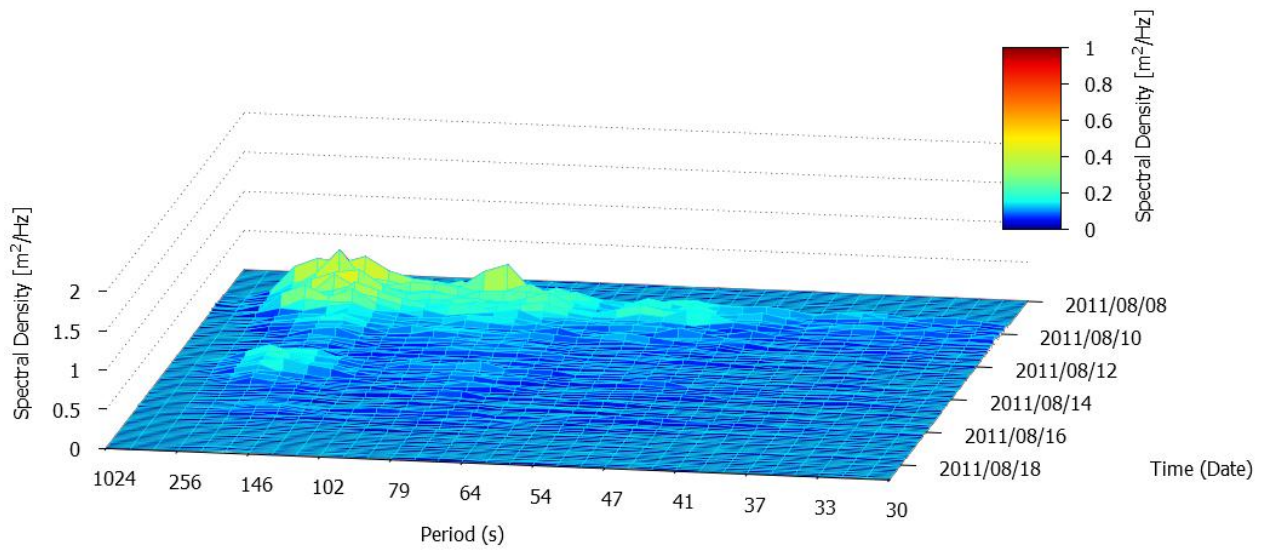


Figure 7-11: 3D Temporal spectrogram (spectral energy-frequency-time) variation, long wave periods only – (2011/08/08 to 2011/08/18). Measured inside the port with the LWrec.

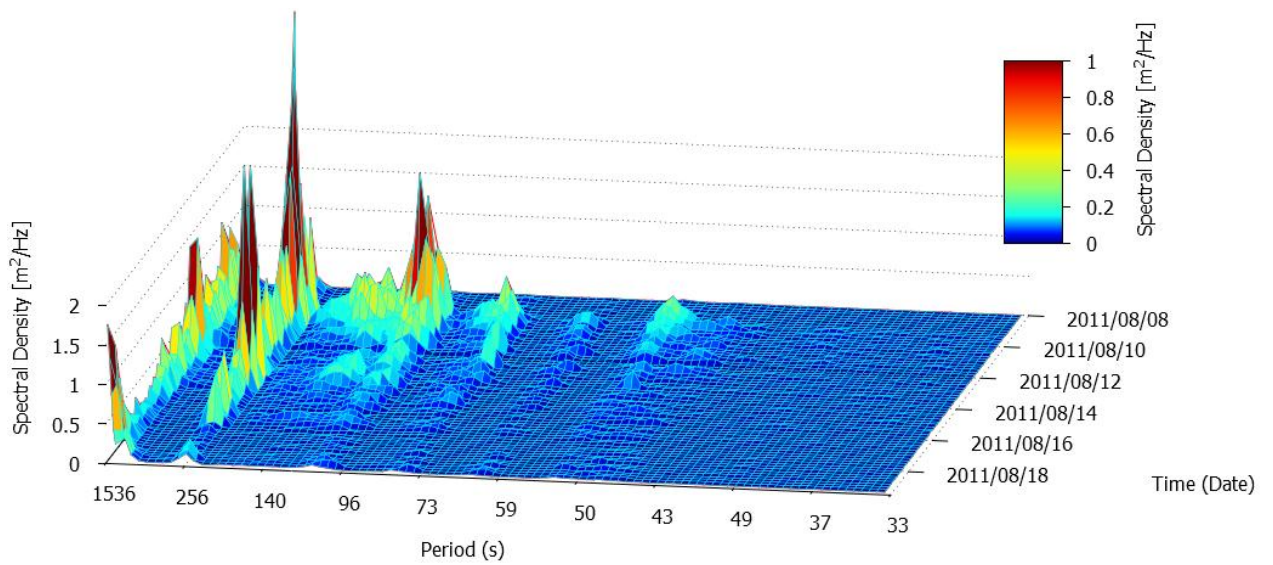


Figure 7-12: 2D Temporal spectrogram (spectral energy-frequency-time) variation, long wave periods only – (2011/08/08 to 2011/08/18). Measured outside the port with the S4DW.

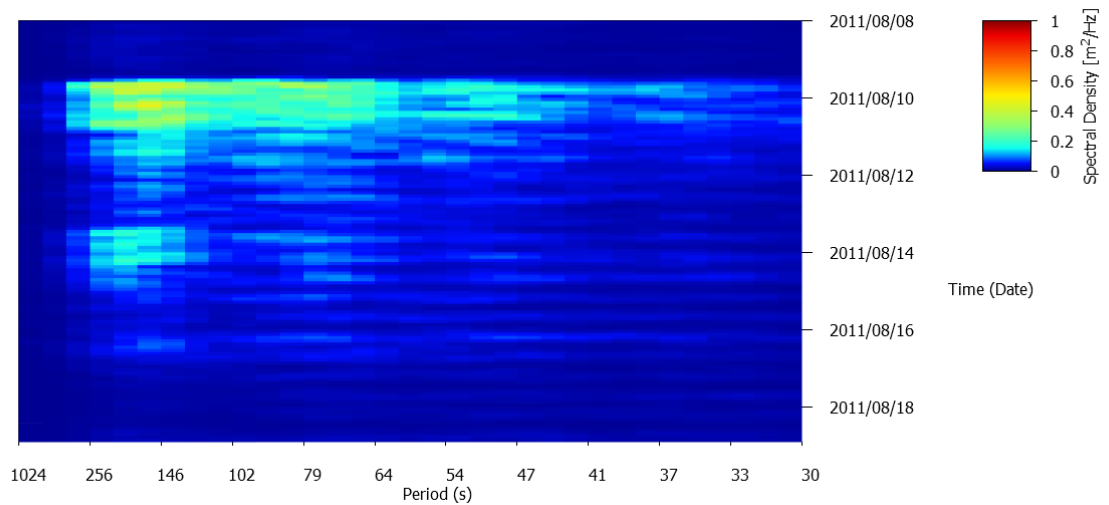


Figure 7-13: 2D Temporal spectrogram (spectral energy-frequency-time) variation, long wave periods only – (2011/08/08 to 2011/08/18). Measured inside the port with the LWrec.

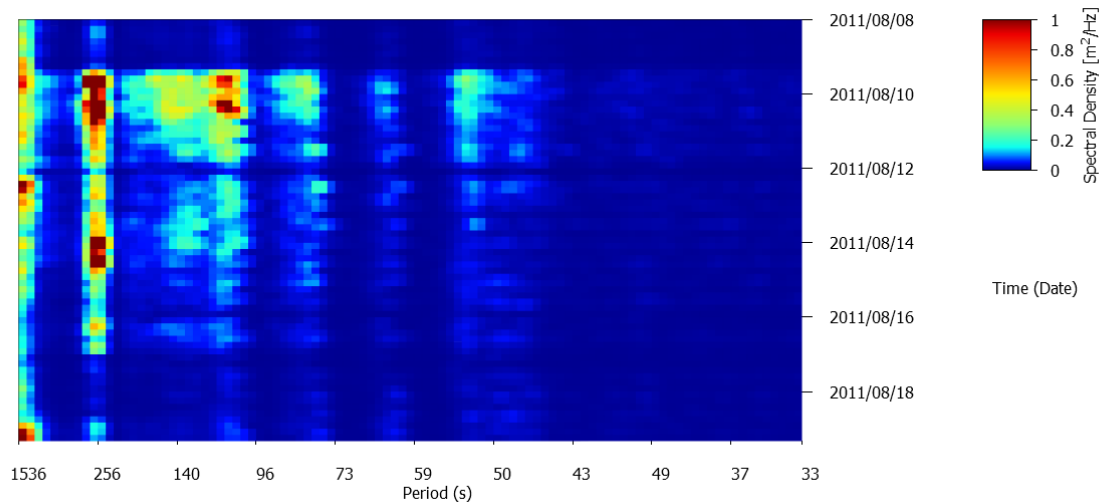


Figure 7-14 to Figure 7-17 represent the 2012 event in similar 3D and 2D spectrograms to the way in which it was used for to the 2011 event figures above. A similar trend is shown between the spectrograms inside and outside the port, namely fairly uniform energy is evident outside the port while inside the port certain period intervals are amplified through resonance. Another important similarity between the two events is that the same period intervals are excited inside the port. Although the 2012 event was smaller, all but the weakest (59 s to 70 s) resonance interval periods identified in the 2011 event are present. This observation, although only supported by two individual

events, supports the theory that the geometry of the port is driving the resonance and the excitation is not driven purely by propagating long waves of a particular period.

Figure 7-14: 3D Temporal spectrogram (spectral energy-frequency-time) variation, long wave periods only – (2012/07/27 to 2012/08/01). Measured outside the port with the RBR1.

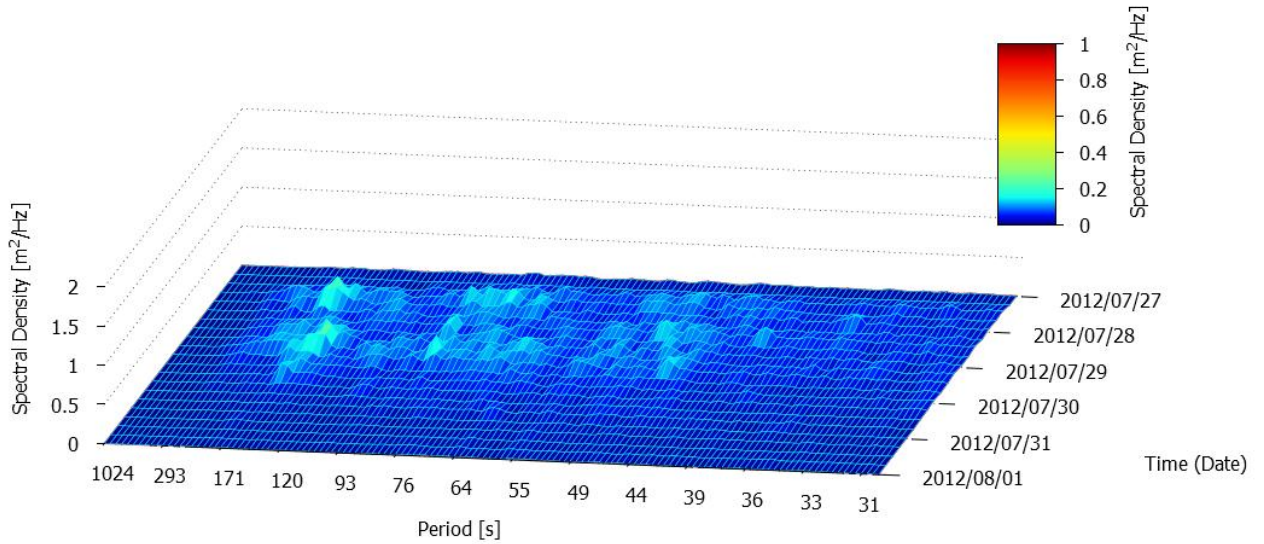


Figure 7-15: 3D Temporal spectrogram (spectral energy-frequency-time) variation, long wave periods only – (2012/07/27 to 2012/08/01). Measured inside the port with the LWrec.

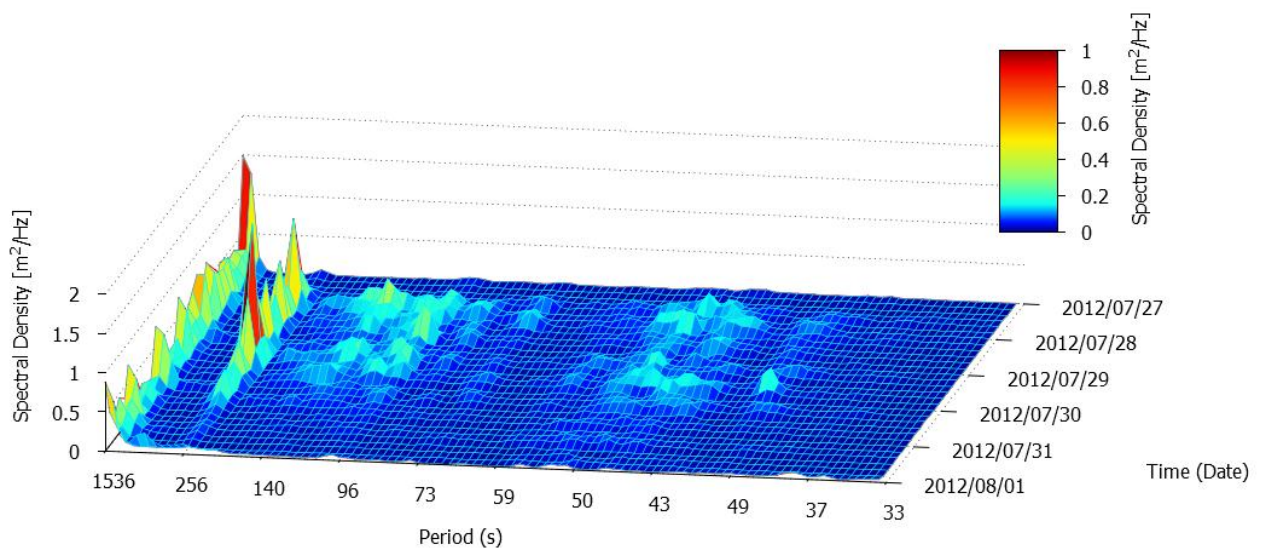


Figure 7-16: 2D Temporal spectrogram (spectral energy-frequency-time) variation, long wave periods only – (2012/07/27 to 2012/08/01). Measured outside the port with the RBR1.

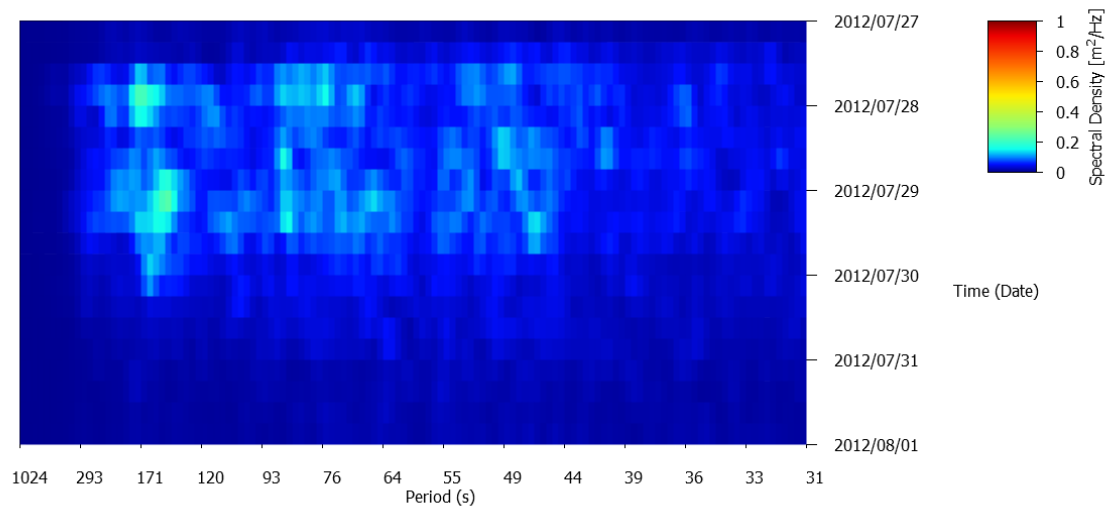


Figure 7-17: 2D Temporal spectrogram (spectral energy-frequency-time) variation, long wave periods only – (2012/07/27 to 2012/08/01). Measured outside the port with the LWrec.

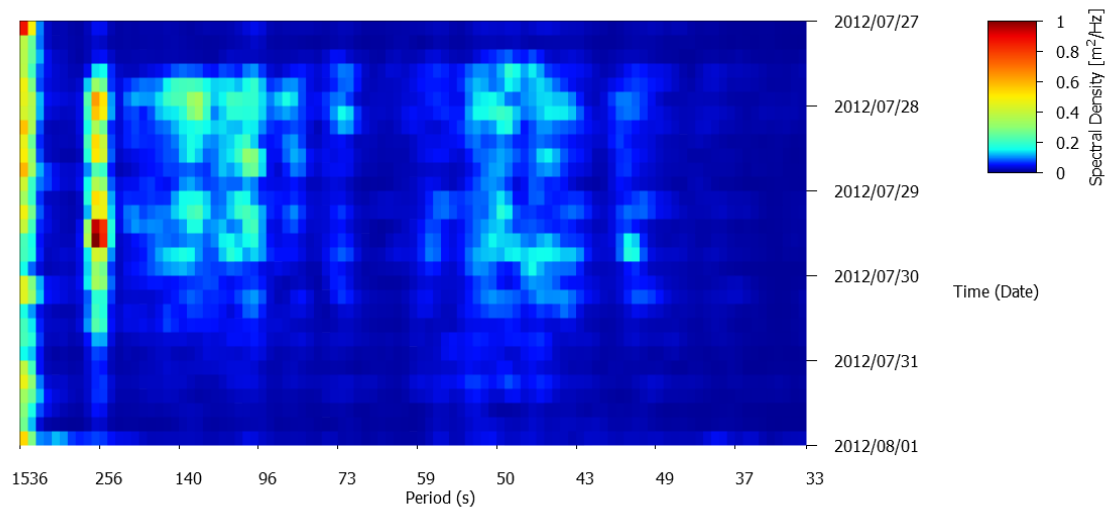


Figure 7-18 and Figure 7-19 show a more traditional perspective of the long wave spectra for the 2011 and 2012 events. The figures show all the spectra outside the port (red) and all the spectra inside the port (blue). The overall maximum spectrum envelope for both inside and outside the port is also shown in bold. The maximum envelope shows the maximum spectrum density at each frequency for its corresponding position. As with the 2D plots above, the peaks of the spectra become easy to read and identify.

Figure 7-18: 2D spectral collation comparison between the outside and inside of the port, long wave periods only – (2011/08/08 to 2011/08/18).

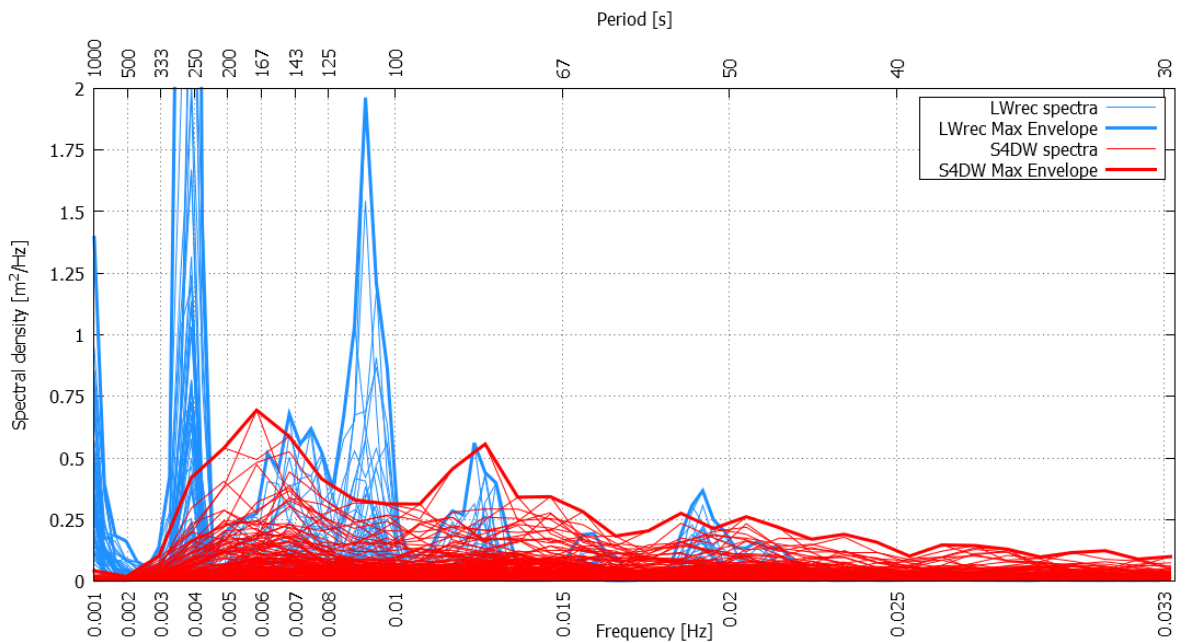


Figure 7-19: 2D spectral collation comparison between the outside and inside of the port, long wave periods only – (2012/07/27 to 2012/08/01).

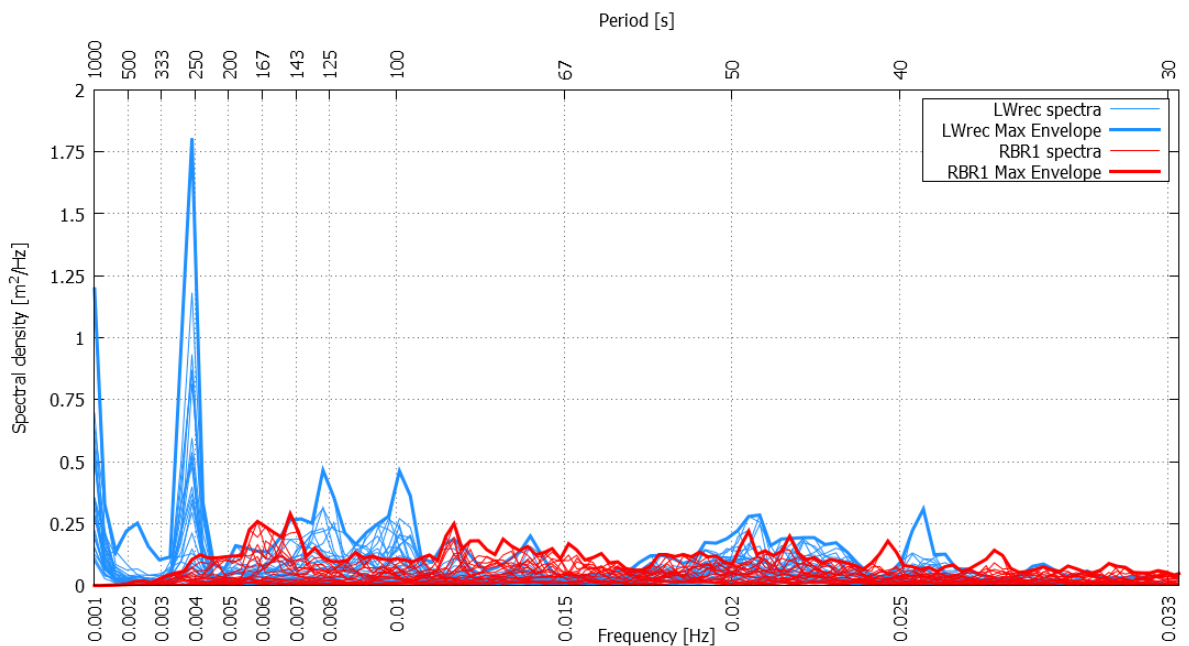
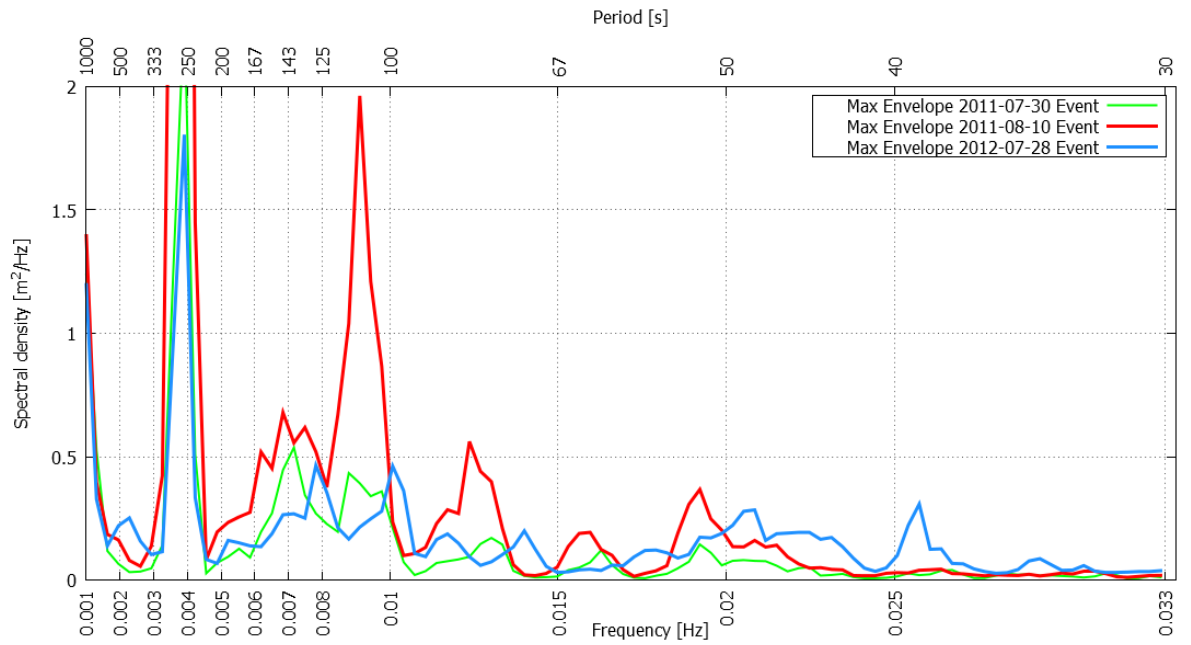


Figure 7-20 below shows a collation of maximum spectra envelopes for three events inside the port. Two of the events have been analysed in detail above namely, 2011-08-08 and 2012-07-27. An additional event, 2011-07-30 has been added in order to gain more confidence in the trends seen. The 2011-07-30 event may be viewed in the form of parametric data in the time-series figure above

(Figure 7-6); the spectral envelope was calculated in similar manner to the other two events and covers a duration of 5 days (2011-07-31 to 2011-08-05).

Figure 7-20: 2D spectral collation showing maximum spectra envelopes for 3 events inside the port from LWrec.



7.5. Meteorological Data

Figure 7-21 and Figure 7-22 show the meteorological observations at the port of Ngqura during the 2011-08-08 and 2012-07-27 events (3D spectrograms and time series of both events have been shown previously in the section above). The figures show that in each case there is a drop in pressure to approximately 1013 hPa one day before the sea storm and the associated increase in long wave heights arrive at the port location. The arrival of the low pressure system over the port location is associated with a change in wind direction and variability in the wind speeds. Data in each figure is hourly averaged data from the Central Data Base South African Weather Service.

Figure 7-23 shows daily synoptic charts for the events; the 2011 and 2012 events are shown on the left and right columns of the figure respectively. The synoptic charts allow for identification and visualization of the progression of the meteorological systems over the days during the events. Both events are driven by typical synoptic pattern types associated with sea storm creation on the South African coastline. In both events a low pressure system is present offshore east of the port of Ngqura. In addition an easterly wave condition is present during the 2011 event and a cut-off low is evident during the 2012 event. These are the systems associated with the short and long wave height increase identified by the two events.

Interestingly, both events are followed by a more extreme drop in pressure 3 days after the wave heights first increased outside the port. In both cases it is evident from Figure 7-23 that the pressure drop is due to the passing of large cold front systems over the port. A rough calculation shows that the front speeds are in both cases faster than the wave group celerity and hence the cold fronts cannot be attributed to the events shown.

Figure 7-21: Comparison of significant long wave heights (m) with meteorological parameters from 2011-08-07 to 2011-08-16. Panels shown (top to bottom): Significant long wave height (outside port), Air pressure, Wind speed, Wind Direction and Temperature.

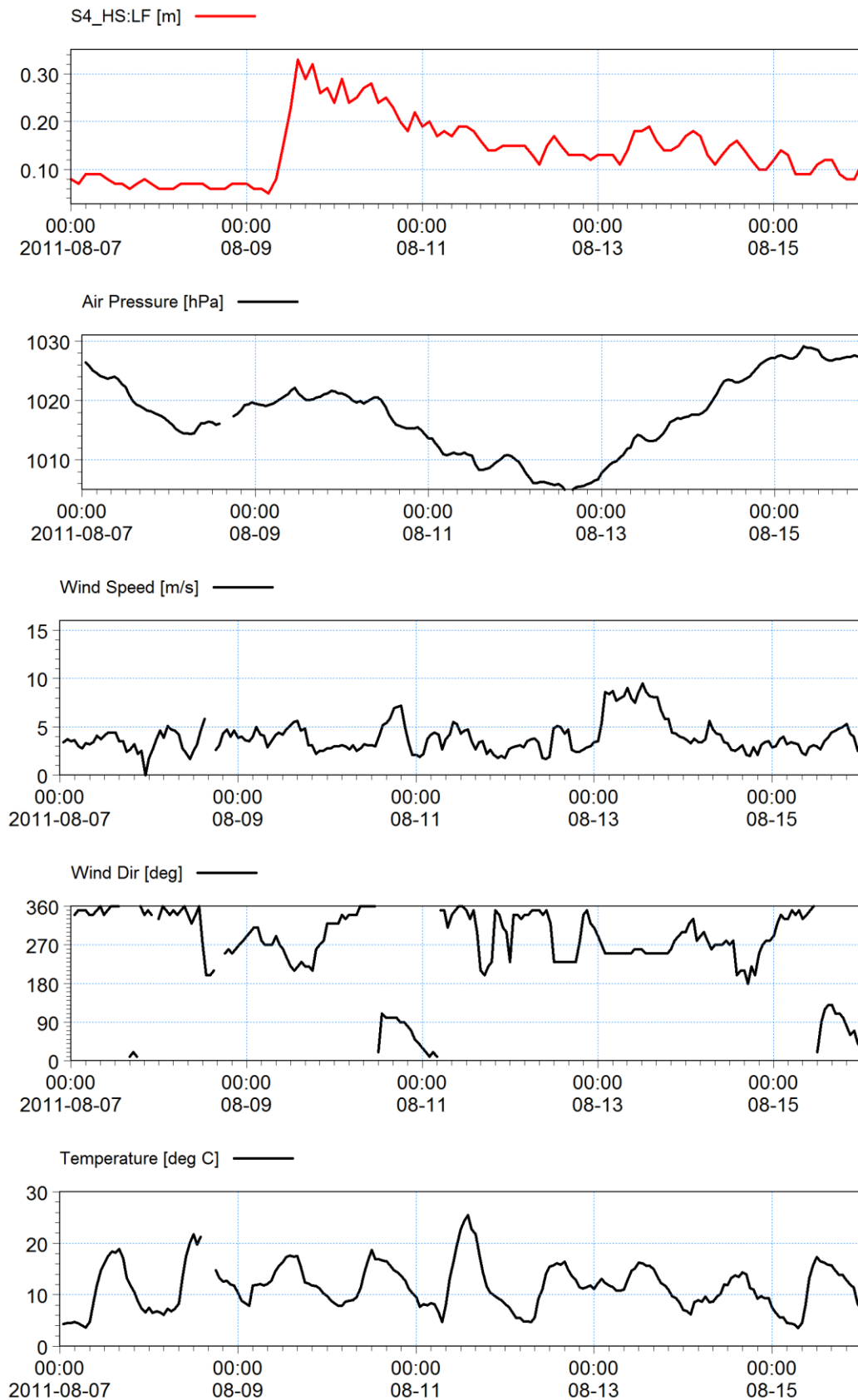


Figure 7-22: Comparison of significant long wave heights (m) with meteorological parameters from 2012-07-23 to 2012-08-01. Panels shown (top to bottom): Significant long wave height (outside port), Air pressure, Wind speed, Wind Direction and Temperature.

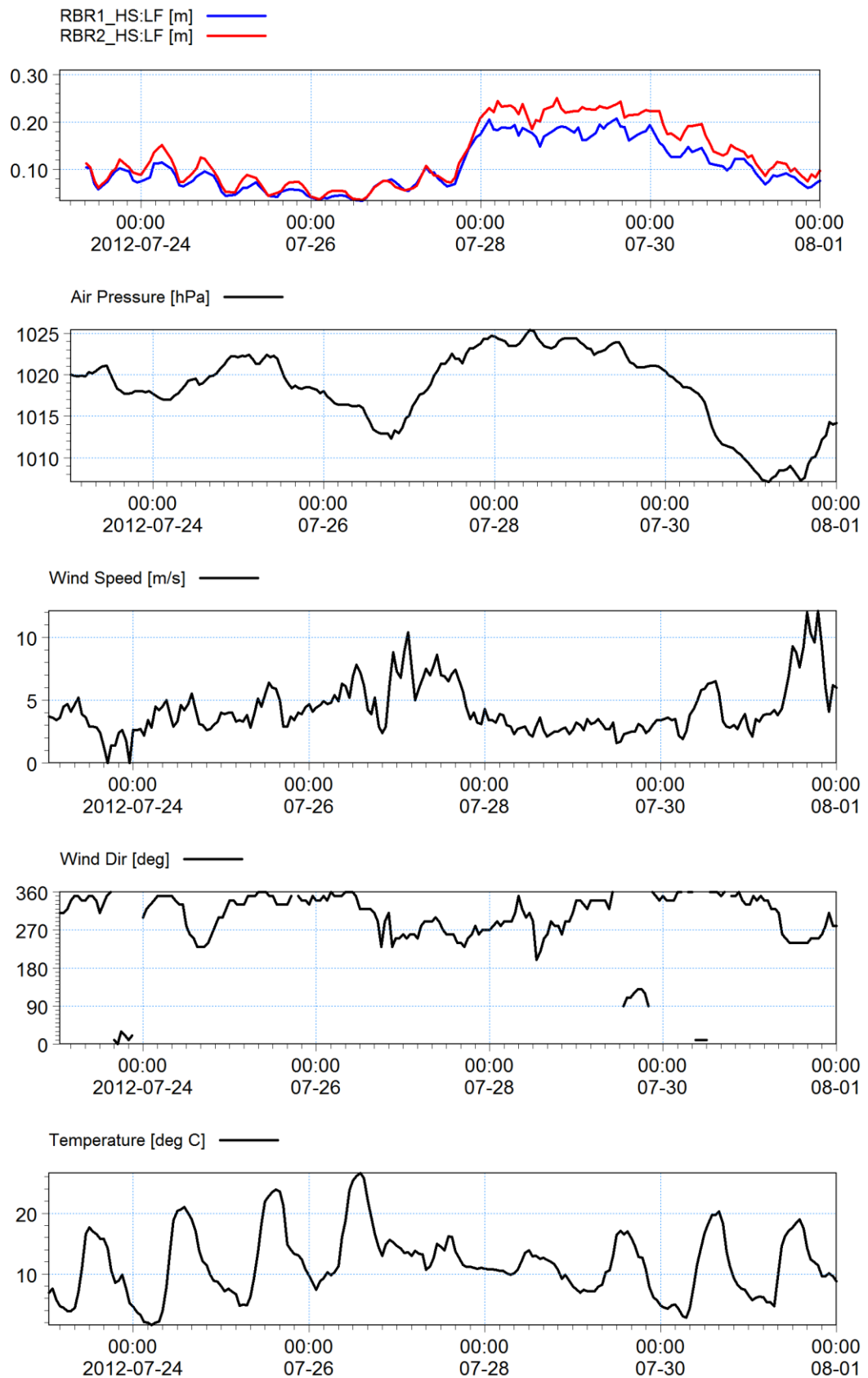
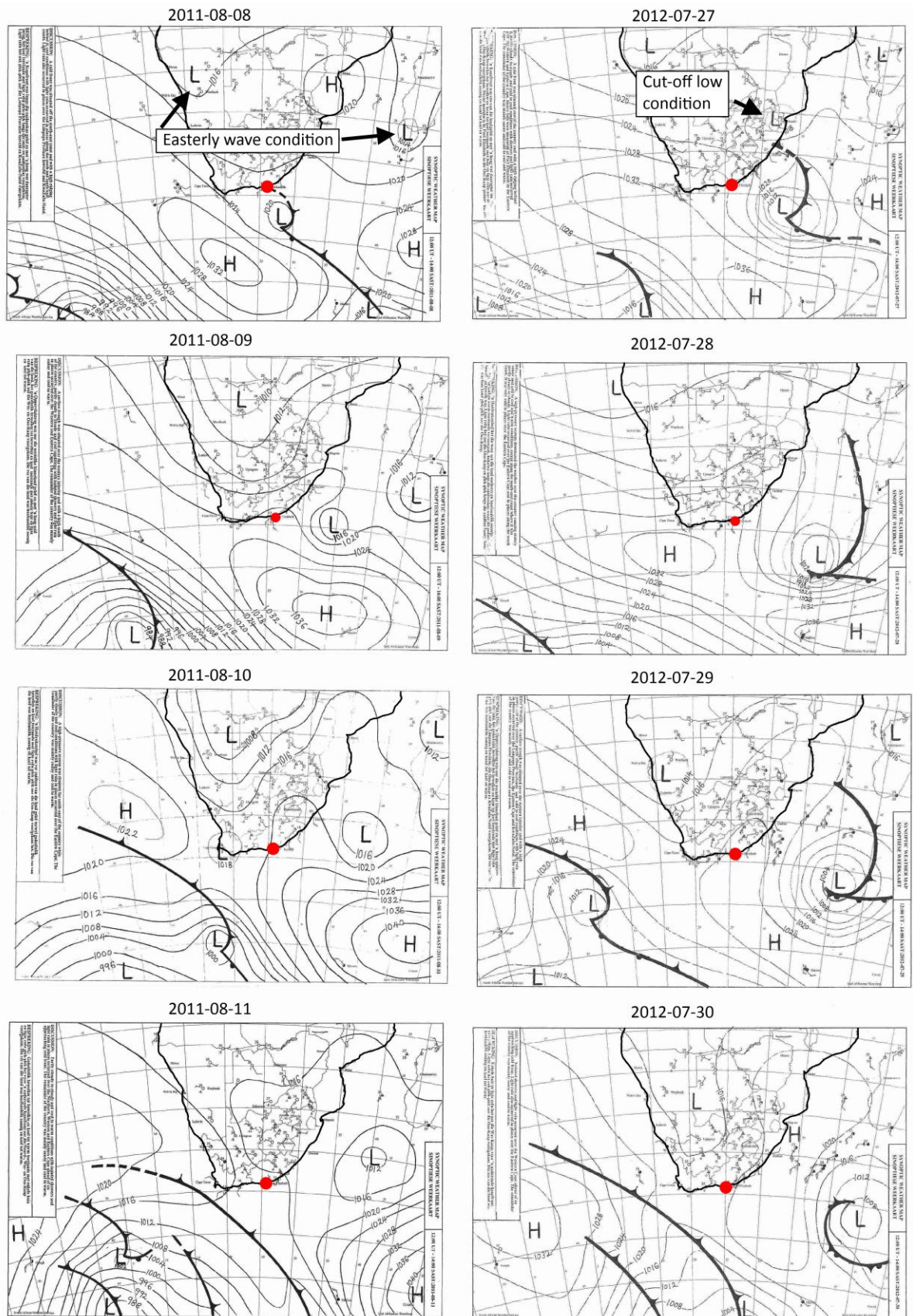


Figure 7-23: Daily synoptic charts, left pane: 2011-08-08, right pane: 27-07-2012. Red dot indicates the port of Ngqura (South African Weather Service, 2011 & 2012).



7.6. Summary and Discussion

Important characteristics have been observed through the various data analysis methods, namely:

A strong correlation between the significant long and short wave height has been observed. On average the long wave heights are 8% of the short wave heights and from time-series comparison the long wave heights appear to be bound to the short wave heights. Importantly, there seems to be little exception to the coupling of long and short wave heights. This suggests that the presence of long waves is predominantly the result of non-linear wave-wave interaction of the short waves and due to the creation of long waves in the surf zone. There appears to be no evidence showing that the long wave energy is a result of either direct atmospheric forcing or seismic activity.

The data analysis did not offer insight into the effect of wave groups on the long wave creation or the explicit effect of the surf zone and long wave reflections off the beach. It is noted that the long wave measurements did not include long wave direction either. The long wave measurements outside the port therefore included both the incident and reflected components to some degree. The analysis did not include a separation of these components. The effects of the beach will be investigated with the use of numerical models in the subsequent chapters.

The effect of tidal modulation on long wave height was evident when inspecting the wave height time-series both outside and inside the port. This phenomenon essentially equates to an increase in the non-linear transfer of energy from long period waves to shorter waves at low tide due to the convex beach profile. This results in a rise and fall of the long wave height which corresponds with the rise and fall of the tide. A more detailed description is included in Section 7.3.3.1. The occurrence of the tidal modulation in the data proves that a reflected component of long wave energy is in the measurements; furthermore it proves that the energy inside the port is partially the result of reflected wave energy off the beach south of the port.

The availability of simultaneous data sets allowed for insight into the correlation of the long wave heights between the inside and outside of the port. It was found that on average the significant long wave height was only reduced by 10% when propagating into the port.

Spectral analysis of the surface elevation measurements both outside and inside the port offered a more detailed and informative perspective on the data. Critically, the effect of the port geometry was clear in resonating and amplifying the long wave energy at certain frequencies. In regard to vessel motion analysis, this resonance of long wave energy at particular frequencies is what is of most importance and not simply the significant long wave heights. It was found that although the energy outside the port was fairly uniformly spread over the frequency range, the energy inside the port was consistently amplified at discrete period intervals, namely:

45 s to 55 s, 59 s to 70 s, 75 s to 90 s, 100 s to 160 s, 250 s to 260 s, 1000 s

Comparison of the long wave events with meteorological parameters showed no evidence of the meso-scale long wave generation, but rather a confirmation that the long waves were bound to short waves driven by fairly typical weather patterns acting off the coast of South Africa.

8. IDENTIFYING LONG WAVE PENETRATION MECHANISMS

8.1. Introduction

In order to gain more insight into how long waves behave in and around the port of Ngqura a Boussinesq wave model was setup to simulate some of the measured events analysed in Chapter 7. The model was an essential aid in the determination of two of the main objectives of the study:

1. Investigate the excitation of the port of Ngqura due to the long wave energy.
2. Identifying how the long waves are entering the port

Once the model was calibrated, the extents of long wave agitation and propagation could be viewed over the entire domain rather than at just two points, as is the case with analysis of measurements. Furthermore a model allows testing of scenarios which can help to identify how waves are propagating in the domain.

8.2. Modelling Approach

Two theories and corresponding model permutations were tested against a base case to identify the mechanisms responsible for how long waves enter the port. The base case was modelled for a typical event and then the two permutations, which included changing the model characteristics and filtering the base case wave input, were modelled. By comparison of the two permutations with the base case, the long wave penetration mechanisms were identified and quantified. The two theories and three models are described as follows:

1. Base Case. The base case was the propagation of a typical event into the port.
2. Beach Reflection Test. In this case the beach south of the port was dug-out and replaced with a sponge. The sponge essentially absorbs all wave energy hitting the beach and hence the only wave energy inside the port is a result of diffraction and refraction. This test was used to quantify the effect of wave energy reflecting off the beach and subsequently propagating into the port by; diffraction, refraction, and reflecting off the lee-side of the main breakwater into the port.
3. Free Long Wave Effect. In this case the short waves were filtered from the input surface elevations, resulting in freed long waves entering the model. This tested the bound wave effect on diffraction of long waves into the port.

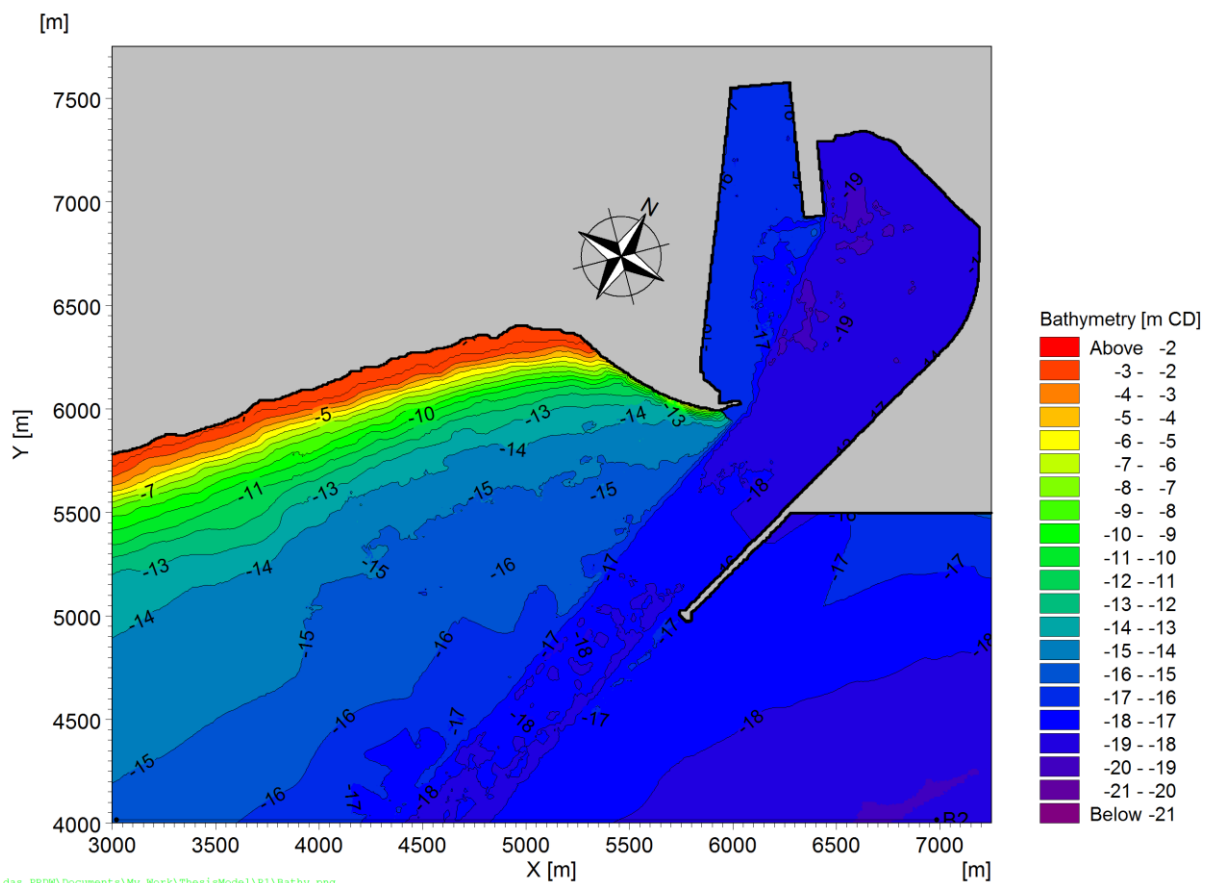
8.3. Model Setup

8.3.1. Bathymetry

Figure 8-1 shows the model bathymetry for the port of Ngqura. Three bathymetry surveys were used to collate the bathymetry;

- A preconstruction survey covering the extents beyond the port
- A single beam post construction survey covering the actual port area and entrance channel
- A beach profile, and single beam survey covering the beaches north and south of the port to the -15 m CD contour (the surf zone was omitted and has been interpolated).

Figure 8-1: Ngqura model bathymetry.



8.3.2. Waves

Surface elevation measurements, of 4.5 hr duration, were used for the preparation of the wave energy flux used as the model inputs. The original data was available in the form of pressure measurements which were converted to surface elevation measurements using linear wave theory, then de-trended, de-gapped and de-spiked. The events were all selected from the 2012 data set

from one moderate storm event occurring over 3 days, with a mean direction of 140°. Only the 2012 data was used because it offered the longest continuous records of surface elevation measurements which were measured simultaneously with the Long Wave recorder inside the port. The 2012 data set is described in Section 6.2.3. The relatively long 4.5 hr input duration was chosen because it allowed for enough data to analyse the long waves with confidence (see Section 4.4.1). This is also in accordance with tests on Boussinesq long wave modelling which conclude that in order to get a stable spectrum the data length should be at least in the order of 3 to 5 hours (Ota et al., 2010). The use of the surface elevations also ensured that no phasing was lost and that the wave groups and bound long waves were conserved.

Two unquantified downfalls of using the measurements is that the long wave directions were not identified and a split between the incident and reflected wave components was not performed. Hence a portion of the energy propagated into the model would have in fact been a reflected wave component travelling back out to sea. Nonetheless, the use of the surface elevation was still the preferred option. The white noise approach in Chapter 9 allowed for a check on the model in regard to sensitivity to the wave input.

Figure 8-2 shows a basic annotation of the preparation of the input data used in creating the wave input for the Boussinesq models. The figure shows the de-trended, de-spiked and de-gapped surface elevation measurements and associated wave parameters. The surface elevation measurements were converted from the raw pressure measurements available from the RBR1 instrument. The lower pane of the figure shows an enlarged version of the surface elevation wave record identified in the upper pane. The surface elevations in the lower pane were used as the wave inputs for the base/validation case modelled in Section 8.5.1.

Figure 8-2: Visualization of boundary input. Top pane: de-trended surface elevation data and corresponding $H_{m0:HF}$ and $H_{m0:LF}$ parameters. Bottom pane: zoom of validation event.

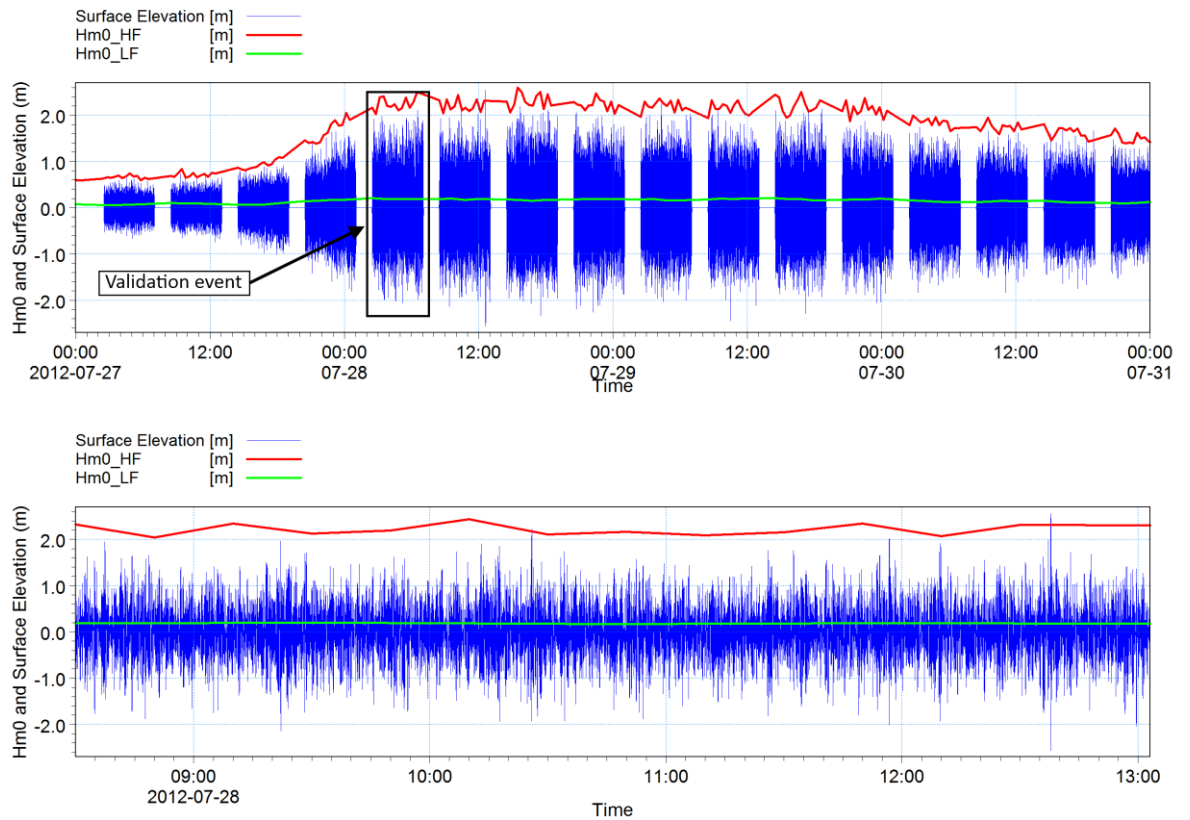
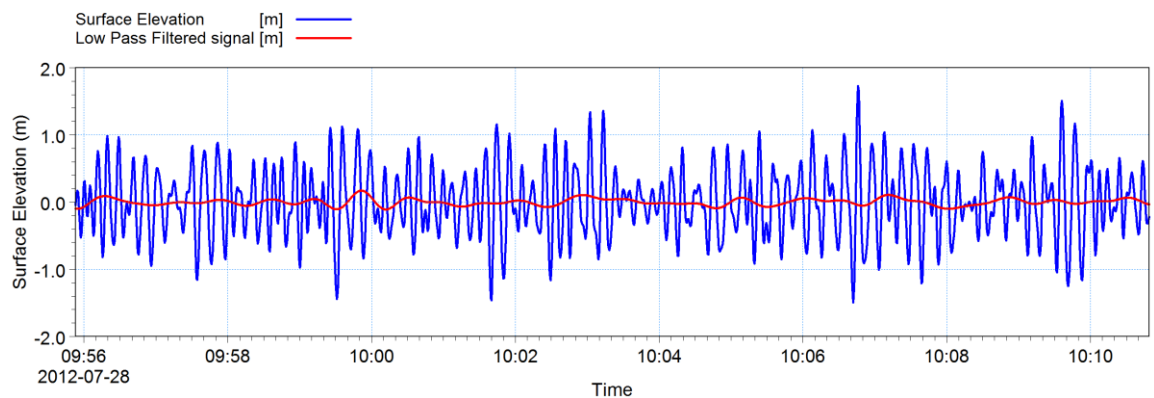


Figure 8-3 shows in red the filtered long wave signal used as input for the free long wave test described in Section 8.5.3. The blue signal shows the surface elevation measurements.

Figure 8-3: Example of filtered long wave signal – validation event



8.3.3. Numerical Parameters

The numerical parameters used in the model are as follows:

- Grid size: 5 m

- Time step: 0.125 s
- Solver: Quadratic upwinding with simple upwinding at steep gradients and near land
- Time extrapolation factor: Factor of 0.8

The above parameters resulted in a Courant numbers of 0.35 ensuring numerical stability for all the modelled wave conditions.

8.3.4. Water Levels

A constant water level of +1 m Chart Datum (CD) was used for all models, corresponding to the mean water level of the predicted tide for Algoa Bay, as taken from the South African Navy tide tables.

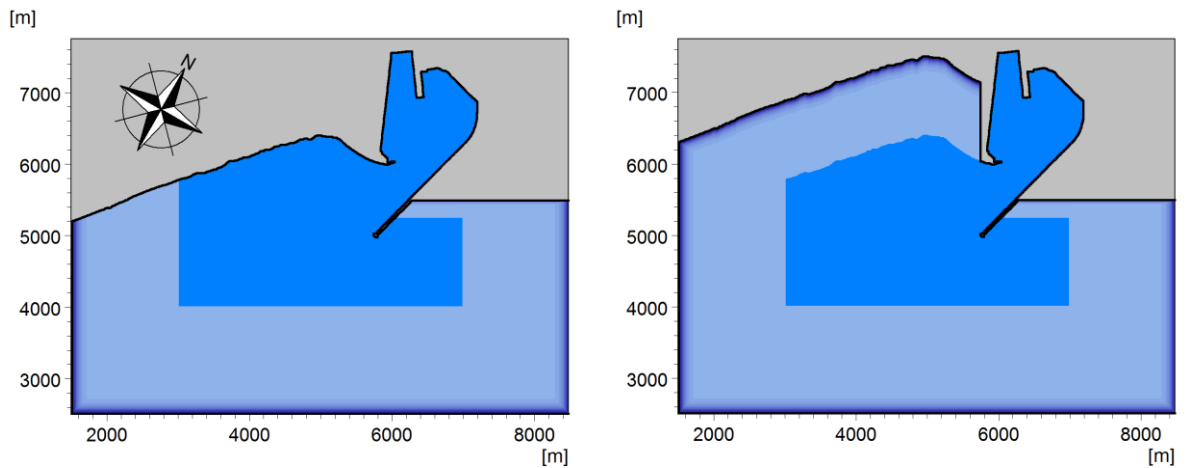
Although evidence of tidal modulation of the long wave heights was apparent, as shown in Section 7.3.3.1, only the mean water level was used. This is partly because varying the mean water level of the model is not possible during a model run, and also because the long duration of the wave records modelled bridged across the mean water level. As the model calibration was successful, a sensitivity test and investigation into the water level and subsequent tidal modulation was not considered necessary. This sensitivity test is recommended in the event of further study.

8.3.5. Sponge Layers

To ensure the models were not affected by false wave reflections sponge layers, 1.5 km wide, equivalent to one wave length of a 150 s wave, were inserted on the open boundaries. According to tests on Boussinesq long wave modelling, this sponge length should be acceptable (Ota, et al., 2010).

Figure 8-4 shows the extent of the sponge layers for the base model and for the beach reflection case; the sponge layers are identified in light blue. The typical model sponge shown in the left pane shows the sponge on all the artificial boundaries. The beach absorber sponge shown in the right pane shows the replacement of the beach with a sponge.

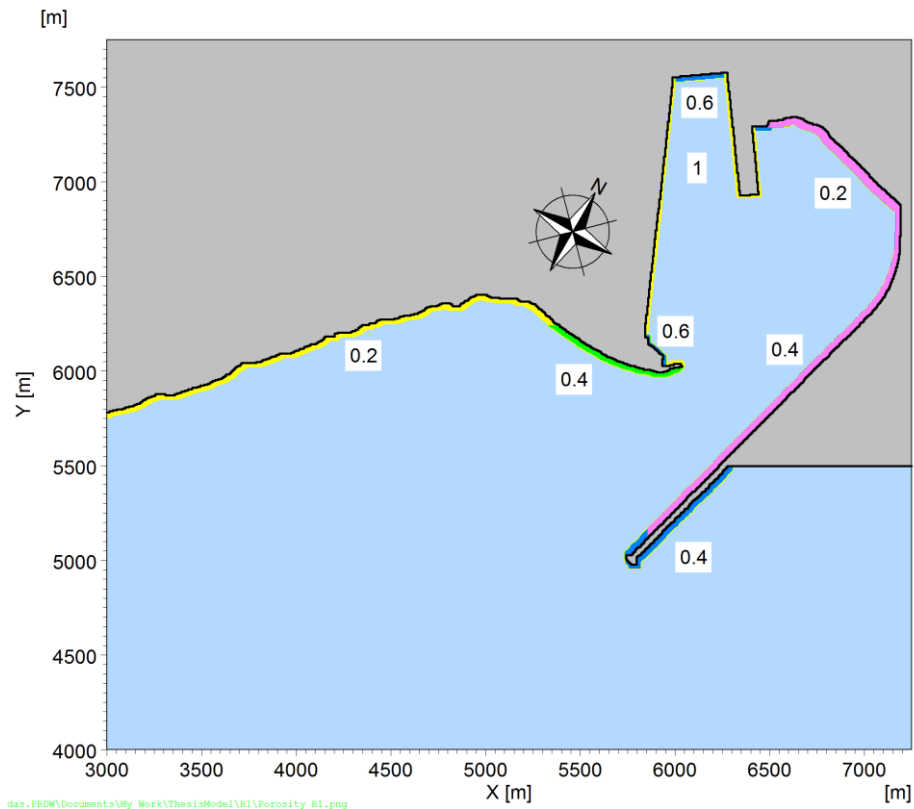
Figure 8-4: Sponge layers for base case (left) and beach reflection test (right).



8.3.6. Reflection Coefficients

The reflection coefficients for the various types of landward boundaries were based on guidelines given for typical structures by Thompson et al. (1996). The desired reflection coefficients at the various structures were obtained by applying representative porosity layers in front of the relevant structures. The reflection coefficients for the various structures are shown below in Figure 8-5.

Figure 8-5: Ngqura reflection coefficients.



das.PRDM\Documents\My_Work\ThesisModel\RI\Porosity_R1.png

8.3.7. Bottom Friction

The effects of bottom friction were included in the model. A Manning number of $32 \text{ m}^{1/3}/\text{s}$ was used to simulate a constant sand bottom across the entire model domain.

8.4. Calibration

8.4.1. Calibration Approach

The calibration of the model was aimed at setting up the model as accurately as possible and adjusting necessary parameters realistically, to achieve a result similar to the measurements available.

The initial step in the calibration process was to ensure that the results given by the model obeyed the expected trends and outputted obvious results. This included inspection of 2D plots showing the significant wave height across the domain, and surface elevation animations showing the propagation of short waves. The next step was to compare the measured wave heights with the modelled wave heights.

The available measurements have been described previously in Chapter 6; essentially surface elevation measurements outside the port were available, sampled at a sufficient sampling interval to accurately resolve the short and long waves for a 4.5 hour period. Inside the harbour simultaneously measured surface elevation measurements were available; however, the measurements were only sampled at a sampling interval sufficient to resolve the long waves. Therefore, in the calibration process, comparison of short wave heights was not possible (except on the input boundary) and only long wave heights could be compared inside the port. The surface elevation measurements were used as input for the model in order to conserve the phasing of the waves, the effect of groups, and hence, conserve the bound long wave energy as accurately as possible.

The most detailed calibration output for comparison between the model and measurements was direct spectral comparison of the long wave spectra inside the port, at the location of the long wave recorder.

8.4.2. Summary of Calibration Progression

The calibration of the Boussinesq model proved to be time-consuming. Each model run took approximately 30 hours. The calibration process developed into a sensitivity test and an exercise in determining the different mechanisms driving particular resonance modes.

The calibration process and sensitivity tests may be broken down into the following three groups:

1. Testing input conditions

2. Changing physical parameters
3. Testing output analysis

8.4.2.1. Testing Input Conditions

As mentioned, 4.5 hr surface elevation measurements were used as input for the model. The Boussinesq model propagates waves from an energy flux; hence, the measurements were converted using the Mike 21 Random Wave Generation Tool. The tool offers three options for the types of wave to be created from the surface elevation measurements; one-dimensional, unidirectional, and directional waves. Initially, the directional wave input was selected as this was perceived to be the most accurate because it produces short crested, irregular waves with a defined spreading. It quickly became apparent that this was not the case as the long wave energy was radically reduced and seemed to lose the phasing associated with the input measurements.

Subsequently both the one-dimensional and unidirectional waves were tested. The one dimensional wave option was dropped as it can only propagate long crested irregular waves perpendicular to the model boundary; this forced the waves to be sent from the wrong direction. The uni-directional waves option propagates long crested irregular waves from the boundary with an option to specify the direction. The unidirectional waves gave the best result. It is noted that using long crested waves is not completely realistic and is likely to increase the long wave energy input into the model however the option was used as it gave the best results and there was doubt about the directional wave input conserving the wave phasing.

A sensitivity test on the wave direction was performed; the best results were attained from the measured mean wave direction of the short waves.

8.4.2.2. Changing Physical Parameters

The effects of friction and porosity were explored in the calibration process. It was found that friction had very little effect on the resonance modes and only marginally reduced energy in the long wave spectrum. Reflection coefficients in the model were not adjusted, but the manner in which the porosity was applied was tested. In one case, all slopes inside the port were removed and replaced with correlating porosity layers to simulate the specified reflection. In another test, the slopes were reintroduced and cut at -2 m CD, a porosity layer was then applied for the remaining slope. The test results were the same in both cases.

The effects of including wave breaking were also tested. At first wave breaking was excluded because the model setup only allowed for a semi-realistic breaking process. This was because the bathymetry near the shore was cut at -2 m CD making the water depth approximately 3 m; which meant only the

larger waves for the event would break before running into the porosity layer. This model setup was required in order to ensure model stability and reasonable run times. To more accurately model wave breaking on a beach using the Mike Boussinesq model, a moving shoreline approach would be required; practically however, the Ngqura model domain was too large to allow for this. Nonetheless the results were found to be best when the wave breaking feature was included and hence all the model results which included short waves include wave breaking.

8.4.2.3. Testing Output Analysis

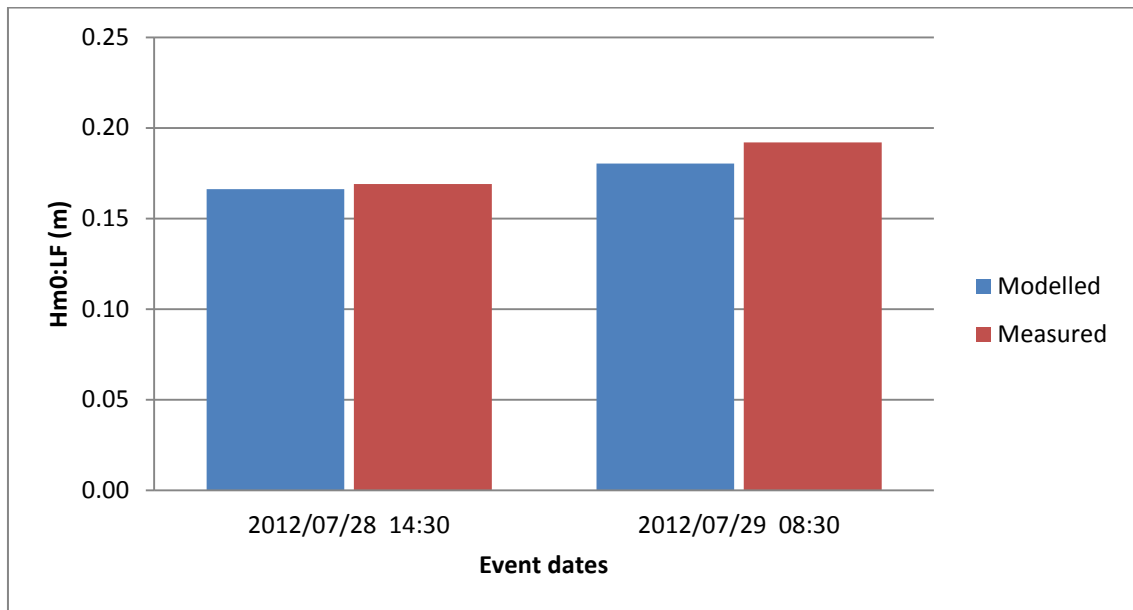
Two methods of spectral comparison were investigated. In one, the best spectra in terms of confidence and resolution were used; in the case of the model a much higher resolution could be attained with the same confidence as more data points existed. In the second method, the model data was sub-sampled reducing data points from the write out frequency of 8 Hz to the equivalent frequency of the measured data of 0.33 Hz. The same spectral analysis was then performed on both data sets. It was found that although the methods resulted in fairly similar looking spectra, sub-sampling the data and performing exactly the same spectral analysis gave the best results.

A sensitivity test on the position of the model output extraction point was performed in order to check how the modelled long wave spectra were affected. The test was necessary as the exact position of the Long Wave Recorder could not be repeated in the model. The Long Wave Recorder was positioned against a wall in the port, in the corner of a basin. In the model, for stability reasons, a porosity layer was inserted against the walls. The extraction point therefore was offset diagonally by approximately 15 m. Multiple output points were tested and the difference in results were minor as the anti-nodes cover a fairly large area. The closest point outside of the porosity layer was used.

8.4.3. Calibration Results

Multiple events were modelled during the calibration process to ensure the model was not biased for a specific event and that the chance of using an event including measurement anomalies was reduced. Figure 8-6 shows a comparison of the significant long wave heights for two events. For each event the long wave height from the model has been compared with the measured data. All the data was extracted from the position of the Long Wave Recorder within the port basin (Figure 6-1). Both modelled events compare well with the measured long wave height as the difference is less than 0.02 m in each case.

Figure 8-6: Significant long wave height comparison between model results and measurements at Long Wave Recorder position inside the port basin.



The long wave spectra for the two events compared above are shown below in Figure 8-7 and Figure 8-8 respectively. In both cases, the modelled long wave spectra has been compared with the measured long wave spectra.

Figure 8-7: Long wave spectrum comparison, model vs. LWrec – Event; 2012/07/28 14h30. Model $H_{m0:LF} = 0.17$ m, LWrec $H_{m0:LF} = 0.17$ m.

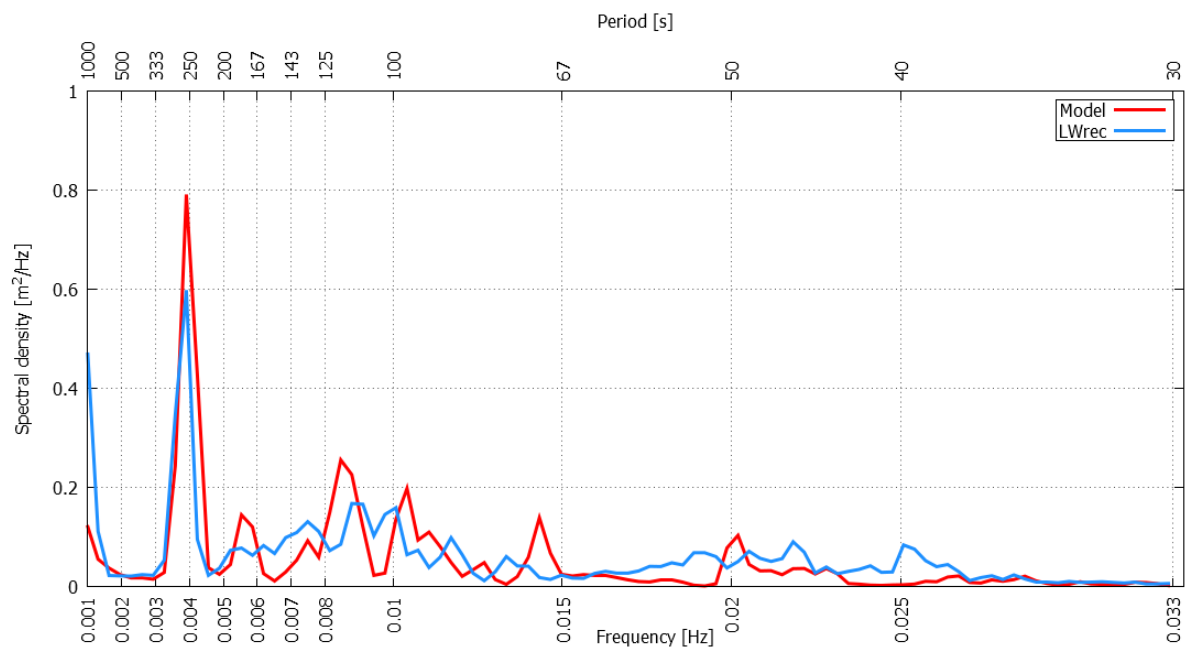
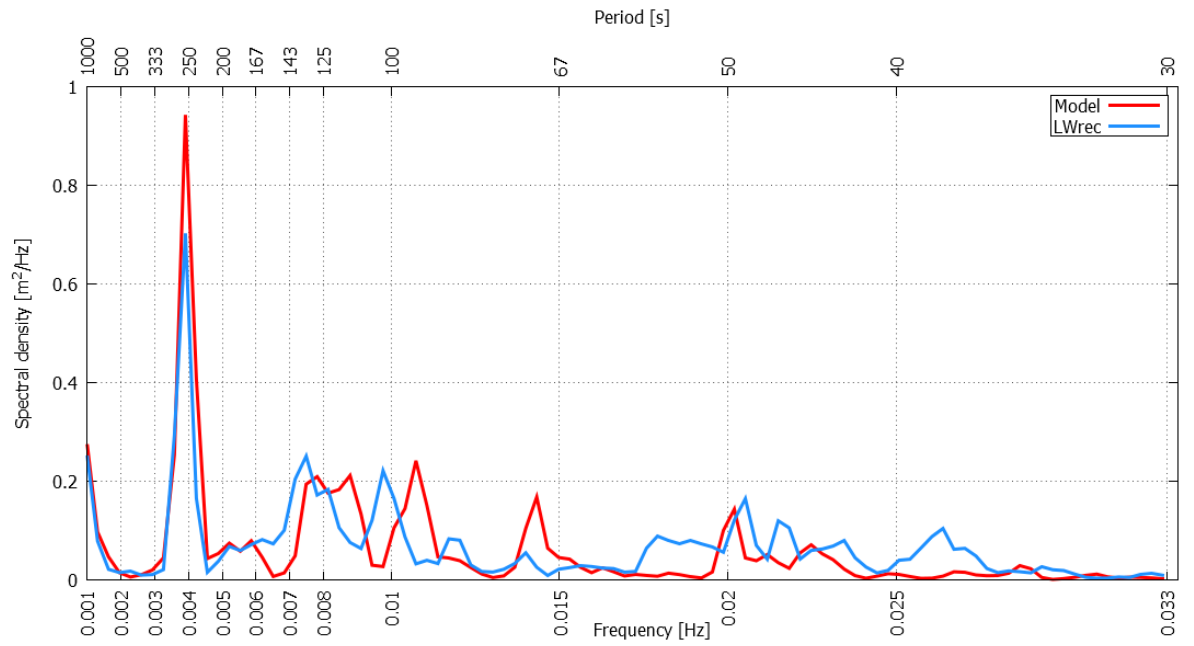


Figure 8-8: Long wave spectrum comparison, model vs. LWrec – Event; 2012/07/29 08h30. Model

$H_{m0:LF} = 0.18$ m, LWrec $H_{m0:LF} = 0.19$ m.



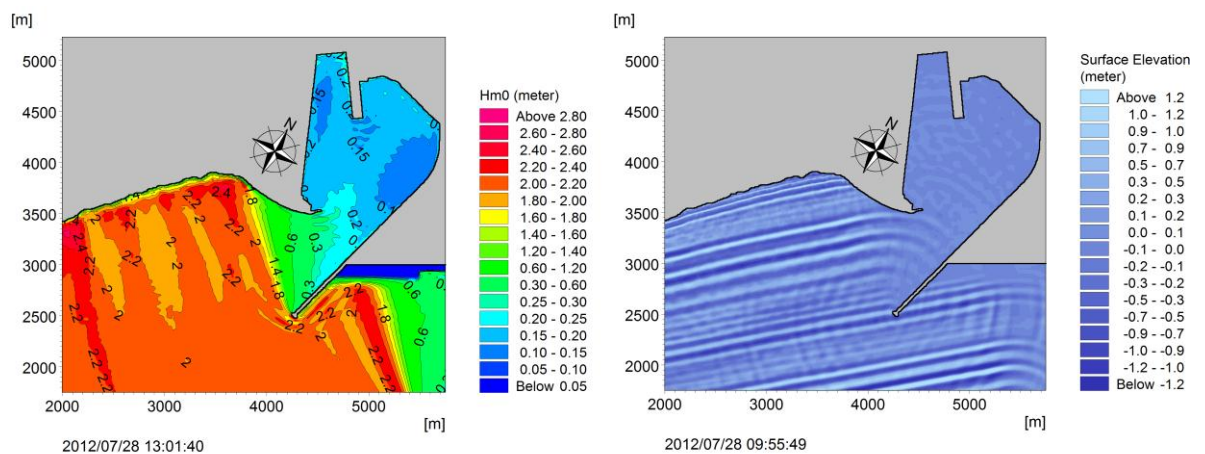
8.5. Results

8.5.1. Base Case

The base case is a model which propagates a typical short wave event into the port. It aims at simulating all the natural processes as accurately as possible in order to develop a “base case” which can be compared subsequently to adapted model permutations. The base case is also a validation of the calibration process described in Section 8.4.

Figure 8-9 and Figure 8-10 show the results of the base case. Figure 8-9 shows the significant short wave height on the left and the instantaneous surface elevation on the right. The significant short wave height is attained and there is no evidence of anomalies in either of the plots. The expected wave crests and diffraction patterns around the main breakwater are seen in the right pane.

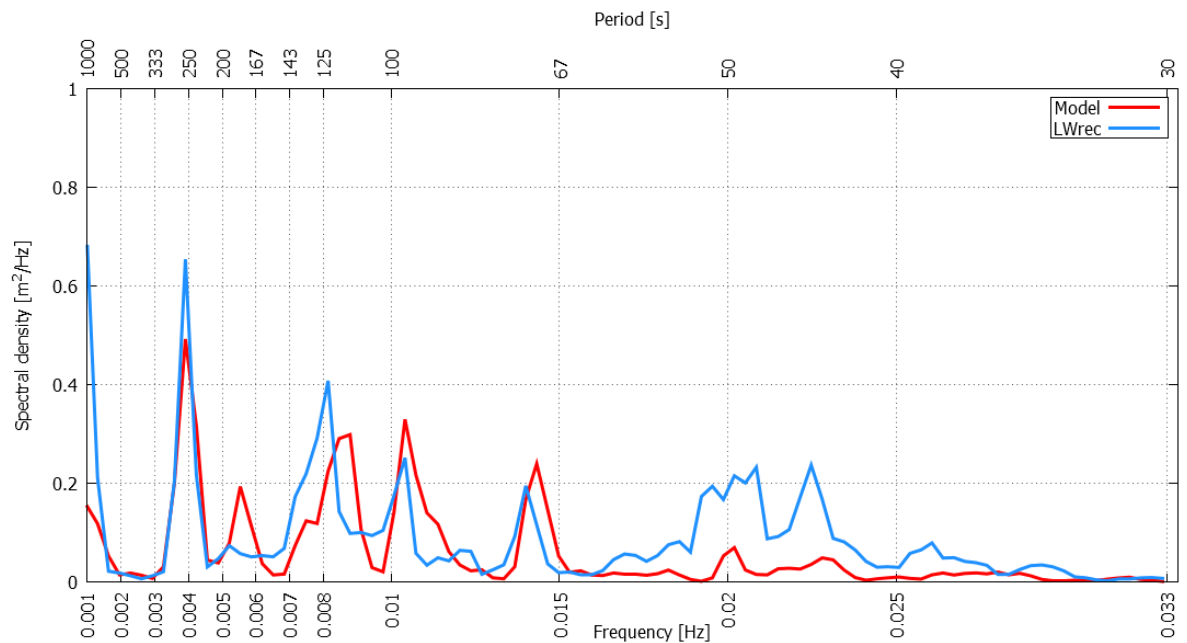
Figure 8-9: Example of modelled significant short wave height (left pane) and instantaneous surface elevation (right pane).



The spectra comparison, in Figure 8-10, shows that as in the calibration events the long wave energy is being fairly well simulated. The main peak at 250 s is aligned exactly with the measurements, another three energy spikes at 125 s, 100 s and 70 s correspond fairly well with the actual measurements. The model seems to slightly over amplify energy between 167 s and 200 s while under predicting energy between 40 s and 55 s. Consideration of the significant long wave heights shows the modelled significant long wave height is 0.18 m in comparison with the 0.21 m wave height calculated from the measurements; the model under predicts the wave height by 0.03 m.

In summary, the base case is considered a fairly typical event exhibiting similar resonance periods to the events analysed in Chapter 7. Furthermore, the modelled results are close enough to the measurements to justify that the model is adequately representing reality. The base case will therefore be used to test the theoretical tests detailed in the Modelling Approach, Section 8.2.

Figure 8-10: Long wave spectra comparison, Model vs. LWrec – 2012/07/28 08h30. Model
 $H_{m0:LF} = 0.18$ m, LWrec $H_{m0:LF} = 0.21$ m.



8.5.2. Beach Reflection Test

The beach reflection test is identical to the base case except a sponge replaces the beach south of the port. As mentioned in Section 8.2, by quantifying the difference between the two models, the aim of the test is to investigate the effect of wave energy reflecting off the beach and subsequently propagating into the port by; diffraction, refraction, and reflection off the lee-side of the main breakwater. The beach sponge in comparison with the base case sponge is shown in Figure 8-4.

Figure 8-11 shows a comparison of the long wave spectra at the position of the LWrec inside the port. The blue spectrum shows the measurements from the LWrec, the red spectrum shows the base case as detailed in Section 8.5.1, and the green spectrum shows the beach reflection test. In assessing the effects of the beach sponge, only the base case and beach reflection test should be compared i.e. the red and green spectra. Thus, in assessing the effect of the beach sponge there is a notable reduction of low period waves above ~ 100 s; in fact the long wave energy seems to reduce as the period increases. For the frequencies higher than ~ 100 s very little change in the results is evident.

The greater reduction in the higher period wave energy is attributed to the characteristics of the longer waves. Longer waves reflect, refract and diffract more than shorter waves; hence the removal of the beach has a greater effect in reducing the longer wave energy. This implies that a larger proportion of the longer wave energy (Periods > 100 s) present in the port is from reflected wave

energy off the beach; whereas, the majority of the shorter wave energy in the port may be attributed to direct diffraction around the main breakwater.

Considering the significant long wave heights, the modelled significant long wave height is 0.15 m in comparison with the 0.18 m wave height calculated from the base case. The reflected wave component can therefore, in this case, be attributed to contribute approximately 17% to the long wave energy inside the port.

Figure 8-11: Long wave spectra comparison, base case vs. beach absorber test, also showing actual LWrec.

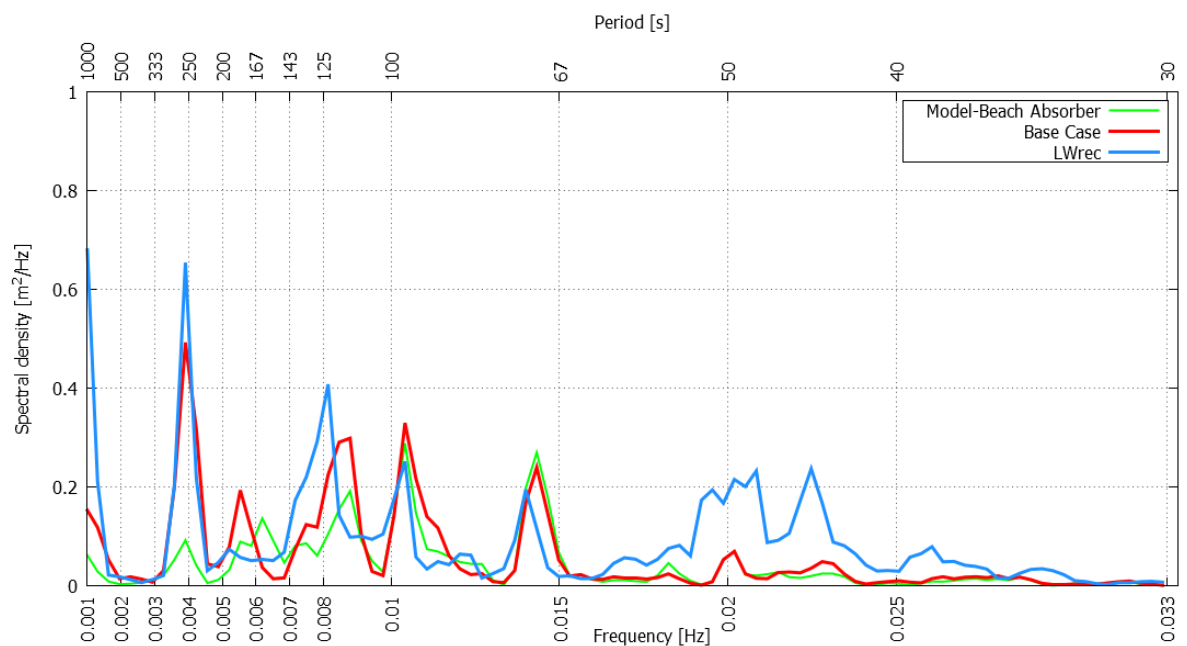
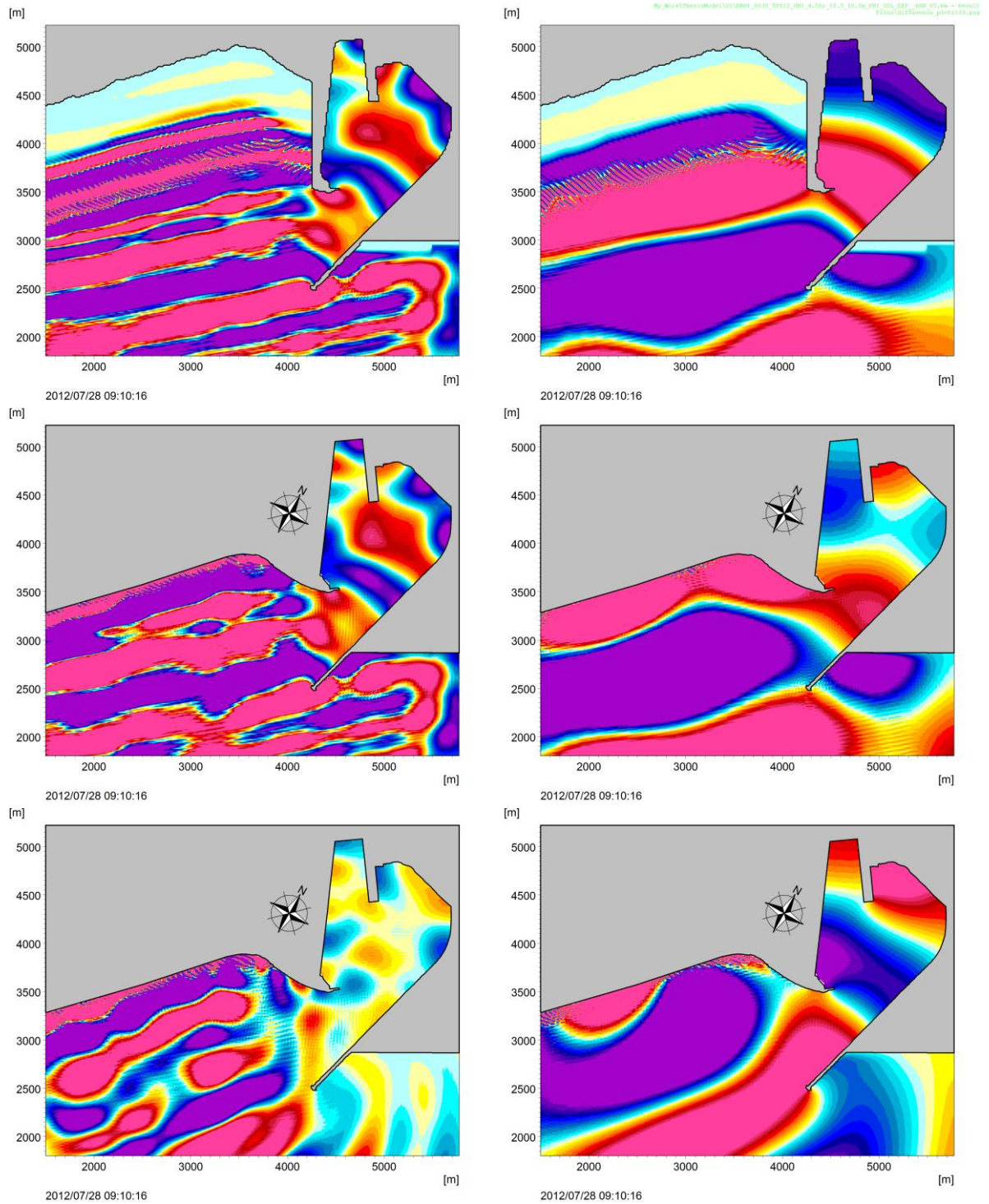


Figure 8-12 visualizes the explanation of the results and was generated in order to aid with the initial understanding of the reduction in the longer period wave energy. All the panes in the figure show the instantaneous surface elevations over the model domain at the same time step. The warm colours represent a rise in the water surface above mean water level; cool colours represent a drop below the mean water level. By band-pass filtering the 2D surface elevation output files from the base case and the beach reflection test, it was possible to visualize the long waves in 2D. The band-pass filtering was performed in order to localize the surface elevations of waves with energy from 30 s to 100 s and 100 s to 1000 s. Hence, the left panes show the surface elevations of the long waves between 30 s to 100 s, the right panes show the long waves between 100 s to 1000 s. Once the long waves of interest were filtered, the beach absorber case (representing incident wave only) was subtracted from the base case (representing both incident and reflected waves) leaving only the reflected waves. The incident waves are shown in the top pane, the incident and reflected waves are shown in the middle pane and finally the reflected wave component is shown at the bottom pane.

The higher degree of refraction of the reflected longer waves is shown in a comparison of the bottom panes. The bottom right pane shows a large portion of the wave front hitting the inside of the main breakwater, in comparison the shorter reflected waves in the bottom left pane appear to travel more directly back out to sea.

Figure 8-12: Reflected long wave components, showing increased wave diffraction, reflection and refraction for energy over 100 s. All panes show instantaneous surface elevation. Upper: Incident waves (no reflection), Centre: Incident and reflected waves, Lower: Isolated reflected waves. Left and right columns represent split in energy for 30 s to 100 s and 100 s to 1000 s.



It is noted that in Figure 8-12 there appear to be some numerical instabilities around the nearshore zone in particular. The instabilities appear more pronounced for the left panes representing the energy between 30 s and 100 s, notably a narrower band-pass filter than the 100 s to 1000 s filter. It is hypothesized that these apparent instabilities are due to the band-pass filtering process and not a result of instabilities in the model output. No instabilities are evident when viewing the significant long wave or the surface elevation figures shown in Figure 8-9. Furthermore, inspection of output time-series of surface elevation points in the vicinity of the beach showed no noise for the unfiltered results. Hence the apparent instabilities are attributed to a lack in data resolution due to the coarse 2D output files that were filtered. The coarse files, in regards to time and spatial steps, were necessary in order to avoid programme crashes when performing the filtering. Interestingly a similar shimmer is visible on the band-pass filtered figure produced by Kofoed-Hansen et al., (2005), shown in Figure 3-14.

8.5.3. Free Long Wave Test

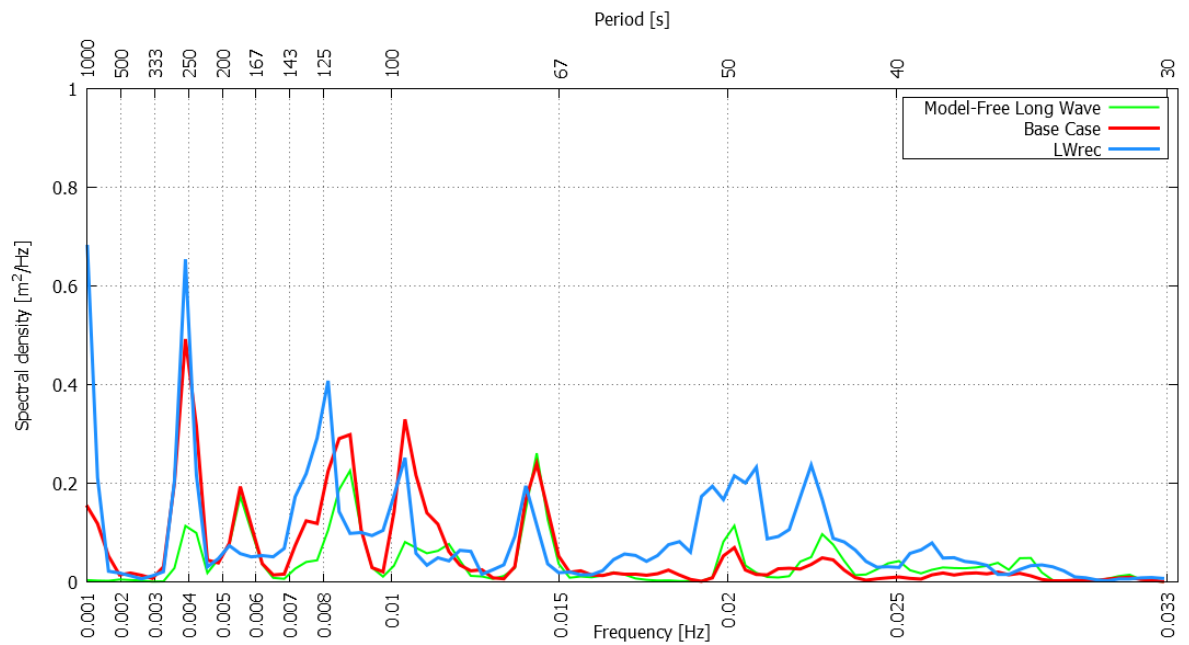
The free long wave test is identical to the base case except for the wave input. The wave input was generated from a filtered signal of the surface elevations used to generate waves for the base case. A low pass filter was applied to the measured surface elevations in order to remove all short wave energy below 30 s, leaving only the long waves; the signal is shown in Figure 8-3 in the Model Setup Section. By removing all the short waves from the surface elevation measurements, the long waves are essentially freed from the groups and can therefore propagate at their own celerity rather than the celerity of the wave groups.

As with the beach reflection test, the results of the free long wave test have been compared with the base case in long wave spectral form at the position of the LWrec inside the port. The blue spectrum shows the measurements from the LWrec, the red spectrum shows the base case as detailed in Section 8.5.1, the green spectrum shows the free long wave test. In assessing the effects of the free waves only the base case and free long wave test case should be compared i.e. the red and green spectra. The comparison shows an unexpected result, a substantial reduction in long wave energy between 75 s to 90 s and 245 s to 260 s with a smaller reduction in energy between 110 s to 145 s; the rest of the energy is fairly similar to the base case.

The reason for the reduction of the long wave energy for only certain frequency bands was discovered with the use of a white noise simulation. This has been detailed in the next chapter, in particular in Section 9.4.3. It was found, by conducting a beach reflection test with the white noise simulation, that certain wave periods that reflected off the beach resonated out of phase with the resonance created by the incident waves.

Additionally, this is unique to when the long waves are free and hence travelling at a slightly faster celerity compared with the bound long waves, which travel at the group celerity. It should be noted that the long waves propagated in a white noise spectrum are also free long waves.

Figure 8-13: Long wave spectra comparison, base case vs. free long wave test, also showing actual LWrec.



Considering the significant long wave heights, the modelled significant long wave height is 0.14 m in comparison with the 0.18 m wave height calculated from the base case.

8.6. Conclusions and Summary

A calibrated Boussinesq model was setup in order to test certain theories aimed at investigating how long waves enter the port. A base case was modelled which was then compared to the other model tests. The model tests investigated the effect of reflection off the beach and free long waves as opposed to bound long waves.

The model calibration gave insight into the optimal modelling setup for incorporating long waves when using a time-series of surface elevation measurements to create the wave input. The resulting calibration trials resulted in a good simulation of the long wave spectra inside the port.

The beach reflection test revealed that wave energy with periods below 100 s predominantly entered the port via diffraction around the main breakwater; little of the reflected wave energy below 100 s contributes to the long wave energy inside the port, for the direction tested. For wave periods of approximately 100 s and greater, a gradual increase of the energy inside the port due to reflection off the beach was apparent. This has been attributed to the characteristics of the longer waves. Longer waves reflect, refract and diffract more than shorter waves; hence the removal of the beach has a greater effect in reducing the longer wave energy. This concept was shown in Figure 8-12.

The free long wave test revealed an interesting difference between bound and free long waves. The results showed that for two specific period intervals energy was reduced inside the port. This case was further investigated using a white noise spectrum in Section 9.4.3 which revealed that the slight change in celerity of the free long waves compared to the bound wave resulted in the incident long wave resonating out of phase with the reflected wave component.

The wave penetration tests have given a better understanding of the effects of the beach south of the port and how the orientation of the beach, port entrance and main breakwater contribute to long wave energy inside the port. Use of simultaneous measurement for the outside and inside of the port allowed for accurate calibration of the model and incorporation of the wave groups; unfortunately as only one measured storm event was available a broader test including multiple events was not possible. Instead the use of the single event for the tests was aimed at identifying trends and ruling out any unexpected phenomena. In Chapter 9 a white noise approach has been followed which is more generic and robust allowing for another broader investigation to the long wave penetration mechanisms. Other limitations, due to the use of the measured surface elevations, water levels and unidirectional wave input, are noted in the model setup Section 8.3.

9. CHARACTERIZING PORT RESONANCE – WHITE NOISE SIMULATION

9.1. Introduction

The data analysis and wave penetration investigation in Chapter 7 and 8 offered in-depth insight into the origin of the long waves, the excitation of the port due to long waves, and an indication of how the waves enter the port. The data analysed and events modelled, although typical, do not necessarily represent all events. A more generic white noise simulation approach is applied here in order to identify and confirm all the resonance frequencies of the port. This approach adds more confidence to the preceding two chapters as it will confirm existing resonance periods. It does not rely on specific input data which could contain existing energy peaks that could have forced less characteristic resonance periods and missed others.

As no measurements were necessary to define the input conditions for the white noise simulation the model could be simulated for an extended period of time. The extended period of time allowed the spectral analysis of the results to be performed on a much larger output data set than was previously possible. Hence, a higher resolution spectrum with a greater degree of confidence could be obtained.

Furthermore, the white noise simulations were used in order to aid in the analysis of the results shown in Chapter 8 as mentioned under the investigation of the beach reflection test in Section 8.5.2.

Thus this Chapter addresses two more objectives:

1. Identifying the resonance frequencies of the port
2. A comparison of the resonance frequencies in the port during its construction phase and the final layout*

*Over the thesis progression the bund present during the construction phase was removed; Figure 9-1 shows a construction stage and completed port view indicating the removed bund. The vessel instabilities persisted with the completed port layout and hence it was deemed of little use to compare the layouts using a white noise simulation, thus the objective was dropped as it was no longer relevant. Additionally, there were no simultaneous measurements available of when the bund was present.

Figure 9-1: Construction Layout and Final Layout on left and right respectively.

9.2. Modelling Approach

9.2.1. White Noise Simulation

The white noise approach involves forcing the boundary of a Boussinesq wave model with a flux generated from a white noise spectrum. A white noise spectrum is characterized as having equal amounts of energy at every period in a defined frequency range. In this study, the white noise spectrum frequency range was set between 30 and 1000 seconds. This is equivalent to propagating waves of every defined period into the model domain in one run. Although this is a synthetic exercise it has the following advantages when considering long wave resonance in a port:

- By analysing various areas in the port it is possible through spectral analysis to identify the resonance periods of the port.
- The method also allows for reduced run times as many wave periods are included in one run.
- No long wave measurements are required for this approach.

It is important to realize that the white noise spectra represents a synthetic sea state and for that reason may only be used to indicate potential resonating frequencies.

The white noise modelling approach has been well documented and used successfully to identify port resonance, e.g. (Kofoed-Hansen et al., 2005) and (Gierlevsen et al., 2001), also detailed in Section 3.3.2.

9.2.2. Band-pass Filtering

In order to visualize and gain better insight into the factors driving resonance in the port certain period intervals have been looked at more closely. By band-pass filtering the output files from the white noise simulations it is possible to look at the long wave energy in specified period intervals. This technique allows for the visualization of the position of nodes and anti-nodes, as well as the surface elevations, for specific period intervals.

9.3. Model Setup

The white noise simulation model was kept as similar as possible to the validated model described in Chapter 8. The only difference between the models was the wave input described below.

Random wave input was created from a one dimensional white noise spectrum. The input energy density was set at $0.1 \text{ m}^2/\text{Hz}$ for a period interval between 30 s and 1000 s. The waves were input as unidirectional waves from the average mean wave direction of 150° . The theoretical input spectrum has been indicated on the spectral results shown in Figure 9-2, below.

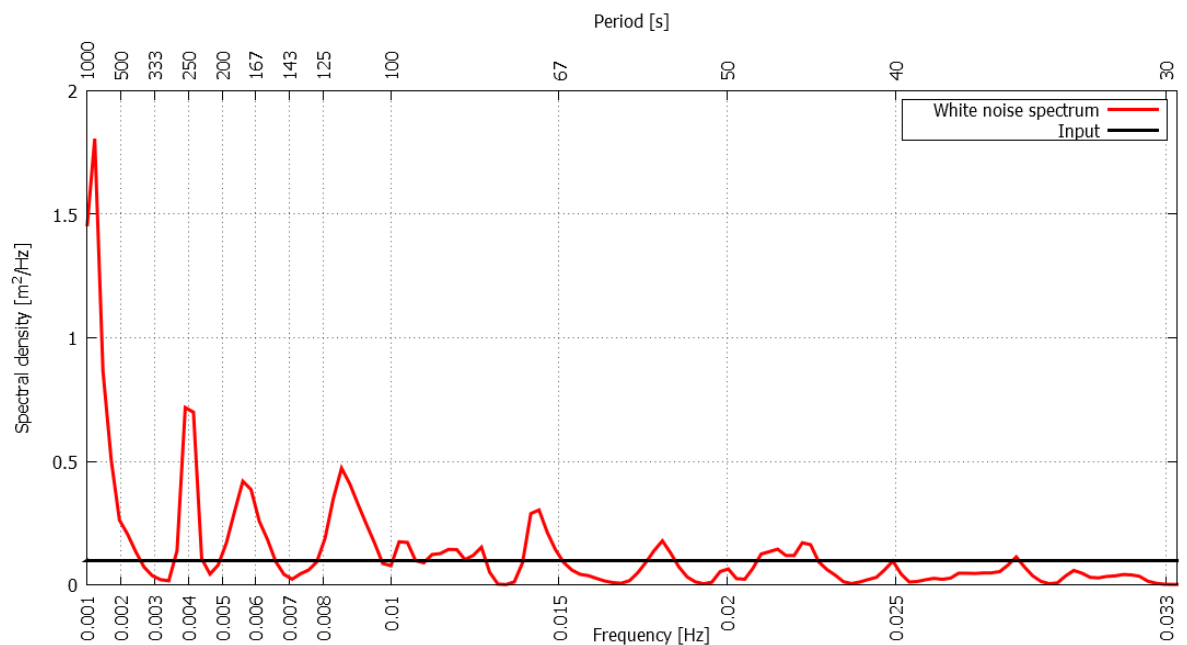
A model duration and wave input duration was set at 12 hrs. As mentioned in the introduction this duration allows for increased resolution and confidence in the output spectrum. The duration is also in accordance with recommendations for modelling long waves with Boussinesq models (Ota et al., 2010).

9.4. Results

9.4.1. Base Case - White Noise Simulation

Figure 9-2 shows the output spectrum for the white noise simulation. The time series used for the spectral analysis was outputted from the position of the long wave recorder inside the port. The following resonance period intervals are clearly defined: 42 s to 49 s, 52 s to 58 s, 67 s to 71 s, 85 s to 105 s, 115 s to 125 s, 155 s to 200 s and 240 s to 260 s. A comparison of the white noise results and the resonance period intervals identified from the measurements is included in the Quasi-Validation section below.

Figure 9-2: Long wave spectrum from white noise simulation, positioned at Long Wave Recorder, inside the port basin.



9.4.2. Quasi-Validation

As mentioned in Section 9.2.1, the white noise approach is synthetic, and hence validation of the results with measurements of an actual sea event will give inconclusive results. Therefore the calibrated model used in “Identifying Long Wave Penetration Mechanisms” (documented in Section 8.4) was used, and hence the model may already be assumed to be calibrated. However, for thoroughness, a quasi-validation has been adopted to further investigate the white noise results.

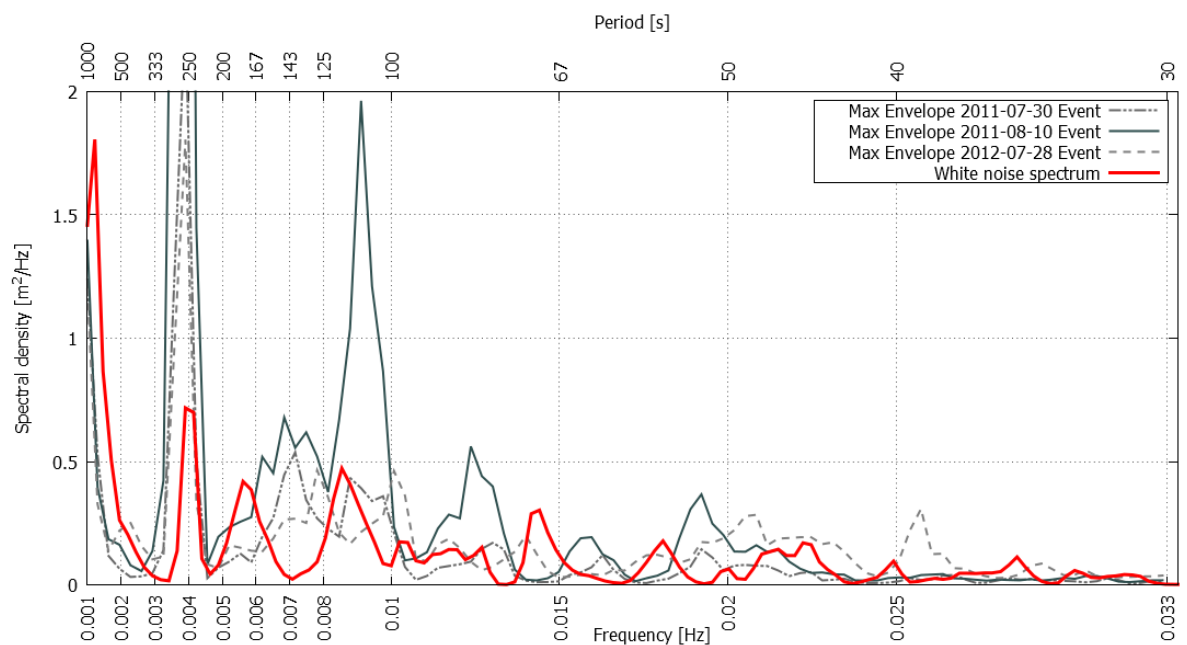
The quasi-validation approach equates to a comparison between the white noise long wave spectrum and the maximum spectra envelopes for three events. The three events have already been analysed in Section 7.4.2. Each event represents a fairly significant storm event with the 10 August

2011 event representing the largest storm event of the three. By taking the maximum spectra envelope for each event all the resonance frequencies of the port during a storm event are visible.

Comparing the white noise results to the maximum spectra envelopes is a cursory approach because there is no proof that the events are typical, and the approach does not account for the non-linearities created by wave-wave interactions more prevalent in larger wave conditions. However, by general inspection of the measured spectra outside the port during the events (also shown in Section 7.4.2) it appears to be an acceptable comparison as the spectra are fairly uniform, with no specific energy spikes.

Thus Figure 9-3 shows the quasi-validation comparison:

Figure 9-3: Long wave white noise results spectrum vs. long wave maximum spectra envelopes for three events.



In general the white noise spectrum (red) has lower energy than the three event envelopes which is expected because the events were high energy events and the event spectra (grey) represent the maximum energy in each frequency over an entire storm duration.

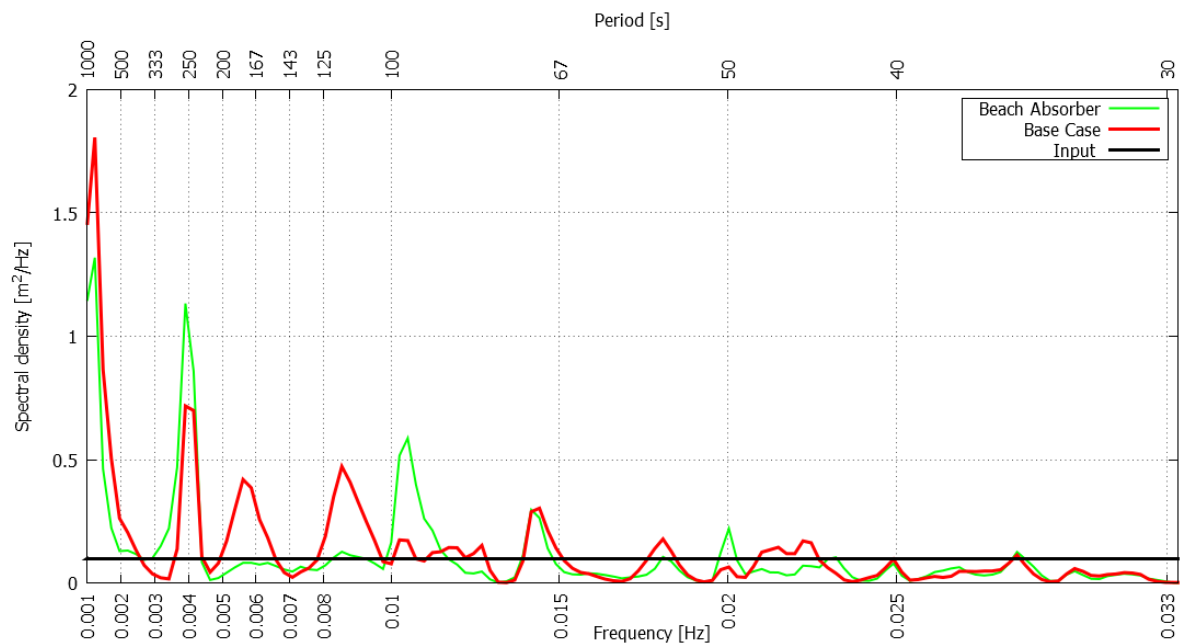
Encouragingly, the strongest two resonant modes viz. ~ 800 s and 250 s are shared by all the events and the white noise simulation. The third and fourth highest peaks lie within an energetic period shared by the three events between 100 s and 200 s. The remaining white noise resonance peaks do not look unnatural in regards to the variability displayed by the event measurements; it also appears that no significant resonant mode shared by all the events is missed in the white noise simulation. Thus the quasi-validation adds another degree of confidence to the white noise simulation results and logically to the identification of the resonance mechanisms as well.

9.4.3. Beach Reflection Test - White Noise Simulation

As the white noise simulation resulted in fairly robust results similar to actual events it was decided that a similar beach reflection test, as was performed in Section 8.5.2, should be executed. As with the initial beach reflection test, the model was identical to the base case, except that the beach south of the port was replaced with a sponge. The beach sponge in comparison with the base case sponge is shown in Figure 8-4.

Figure 9-4 shows a comparison of the long wave spectra at the position of the LWrec inside the port. The red spectrum shows the base case as detailed in Section 9.4.1, the green spectrum shows the beach reflection test. The expected result was a gradual increase in the reduction of wave energy starting with waves with periods of approximately 100 s as was the case with the Beach Reflection test in Section 8.5.2. Surprisingly, two period intervals bucked the trend and actually increased in energy. The two period intervals may be identified where the green spike is greater than the red spikes viz. 85 s to 105 s and 245 s to 260 s.

Figure 9-4: Long wave spectra comparison, normal white noise case vs. beach absorber white noise case, also white noise input spectra.



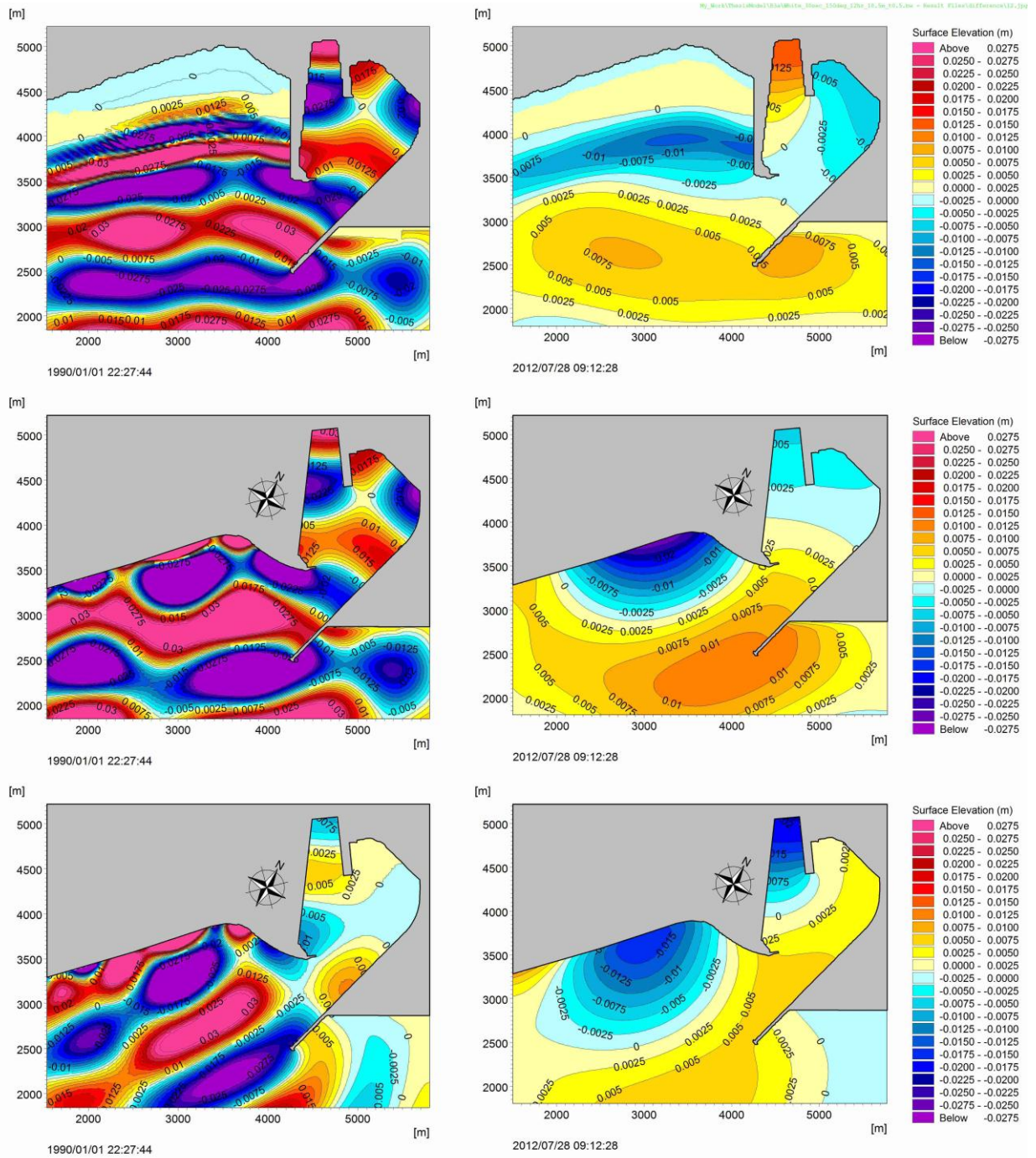
In order to investigate the unexpected results, a similar post processing methodology to that used in the first beach reflection test was performed. The results of this test may be viewed in Figure 9-5. The left panes of the figure show the surface elevations at the same instant for the band-pass filtered long waves between 85 s to 105 s. The right hand panes show the band-pass filtered surface elevations for the same instant for long waves between 230 s and 270 s. By subtraction of the Beach reflection case from the Base Case the reflected wave component has been localized. Thus the

incident (no reflection), incident and reflected and isolated reflected waves are shown in the upper, centre and lower panes respectively.

Through a close inspection of the surface elevations in the vicinity of the LWrec, the reason for the surprising results becomes clear. In the top pane showing only the incident wave, the surface elevation is positive; whereas, in the lower pane the reflected wave component surface elevations are negative. This discrepancy indicates that the reflected wave components for the two period intervals actually resonate out of phase with the resonance of the incident waves. The out of phase resonance has the effect of reducing the energy for the specific period intervals in which it occurs

A further observation regarding these results is that the white noise approach is synthetic and includes no short wave energy; hence, the test should actually be regarded as a free long wave test with a beach absorber. This is important to note when considering the results of Free Wave Test in Section 8.5.3. The results in the free wave test revealed an unexpected reduction of energy for the same two period intervals investigated above. With the help of Figure 9-5, below, it is clear that the reason for the energy reduction is out of phase resonance of certain reflected wave components. Furthermore, the reduction only occurs for free long waves because the free long waves travel at a slightly faster celerity in comparison with the bound long waves. This slight change in celerity initiates the out of phase resonance.

Figure 9-5: Out of phase resonance between reflected and normal wave components. All panes show instantaneous surface elevation. Left column: 85 s to 105 s. Right column 230 s to 270 s wave. Upper: Incident waves (no reflection), Centre: Incident and reflected waves, Lower: Isolated reflected waves.



9.4.4. Band-pass Filtering

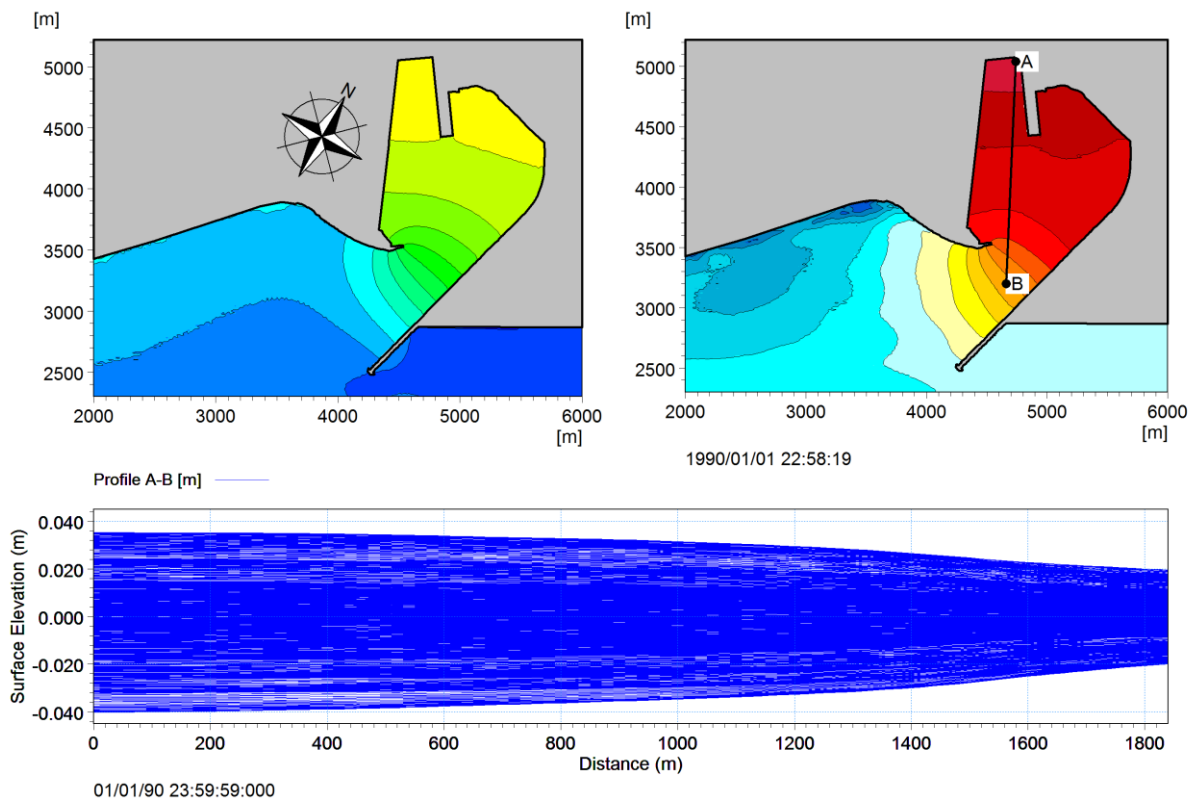
In order to visualize and gain better insight into the factors driving resonance in the port the resonance period intervals have been looked at more closely. By band-pass filtering the surface elevation output files from the white noise simulation, it is possible to look at the long wave energy and surface elevation in specified period intervals. This technique allows for the visualization of the position of nodes and anti-nodes as well as the surface elevations for specific period intervals.

Figure 9-6 to Figure 9-13 show, in the left panes, the position of long wave energy in the port vicinity for specific period intervals identified from the white noise spectrum (see Figure 9-2 above). In the right panes, a snapshot of the instantaneous surface elevation corresponding to the same period interval is shown. The lower pane of each figure shows a surface elevation envelope corresponding to the section indicated on the surface elevation plot above. All the energy plots are to the same scale, warm colours are high energy and cold colours show less energy. All the surface elevation plots are also to the same scale, warm colours indicate a rise in water surface and cold colours a drop below the mean water level. The long wave energy panes on the left of each figure indicate the position of nodes and anti-nodes. The surface elevation panes on the right of each figure show the synchronization of the nodal pattern; the contrast of warm and cool colours shows which anti-nodes are above the mean water level when the others are below the mean water level.

9.4.4.1. 820 s - Long Open Basin - Helmholtz Mode

Figure 9-6 shows the entire harbour basin as an anti-node and the surface elevation envelope confirms a nearly uniform rise and fall of the surface elevation inside the basin. Hence this resonance period is defined as the Helmholtz mode.

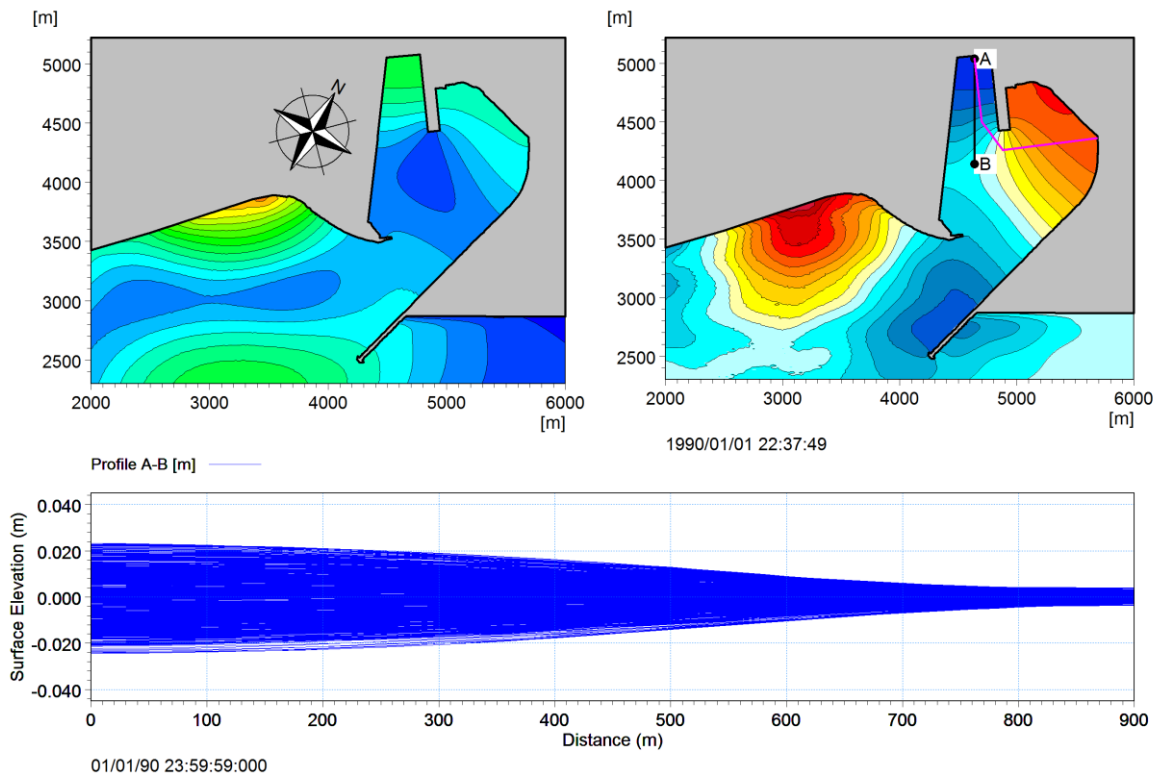
Figure 9-6: ~820 s - Long Open Basin - Helmholtz –. Left: normalized long wave energy, Right: surface elevation, Lower: surface elevation profile envelope.



9.4.4.2. 230 s to 270 s - Short Open Basin coupled with Short Closed Basin

Figure 9-7 shows the 230 s to 270 s resonance interval driven by two mechanisms acting together; the “fundamental mode” of an open ended basin coupled with the “fundamental mode” of a closed basin. The open basin mechanism is driven simply by the length of the rectangular shaped basin enclosing the D100 and D101 berths which corresponds approximately to a quarter of a wave length (axis shown by profile A-B). The anti-node positioned at the top of the basin is further amplified by a coupling with the fundamental mode of a closed basin mechanism. The secondary mechanism resonates a half wave length between the top of the D series basin and the spending beach positioned at the eastern side of the port (axis shown by curved magenta line). The two mechanisms resonate in sync with one another i.e. as the surface elevation within the rectangular basin rises it is driven by both mechanisms and vice a versa.

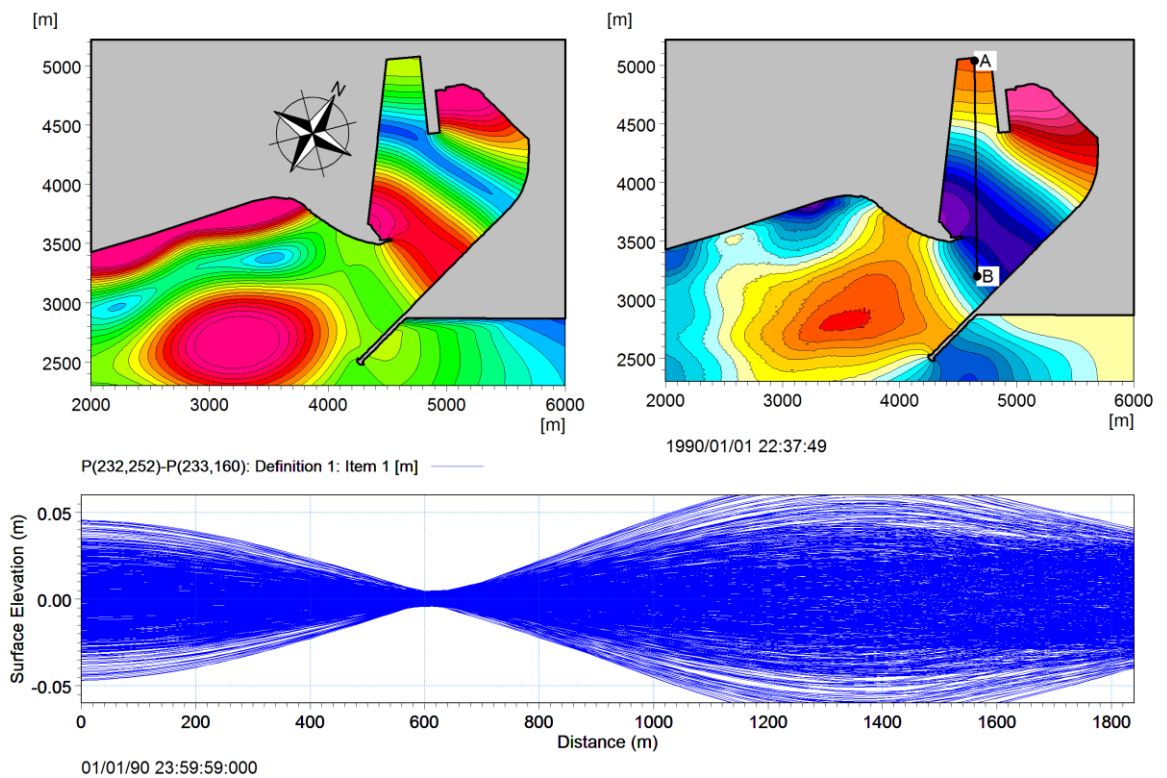
Figure 9-7: 230 s to 270 s - Short Open Basin coupled with Short Closed Basin – Fundamental Modes. Left: normalized long wave energy, Right: surface elevation, Lower: surface elevation profile envelope.



9.4.4.3. 155 s to 200 s - Long Open Basin - Mode 2

Figure 9-8 shows the 155 s to 200 s resonance interval which corresponds to the second mode of a closed basin. The port acts similarly to a rectangular basin with an anti-node at the top of the port and a second anti-node positioned just within the entrance of the port (axis shown by the straight black line). The actual shape of the port and presence of the bulk terminal jetty, splitting the spending beach and container berths, focuses the anti-node energy on the spending beach rather than in the rectangular shaped basin enclosing the D100 and D11 berths.

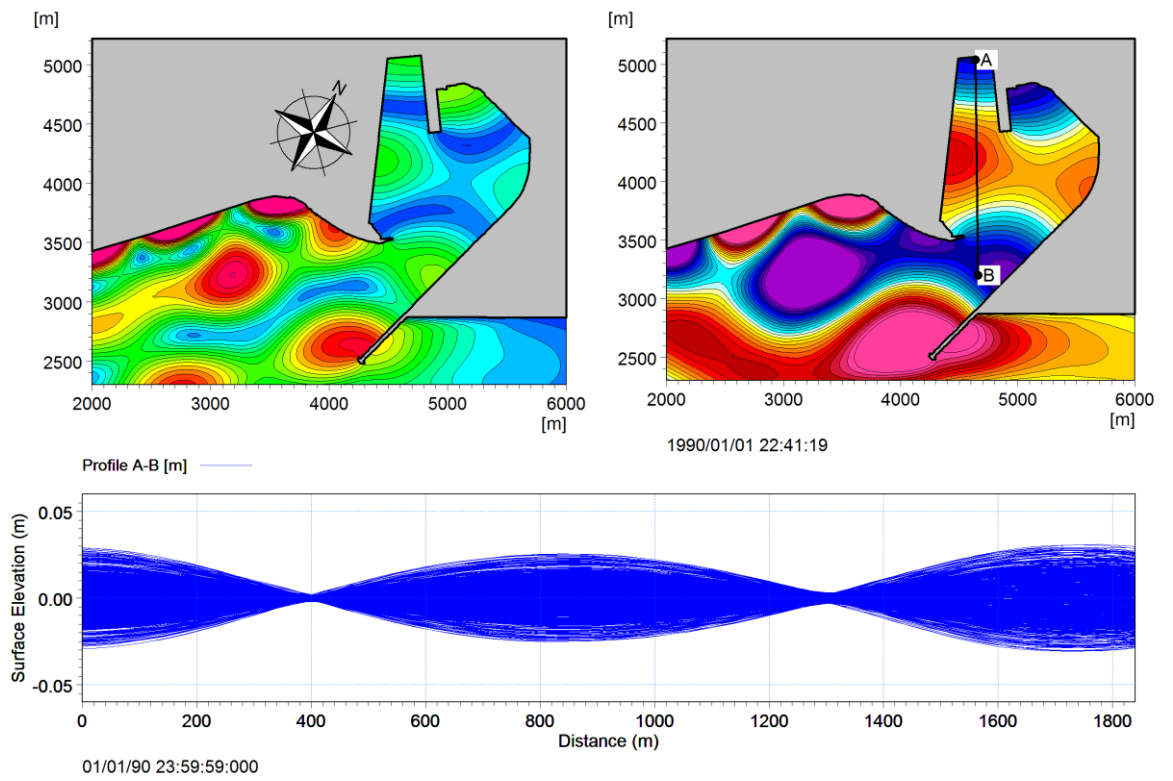
Figure 9-8: 155 s to 200 s - Long Open Basin - Mode 2. Left: normalized long wave energy, Right: surface elevation, Lower: surface elevation profile envelope.



9.4.4.4. 115 s to 125 s - Long Closed Basin Mode 2

Figure 9-9 shows the 115 s to 125 s resonance interval which corresponds to the second mode of a closed basin, this mode is indicated by profile A-B. Three anti-nodes are present along the profile line A-B.

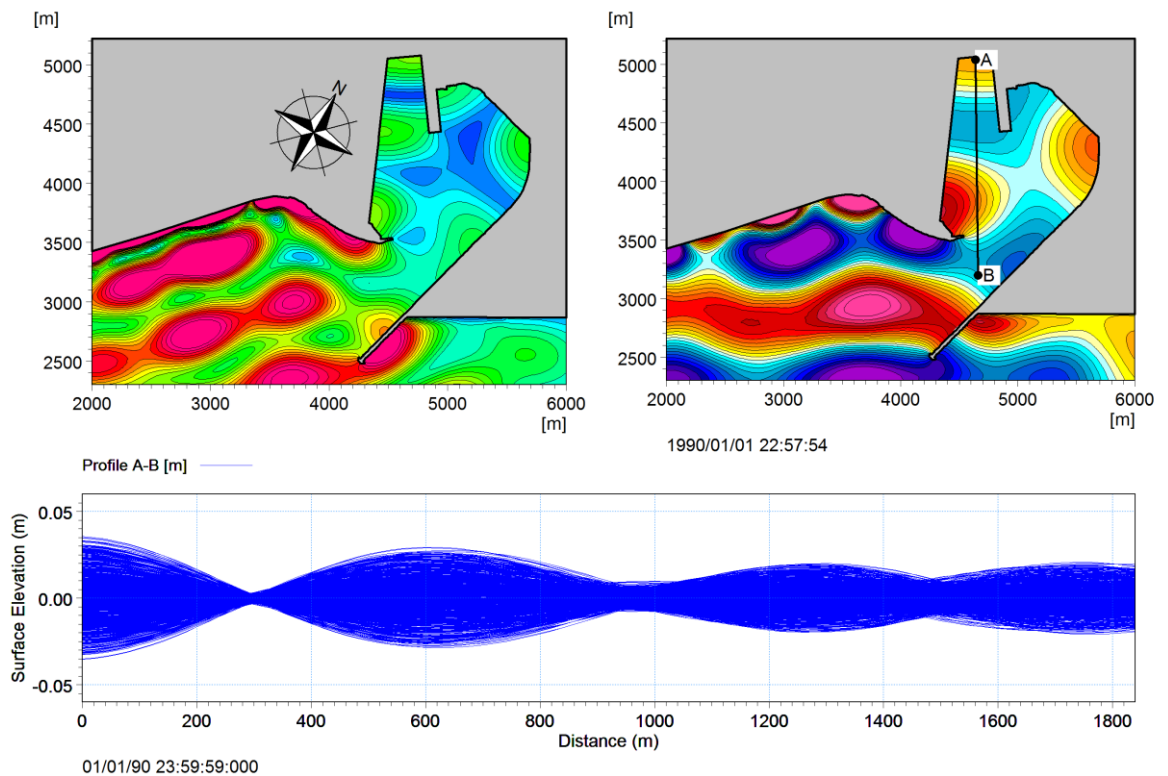
Figure 9-9: 115 s to 125 s - Long Closed Basin – Mode 2. Left: normalized long wave energy, Right: surface elevation, Lower: surface elevation profile envelope.



9.4.4.5. 85 s to 105 s Long Closed Basin Mode 3

Figure 9-10 shows the 85 s to 105 s resonance interval which corresponds to the third mode of a closed basin; this mode is indicated by profile A-B. Four anti-nodes are present along the profile line A-B.

Figure 9-10: 85 s to 105 s - Long Closed Basin - Mode 3. Left: normalized long wave energy, Right: surface elevation, Lower: surface elevation profile envelope.



9.4.4.6. < 71 s - Higher Modes

Figure 9-11 to Figure 9-13 show various higher modes acting in the predominant rectangular basin as shown by profiles A-B. The surface elevation envelopes show that even though the modes are fairly high, and hence the energy more spread out, the three sided enclosed basin in the vicinity of the D berths defines the nodes clearly within the basin.

Figure 9-12 and Figure 9-13 show a coupling of the longitudinal basin higher modes with the fundamental mode of a closed basin in the transverse direction at approximately 56 s. This leads to the diagonal antinodes present at the top of the rectangular basin.

Figure 9-11: 67 s to 71 s - Long Open Basin - Mode 4. Left: normalized long wave energy, Right: surface elevation, Lower: surface elevation profile envelope.

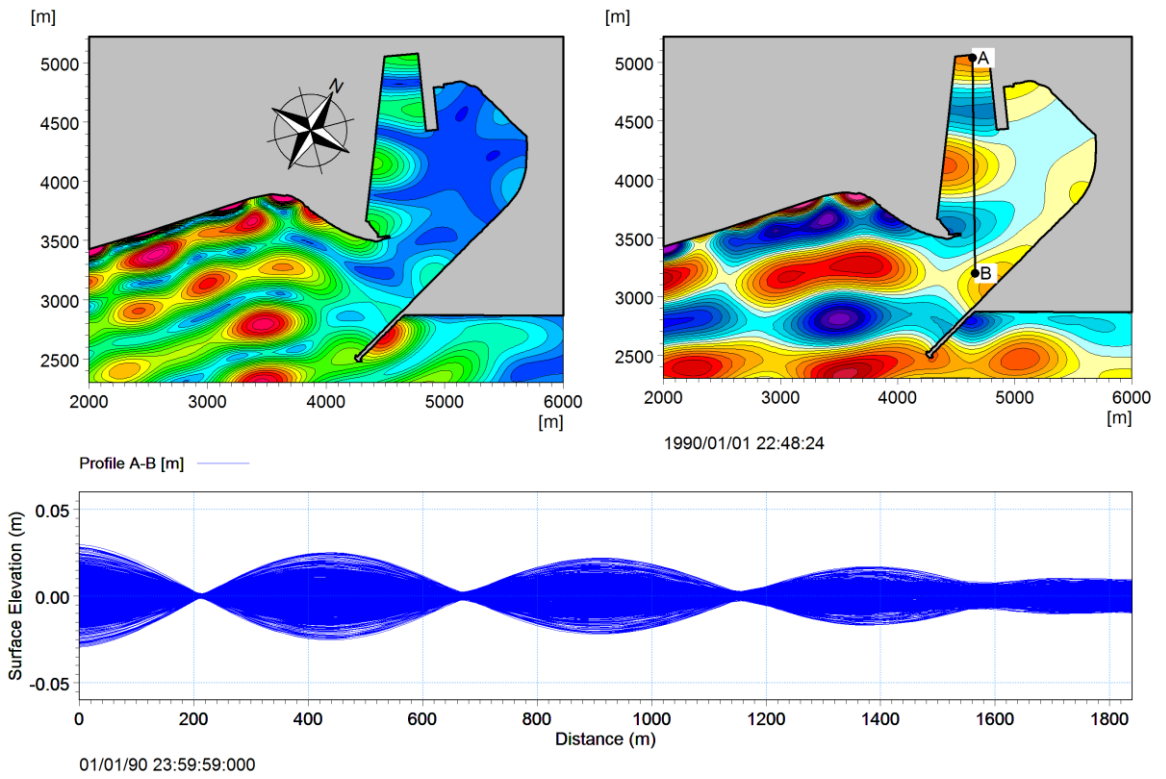


Figure 9-12: 52 s to 58 s - Long Open Basin - Mode 5. Left: normalized long wave energy, Right: surface elevation, Lower: surface elevation profile envelope.

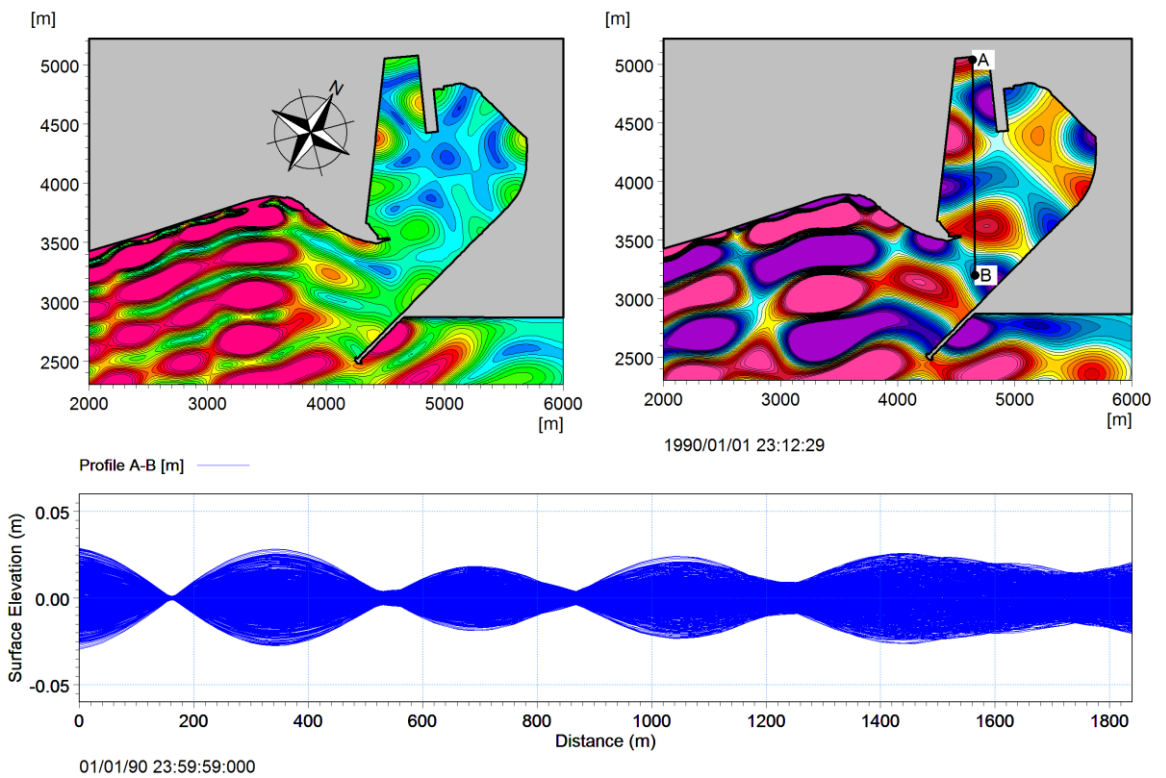
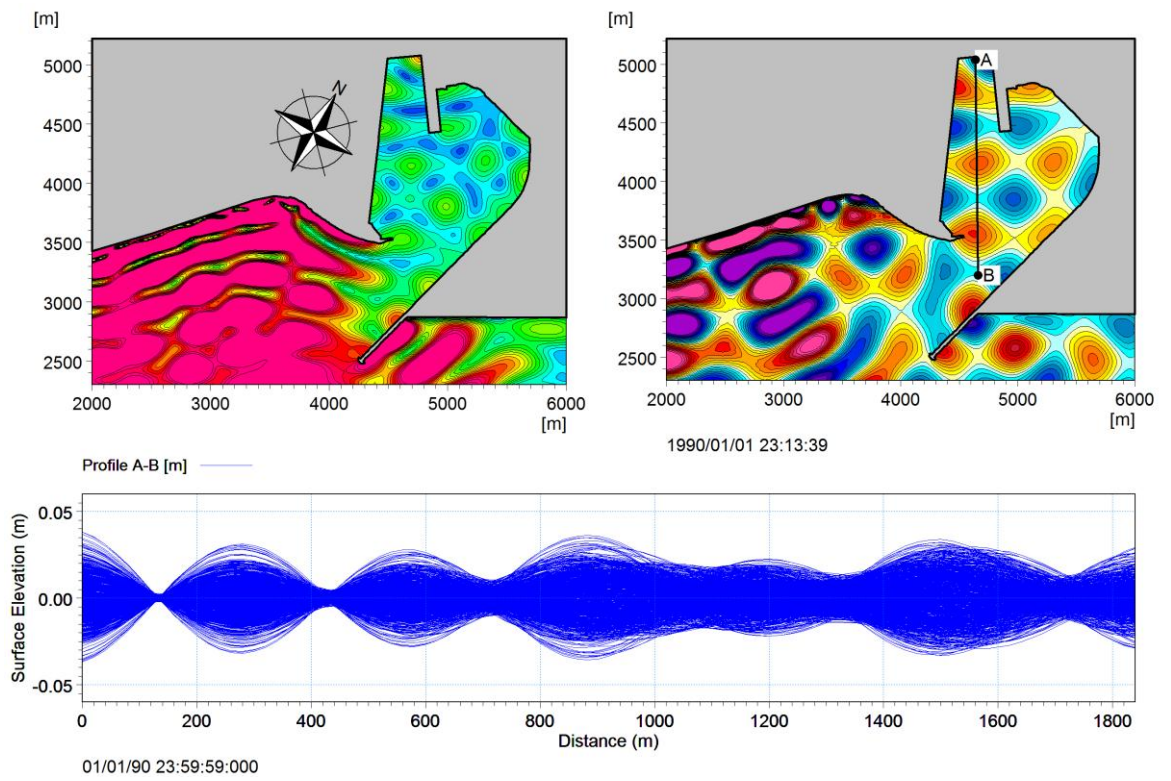


Figure 9-13: Long Open Basin - Mode 6 – 42 s to 49 s. Left: normalized long wave energy, Right: surface elevation, Lower: surface elevation profile envelope.



9.4.5. Conclusions and Summary

In comparison with the previous data analysis and wave modelling, in Chapters 7 and 8, the white noise simulations have added a more generic and robust method for investigating the propagation of long wave energy at the port.

A quasi-validation of the white noise results showed strong similarities with actual events inside the port therefore increasing the confidence in the white noise simulation and subsequent identification of the resonance mechanisms.

The similarity of results with actual events is attributed to the fairly uniform long wave spectra, outside the port (identified in the Data Analysis Section 7.4.2), which is similar to the uniform white noise input spectrum. The strong influence of the port geometry on resonating particular wave periods also contributes to the positive results.

A beach reflection test performed with the white noise spectrum helped to clarify results from the Free Long Wave Test in Section 8.5.3. Out of phase resonance of the incident wave component with the reflected wave component off the beach south of the port was identified as influencing the results. It was determined that the out of phase resonance was a result of “freeing” the long waves and hence changing the celerity of the incident long waves slightly. It should be noted that in the case of the port of Ngqura the out of phase resonance does not occur naturally because the incident long waves are bound. The result shows the importance of in-depth understanding of the site and promotes a cautious approach when using white noise simulations.

Band-pass filtering of the 2D output files from the white noise simulation provided visualizations of the various geometric mechanisms driving resonance inside the port. All the modes identified in the band-pass filtering agreed well with hydrodynamic theory. In general, the port acts as a rectangular basin; this is driven predominantly by the small rectangular basin partially enclosing berths D100 and D101, and the continuation of the quay wall toward the entrance. Coupling of the predominant rectangular basin mechanism was evident for specific resonance periods when the port also acted as a closed basin with an anti-node positioned at the base of the main breakwater.

Although idealization of the mechanisms allows for a useful simple understanding of the processes, the complex shape of the port makes generalizing the geometric mechanisms difficult. In particular, because of the diagonal orientation of the main breakwater with the rectangular shaped port, there are times when the long basin can act as either an open or closed basin, depending on the length assumed for the basin.

The surface elevation envelopes have shown, in the band-pass filtering results well defined nodal patterns, particularly in the vicinity of the container berths D100 and D101. It is hypothesized that it

is the presence of these nodes, and the strong horizontal currents associated with them, which are the drivers of the excessive vessel motions mentioned in Chapter 5. The main conclusion continues this observation with an overall comment on the vessel motions at the port.

10. CONCLUSIONS

10.1. Introduction

The main objective of this thesis was to characterize long wave agitation in the port of Ngqura.

A review of literature revealed the complexity surrounding the processes required for the generation of long waves. Although there are some accepted general theories regarding the generation and propagation of long waves there is still much that is not understood, in particular the transformation of energy between the high and low frequencies within the surf zone is complex. The radiation of this released and created long wave energy from the surf zone seawards and landwards, coupled with reflections of long waves from the shoreline, provides further complexity. Understanding and quantification of these processes is under development.

A large portion of the literature review was devoted to assessment of the conclusions and historical methods used to characterize long waves on the South African coastline and in its ports. Historically, ports on the western coast of South Africa have suffered from the effects of seiching created by long wave resonance. Two generation mechanisms were identified; higher period resonance (over 15 min) was correlated with frontal storms (resonant air-water coupling) while lower period resonance (30 s to 6 min) was observed whenever there was presence of high swell.

The literature review also collated recent work performed on numerical modelling of long waves with the use of Boussinesq wave models. Many of the techniques documented were used in the latter half of this study.

10.2. Long Wave Characteristics and Generation Mechanism

An in-depth analysis of wave measurements, both inside and outside the port, was used to initially characterize long waves at the port. The data analysis showed that the long wave heights outside the port were correlated to the coincident short waves. On average the significant long wave heights were 8% of the short wave heights. This correlation and a close inspection of direct time series comparisons suggests that the majority of the long wave energy is linked to the short wave energy; hence it may be termed as bound long waves with an un-quantified component resulting from reflections off the beach and generation in the surf zone. The contribution of the reflected wave component from the beach south of the port was identified in the measurements by identification of tidal modulation of the significant long wave heights both outside and inside the port.

The generation mechanism for the long wave energy between 30 s and 300 s, for two events, was attributed to fairly typical weather patterns off the coast of South Africa. These typical weather patterns create sea storms and generate the short waves which in turn form wave groups and the

stresses associated with creation of bound long waves. From this analysis and the constant correlation of long and short wave energy found in historic measurements it is hypothesized that the long wave generation mechanisms are always sea storms. The wave breaking and nearshore processes occurring on the beach south of the port are also attributed with creating long wave energy that propagates into the port.

10.3. Long wave Penetration Mechanisms

The data analysis showed on average the significant long wave height inside the port was 90% of the significant long wave height outside the port. A Boussinesq model was calibrated in order to investigate how long waves penetrate into the port. The tests, based on one event, confirmed that long waves enter the port partially by direct diffraction around the main breakwater and partially by reflection off the beach south of the port.

The beach south of the port reflects long waves into the port directly, by diffraction and by subsequent reflection off the lee side of the main breakwater. Moreover the longer wave energy above ~100 s wave period was found to reflect and propagate into the port more effectively than the shorter waves. This result showed that the shorter period long waves enter the port predominantly by diffraction and the longer period long waves enter by a combination of diffraction and reflection. These trends are expected to vary depending on the incident wave direction.

An investigation into the effects of propagating free long waves into the model highlighted that at certain periods an out of phase resonance occurred between the incident and reflected waves. The corollary of the test proves that, at least for the wave periods exhibiting out of phase resonance, the energy in reality is bound to the short wave groups before entering the port.

10.4. Port Resonance

White noise simulations offered another perspective on the penetration mechanisms and allowed for a robust test of the penetration model. The white noise simulation compared well with measurements and the wave penetration models. Band-pass filtering of the model results identified the position of the nodal patterns for specific resonance periods; this helped clarify how the port geometry contributes to each resonance period. Figure 10-1 below, shows the predominant axes of resonance inside the port.

The predominant resonance periods found in the port are as follows:

42 s to 49 s, 52 s to 58 s, 67 s to 71 s, 85 s to 105 s, 115 s to 125 s, 155 s to 200 s and 240 s to 260 s

10.5. Excessive Vessel Motions

In lieu of a vessel motion study and in the absence of any detailed measurements recorded during a vessel motion event the following high level link to vessel motions is hypothesized.

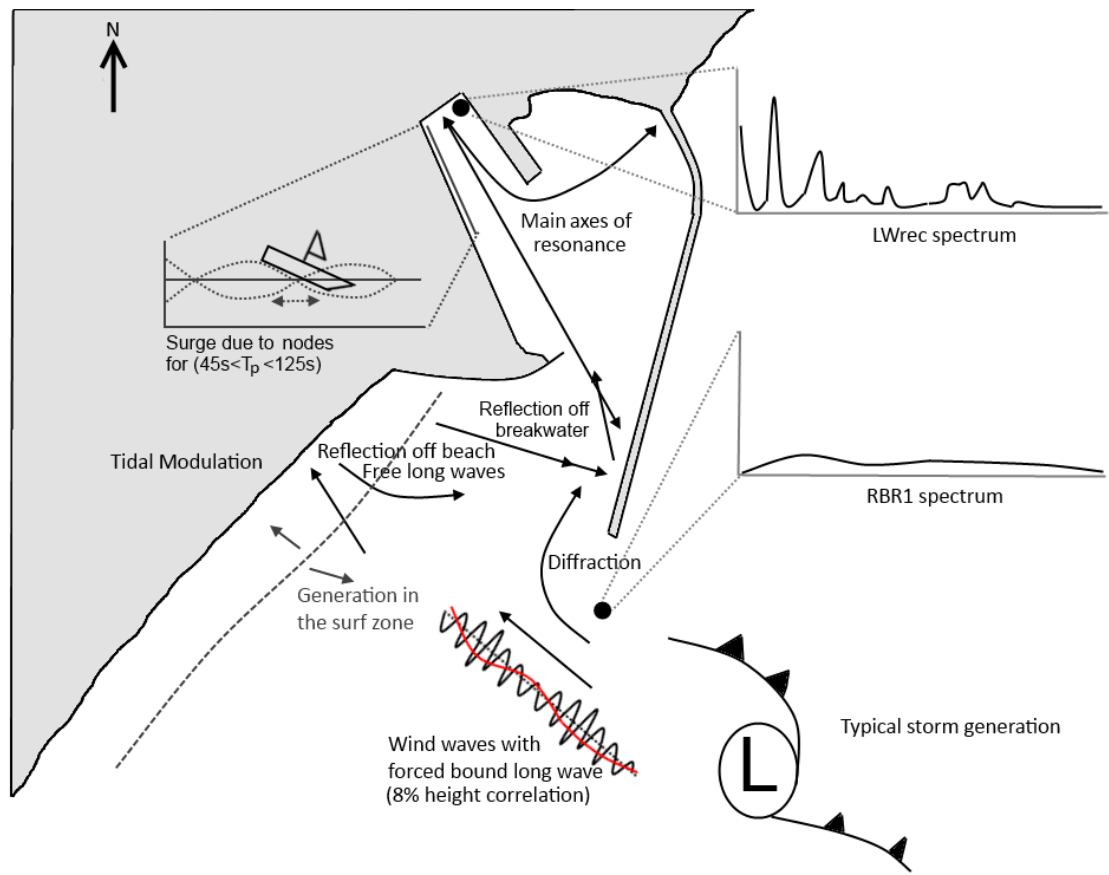
Anecdotal evidence (Table 6-2), states that the predominant vessel motion creating problems is surge which is typically the problem motion for container vessels due to container crane limitations. Moreover, the surge motions are likely to be the result of the vessels positioned over nodes which are characterized by strong horizontal current velocities (see Chapter 5). Through an examination of the surface elevation envelopes in Chapter 9, the position of nodes can be identified. The nodes are present at the berth for resonating waves with periods between 45 s to 125 s. This period range sits in the middle of the typical problem range for vessel motions of between 30 s and 300 s. Although the precise natural period of the vessels is not known, and will vary depending on mooring setup and vessel type, this correlation of wave resonance, node vicinity and mooring resonance is likely to create problems for vessel motions whenever the long wave energy rises above a general height threshold.

From the results already concluded, the correlation of long wave energy to short wave energy is clear, and spectral analyses have shown the energy to be fairly uniformly spread over the 30 s to 300 s period range outside the port. Thus it is likely that no unique generation event is creating the vessel motions but rather that the vessel motions will occur during times of high swell.

Thus in regard to the long wave height threshold, parametric wave height data recorded during two occurrences when vessels parted their lines (2010-04-23 & 2012-08-08), shows during both events that a significant short wave height of ~3 m with a peak period over 10 s occurred. Using the average correlation of 8% shows the significant long wave heights to be in the vicinity of 0.25 m outside the port. Figure 7-2, shows that the long wave height exceedence for 0.25 m is ~2%. It is noted however that downtime may start occurring for smaller wave heights and hence occur more frequently than these extreme events. Maritime guidelines (Puertos del Estado, 2003) recommend that downtime does not exceed 2% for a container port; hence it is unsurprising that the port is subject to complaints from its users.

Figure 10-1 which follows shows an annotation summary of the study.

Figure 10-1: Conclusion annotation summary.



11. RECOMMENDATIONS

With regard to the position of the Long Wave Recorder, the general position seems well sited. The recorder is near the berths of interest and is positioned where anti-nodes will occur, hence modes of resonance will not be missed. It would be best to have the recorder some meters away from the walls and 100 m away from the revetment to avoid local reflection and shoaling effects.

With regards to prevention of the practical problem experienced by the port during long wave induced ship motion events, some ideas on potential mitigation mechanisms are suggested below:

- The first and probably cheapest solution is to develop a long wave prediction system which becomes a part of the port management. Dangerous accidents can hence be avoided by leaving the berth or by adopting alternative moorings when high long waves are predicted. Vessels may also be requested to slow steam to avoid poor conditions. At the simplest level, problematic long waves should be expected when the short wave significant height is above 3 m. A more complex system would make allowance for wave direction, tidal level and short wave period.
- Another alternative is to implement different mooring lines and setups in order to move the natural frequency of the moored vessels out of the range of the port resonance frequencies, identified in Chapter 9. This should be based on at least a high level vessel resonance assessment and the results of this study. There is merit in attempting this approach as up until now only soft/flexible moorings have been used. When using stiffer moorings the resonance period of the vessel mooring system will decrease, hopefully below the higher energy bands identified above 90 s. It should be noted that the designers of the port identified long waves as a downtime issue and defined stiff moorings using Dyneema lines to counteract them (PRDW, 2002). This aspect of PRDW's design seems to have never been implemented at the port.
- Where the first two recommendations do not aid in prevention of the problem, more elaborate solutions would involve the use of advanced mooring systems (Moormaster or similar), or changes to the port infrastructure. Both of these options would require an advanced vessel motions study and resonance tests before implementation.

With regards to the academic progression of this study a number of interesting and useful areas of further research arose which were unfortunately beyond the already broad scope of this study. They are briefly described below:

- The most obvious next step is to recreate an excessive vessel motion event. The models in this study could provide the wave inputs to be coupled with an appropriate vessel motion

model. This would require wave measurements recorded during an event, a detailed description of the vessel and moorings and preferably measurements from on the vessel.

- Using the calibrated Boussinesq wave model to test basic wave inputs created from parametric data and a JONSWAP spectrum. If the results compared well with the models in this study, which were input with surface elevations, many new scenarios could be tested with confidence and without the long wave records.
- A better understanding of the effects of the breaking process and beach on creation of the long wave energy. This is a large topic which is still developing often with the help of complex numerical models however the following two tests would be interesting and practical.
 - The splitting of the measurement record outside the port into reflected and incident wave components. This will require a new measurement campaign with an array of pressure reading instruments or at least an ADCP instrument (with advanced post-processing techniques). One pressure reading cannot be used.
 - Secondly the use of a Boussinesq wave model as a 2D flume (in order to simplify and reduce the domain size) where the full functions of the model including breaking and a moving shoreline can be set to task. With results from these tests the effects of tidal modulation and effect of the near-shore processes could be investigated (this would require full beach profile measurements).
- An analysis on the effects of wave grouping of the long wave heights.
- Improved representation of wave groupiness in the numerical model input.

12. REFERENCES

- Baldock, T. E. & Huntley, D. A., 2002. Long-wave forcing by the breaking of random gravity waves on a beach. *Proc. R. Soc. Lond. A*, Volume 458, pp. 2177-2201.
- Botes, W. A. M., Russel, K. S. & Huizinga, P., 1982. *Resonance in South African Harbours*. Cape Town, ICCE.
- Botes, W. A. M., Russel, K. S. & Huizinga, P., 1984. *Model Harbour Seiching Compared to Prototype Data*. Texas, ICCE.
- Council for Science and Industrial Research, 2008. *Module W03-2 : Numerical and physical modelling (including ship motions): WEEK 5 & 6 – Lecture 6. Unpublished class notes*. Stellenbosch: s.n.
- Darbyshire, J. & Darbyshire, M., 1964. Range Action in Table Bay Harbour. *South African Journal of Science*, pp. 173-182.
- de Bont, J., 2009. *Validation of a numerical model for motions of ships moored with MoorMaster units, in a harbour under the influence of ocean waves*. Msc. thesis. s.l.:Delft University of Technology.
- De Jong, M. P. C., 2004. *Origin and prediction of seiches in Rotterdam harbour basins*. PhD thesis. Netherlands: PrintPartners Ipskamp.
- De Jong, M. P. C. & Battjes, J. A., 2004. Seiche Characteristics of Rotterdam Harbour. *Coastal Engineering*, Volume 51, pp. 373-386.
- DHI, 2012. *Mike 21 BW, Boussinesq Waves Module, Scientific Documentation*, Copenhagen, Denmark: Danish Hydraulics Institute.
- Gierlevsen, T., Hebsgaard, H. & Kirkegaard, J., 2001. *Wave Disturbance Modelling in the Port of Sines, Portugal - with special emphasis on the long period oscillations*. Singapore, International Conference on Port and Maritime R&D and Technology .
- Goda, Y., 2000. *Random Seas and Design of Maritime Structures. Advanced Series on Ocean Engineering – Volume 15*. 2nd ed. Singapore: World Scientific Publishing Co. Pte. Ltd..
- Google Earth, 2013. *Google Earth 6.0. Ngqura Port 33.796434S, 25.684401E, elevation 5.74km*. Available through:<http://www.google.com/earth/index.html> [Accessed 26 July 2013], s.l.: s.n.
- Holthuijsen, L. H., 2007. *Waves in Oceanic and Coastal Waters*. First ed. New York: Cambridge University Press.

Hwang, P. A., Huang, N. E. & Wang, D. W., 2003. A note on analyzing nonlinear and nonstationary ocean wave data. *Applied Ocean Research*, Volume 25, pp. 187-193.

International Towing Tank Conference and Norrbin, N.H., 1984. *7th International Towing Tank Conference*. Goteborg, s.n.

Jacques, L., Lee, H. J., Locat, P. & Imran, J., 2004. Numerical analysis of the mobility of the Palos Verdes debris avalanche, California, and its implication for the generation of tsunamis. *Journal of Marine Geology, Geochemistry and Geophysics*, Volume 203, pp. 269-280.

Jansa, A., Monserrat, S. & Gomis, D., 2007. The rissaga of 15 June 2006 in Ciutadella (Menorca), a meteorological tsunami. *Adv. Geosci.*, Volume 12, pp. 1-4.

Johnson, D. & McComb, P., 2011. *Modelling long wave generation and propagation around and within ports*. Perth, Western Australia, Proceedings of the 2011 Coasts and Ports Conference.

Journée, J. M. J. & Massie, W. W., 2001. *Offshore Hydromechanics*. 1st ed. Delft: Delft University of Technology.

Kennedy, A. B., Chen, Q., Kirby, J. T. & Dalrymple, R. A., 2000. Boussinesq Modeling of Wave Transformation, Breaking, and Runup. I: 1D. *Journal of Waterway, Port, Coastal and Ocean Engineering*, 126(1).

Kinsman, B., 1965. *Wind Waves: Their Generation and Propagation on the Ocean Surface*. New Jersey: Prentice-Hall.

Kofoed-Hansen, H., Kerper, D. R., Sorensen, O. R. & Kirkegaard, J., 2005. *Simulation of Long Wave Agitation in Ports and Harbours using a Time-domain Boussinesq Model*. Spain, Madrid, Paper in the Proceedings of Fifth International Symposium on Ocean Wave Measurement and Analysis-Waves.

Kofoed-Hansen, H., Kerper, D. R., Sørensen, O. R. & Kirkegaard, J., 2005. *Simulation of Long Wave Agitation in Ports and Harbours using a Time-domain Boussinesq Model*. Madrid, Spain, Proceedings of Fifth International Symposium on Ocean Wave Measurement and Analysis-Waves.

Ligteringen, H. & Moes, J., 2001. *Motions of Moored Ships in Long Waves*. s.l., Paper in Proceedings of the International Conference on Port and Marine R&D and Technology.

Longuet-Higgins, M. S. & Stewart, R. W., 1964. Radiation stresses in water waves; a physical discussion, with applications. *Deep-sea Research*, Volume II, p. 529.

MacHutchon, K. R., 2006. *The Characterization of South African Sea Storms*, MSc Thesis University of Stellenbosch. Stellenbosch: s.n.

Madsen, P. A. & Hemming, A. S., 1999. A review of Boussinesq-type equations for surface type gravity waves. *Advances in Coastal and Ocean Engineering*, Volume 5.

Madsen, P. A., Murray, R. & Sørensen, O. R., 1991. A new form of Boussinesq equations with improved linear dispersion characteristics (Part 1). *Coastal Engineering*, Volume 15, pp. 371-388.

Madsen, P. A. & Sørensen, O. R., 1992. A new form of Boussinesq equations with improved linear dispersion characteristics. Part 2 A slowly varying bathymetry. *Coastal Engineering*, Volume 18, pp. 183-204.

Madsen, P. A., Sørensen, O. R. & Schäffer, H. A., 1997a. Surf zone dynamics simulated by a Boussinesq type model. Part 1. Model description and cross-shore motion of regular waves. *Coastal Engineering*, Volume 32, pp. 255-287.

Madsen, P. A., Sørensen, O. R. & Schäffer, H. A., 1997b. Surf zone dynamics simulated by a Boussinesq type model. Part 2. surf beat and swash oscillations for wave groups and irregular waves. *Coastal Engineering*, Volume 32, pp. 289-319.

McComb, P., Gorman, R. & Goring, D., 2005. *Forecasting infragravity wave energy within a harbour*. Madrid, Ocean Wave Measurement and Analysis.

McComb, P., Johnson, D. & Beamsley, B., 2009. *Numerical model study to reduce swell and long wave penetration to Port Geraldton*. Wellington, New Zealand, Proceedings of the 2009 Pacific Coasts and Ports Conference.

Morelet, J., Arens, G., Fourgeau, E. & Giard, D., 1982. Wave propagation and sampling theory: part 2. Sampling theory and complex waves. *Geophysics*, 47(2), pp. 222-236.

Munk, W. H., 1949. Surf Beats. *Transaction, American Geophysical Union*, 30(6), pp. 849-854.

Ndarana, T. & Waugh, D. W., 2010. The link between cut-off lows and Rossby wave breaking in the Southern Hemisphere. *Quarterly Journal of the Royal Meteorological Society*, Issue 136, pp. 869-865.

Ota, K., Yoshida, A., Yamashiro, M. & Nishii, Y., 2010. *On Basic Conditions for Long-Wave Simulations in Harbours by the Boussinesq Model*. Shanghai, China, International Conference on Coastal Engineering.

PAHRI, 1998. *Low-Frequency Ship Motions Due to Long-Period Waves in Harbours, and Modifications to Mooring Systems That Inhibit Such Motions*, Vol. 37 No. 4, Nagase, Yokosuka, Japan: s.n.

Peregrine, D. H., 1967. Long waves on a beach. *Journal of Fluid Mechanics*, 27(4), pp. 815-827.

PIANC, 2012. *Criteria for the (Un)Loading of Container Vessels*. Report no. 115-2012, s.l.: s.n.

PRDW, 2001. *Coega Port: Maritime Works. Sub-Task J: Coastal Processes. Volume 1 Summary of Field Date on Coastal Processes. Report No. 256/J01/s001 Rev 03*, s.l.: s.n.

PRDW, 2002. *Coega Port: Maritime Works. Sub Task: Port Layout. Optimization of Mooring Layout and Estimation of Vessel Downtime using Physical Model Results. Technical Note: 256/B15/01 Rev 01.*, Cape Town: PRDW.

PRDW, 2004. *Coega Port: Maritime Works. Sub-Task J: Coastal Processes. Wave Data Recorded at S4. Interim Report No. 256/J03/s004 Rev 02.*, s.l.: s.n.

PRDW, 2005. *Coega Port: Maritime Works. Sub-Task J: Coastal Processes. Wave Data Recorded at S4. Interim Report No. 256/J03/s006 Rev 03*, s.l.: s.n.

PRDW, 2010a. *Port of Ngqura Parted Moorings, Mooring Layout. DWG no. 0/620/1002 Rev AA*. Cape Town: s.n.

PRDW, 2010b. *Port of Ngqura Parted Moorings, Enviromental Data. DWG no. 0/620/1001 Rev AA*. Cape Town: s.n.

Puertos del Estado, 2003. *ROM 3.1-99. Designing the maritime configuration of ports, approach channels and flotation areas*, Madrid: Gráficas Calima.

Rabinovich, A. B., 2009. Seiches and Harbour Oscillations. In: C. K. Y, ed. *Handbook of Coastal Engineering*. Singapore: World Scientific Publ., pp. 193-236.

Rossouw, J., 1989. *Design waves for the South African coastline. Phd thesis*, s.l.: s.n.

Shillington, F. A., 1984. Long period edge waves off southern Africa. *Continental Shelf Research*, 3(4), pp. 343-357.

Sørensen, O. R., Schäffer, H. A. & Madsen, P. A., 1998. Surf zone dynamics simulated by a Boussinesq type model. III. Wave-induced horizontal nearshore circulations. *Coastal Engineering*, Volume 33, pp. 155-176.

Sørensen, O. R., Schäffer, H. A. & Sørensen, L. S., 2004. Boussinesq type modelling using an unstructured finite element technique. *Coastal Engineering*, Volume 50, pp. 181-198.

South African Weather Service, 2011 & 2012. *Daily Weather Bulletins*, s.l.: s.n.

Symonds, G., Huntley, D. A. & Bowen, A. J., 1982. Two Dimensional Surf Beat: Long Wave Generation by a Time-Varying Breakpoint. *Journal of Geophysical Research*, Volume 87, pp. 492-498.

The Weather Channel, 2012. *Weather Glossary*. [Online]

Available at: <http://www.weather.com/glossary/c.html>

[Accessed 26 October 2013].

Thompson, E. F., Chen, H. S. & Hadley, L. L., 1996. Validation of Numerical Model for Wind Waves and Swell in Harbours. *Journal of Waterway, Port, Coastal and Ocean Engineering*, 122(5), pp. 245-257.

Thomson, M. T., 2006. *Infragravity Waves over Topography: Generation, Dissipation, and Reflection*. PhD thesis. s.l.:Massachusetts Institute of Technology.

USACE, 2006. *Coastal Engineering Manual, Part II, Chapter 7 Harbour Hydrodynamics*, Washington, USA: United States Army Corps of Engineers.

Van der Molen, W., 2006. *Behaviour of Moored Ships in Harbours*, PhD thesis. Netherlands: Gildeprint Drukkerijen BV.

Wilson, B. W., 1953. *Table Bay as an oscillating basin*. Minneapolis, Proc. of Joint Convention of International Assoc. Hydraulic Research and Am. Soc. Civ. Engrg..

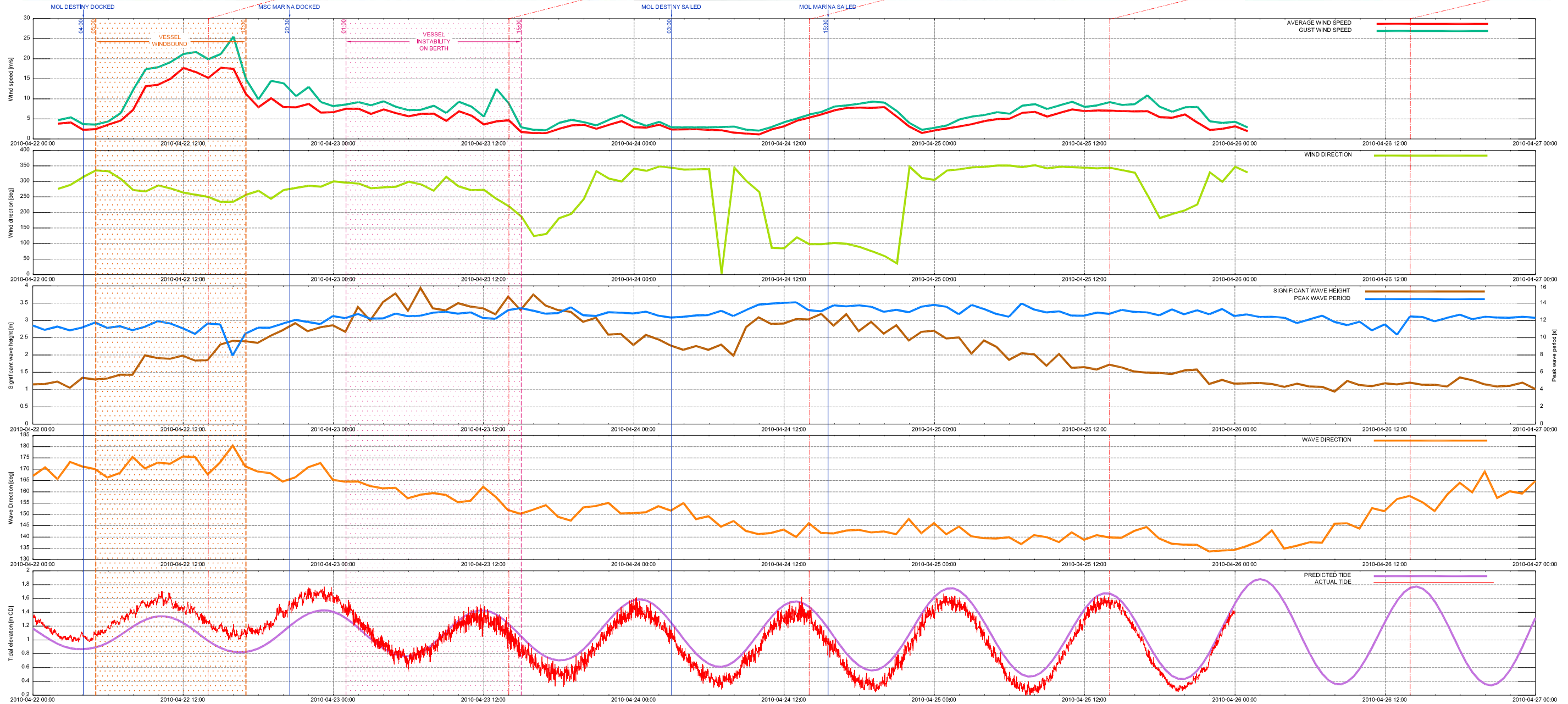
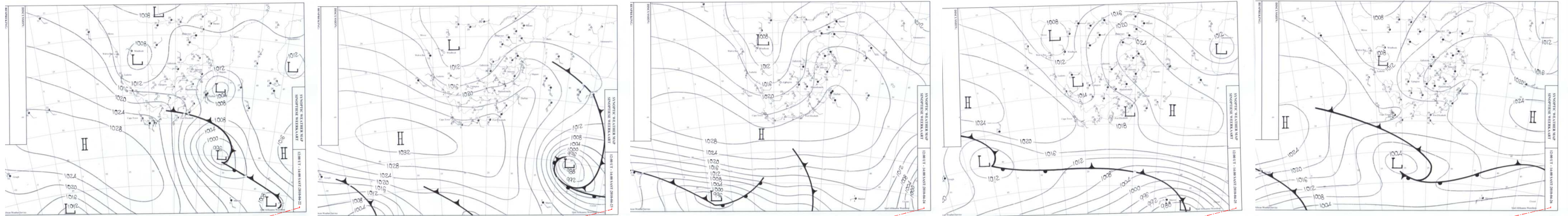
Wilson, B. W., 1954. *The mechanism of seiches in Table Bay Harbour, Cape Town*. Berkeley, Proceedings 4th Conference Coastal Engineering.

Wilson, B. W., 1957. *Origin and effects of long period waves in ports*. s.l., Proc. 19th Navigation Congr..

Wilson, B. W., 1972. Seiches. In: *Advances in Hydrosience*. California: s.n., pp. 1-94.

APPENDIX A: DRAWINGS OF VESSEL MOTION EVENT – APRIL 2010

DO NOT SCALE - IF IN DOUBT, ASK



DRAWING NO.	REFERENCE
1	REFERENCE DRAWINGS

NOTES:

CONSULTANT:
PRESTEDGE RETIEF DRESNER WINBERG (PTY) LTD

CONSULTING PORT AND COASTAL ENGINEERS
CAPE TOWN
TEL: (021) 418-3830 FAX: (021) 418-3834
E-MAIL: info@prdw.co.za

DRAWING NO:
0/620/1001 REV AA

NO.	DESCRIPTION	BY	CHKD	APPD	DATE
AA	ISSUED FOR INFORMATION				
REVISIONS / ISSUE AUTHORIZATION					

This Document including all design and information therein is Confidential Intellectual Property of Transnet and/or PRDW/Copyright and all other rights are reserved by Transnet and/or PRDW. This Document may only be used for the intended purpose.

EPCM CONSULTANT: TRANSNET PROJECTS				ORIGINATOR: PRDW			
TITLE	NAME	SIGNATURE	DATE	TITLE	NAME	SIGNATURE	DATE
LEAD DES. ENG.				DRAWN			
ENG. COORD.				CHECKED			
ENG. MANAGER				ENG. COORD.			
AREA MANAGER				DISCIP. ENG.			
PROJECT MGR.				ENG. MANAGER			
DIVISION				AREA MANAGER			
DIV.	TITLE	NAME	SIGNATURE	DATE	PR. ENG. / PR. TECH.		
					NAME	J. DRESNER	DATE
					SIGNATURE		
					REG. NUMBER	790005	
					SCALE:	AS SHOWN	

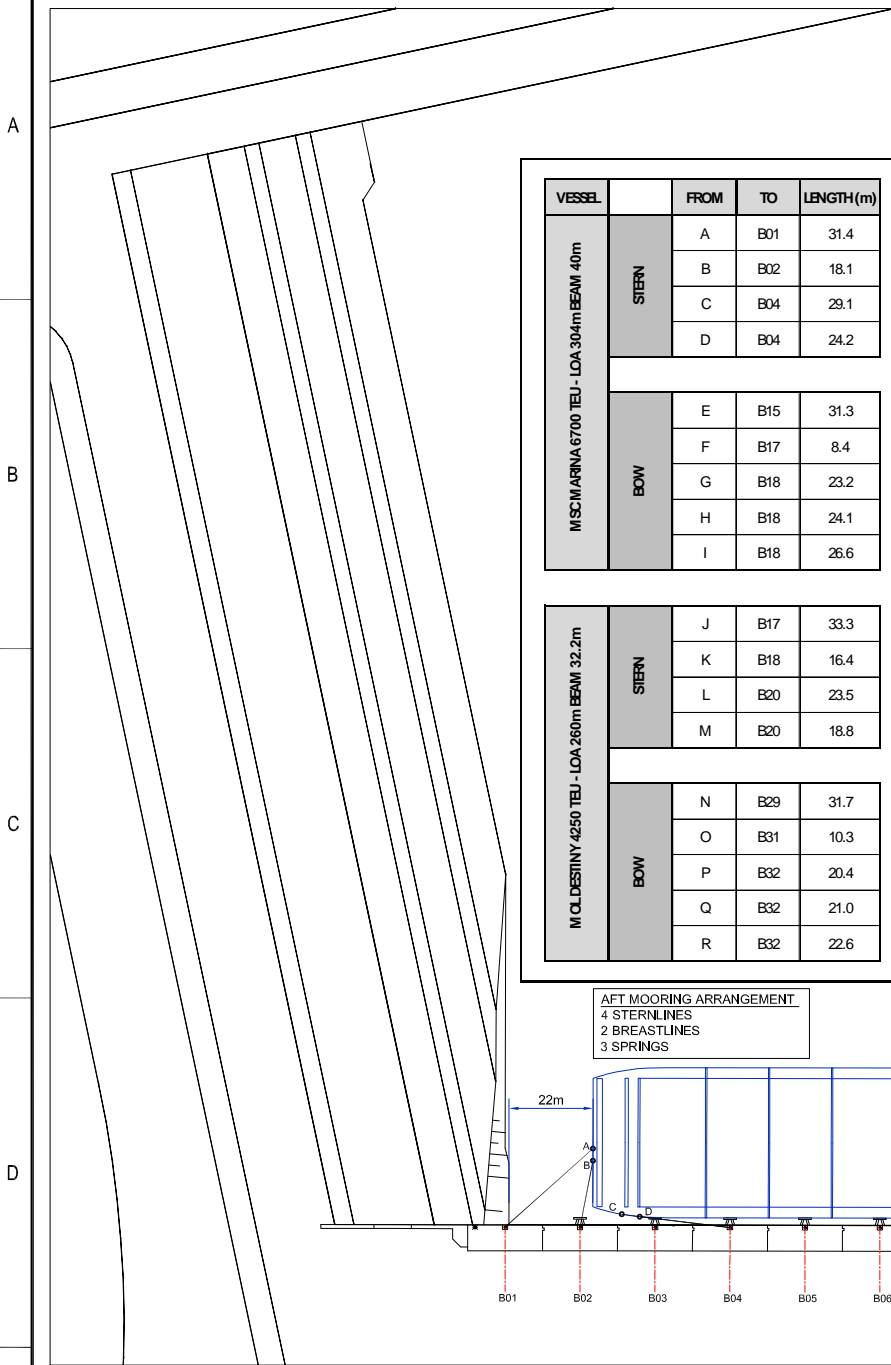
PROJECT NUMBER	DIV	FBS	DIS	TYPE	DRG. NO.	SHT	REV.	ID
----------------	-----	-----	-----	------	----------	-----	------	----

PORT OF NGQURA
PARTED MOORINGS

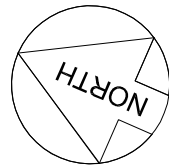
ENVIRONMENTAL DATA

DO NOT SCALE - IF IN DOUBT, ASK

DRAWING NUMBER



VESSEL		FROM	TO	LENGTH(m)
MSC MARINA 6700 TEU - LOA 304m BEAM 40m	STERN	A	B01	31.4
		B	B02	18.1
		C	B04	29.1
		D	B04	24.2
	BOW	E	B15	31.3
		F	B17	8.4
		G	B18	23.2
		H	B18	24.1
I	B18	26.6		
MOL DESTINY 4250 TEU - LOA 260m BEAM 32.2m	STERN	J	B17	33.3
		K	B18	16.4
		L	B20	23.5
		M	B20	18.8
	BOW	N	B29	31.7
		O	B31	10.3
		P	B32	20.4
		Q	B32	21.0
R	B32	22.6		

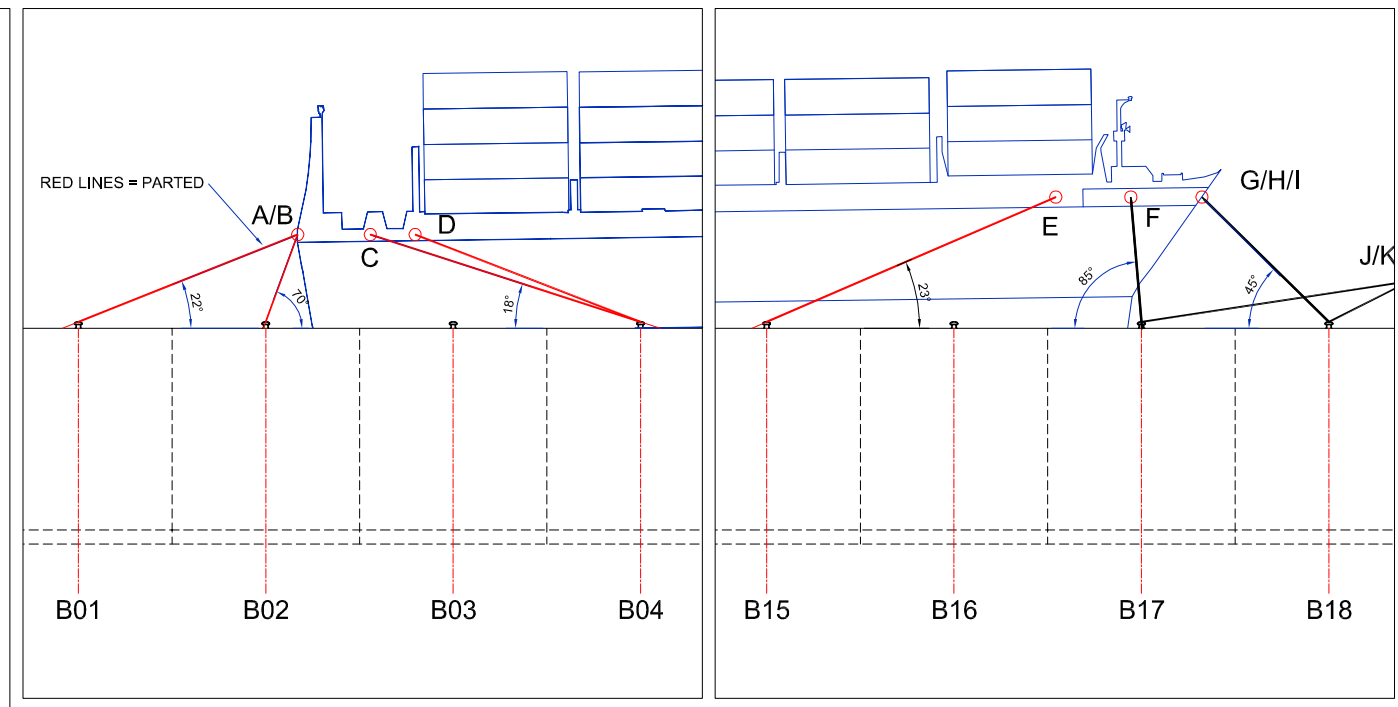


OCIMF MOORING EQUIPMENT GUIDELINE RECOMMENDATIONS

Moorings to be arranged as symmetrically as possible
 Vertical angle of mooring lines to be kept to a minimum
 Avoid mooring lines with vertical angles in excess of 25°
 A mooring line angle of 45° will render the line only 75% effective
 Sternlines should be orientated longitudinally in order to reduce vessel surge
 Differences in the length or vertical angle of spring lines will induce vessel surge
 A reduction in mooring load can be achieved with a specific rather than generic mooring layout
 Mooring layouts with dominant longitudinal forces should provide additional spring lines
 Effect of material and use of mixed moorings on load distribution is critical, in particular springs
 Mooring lines performing the same service should be the same length

BS 6349-4:1994 MOORING RECOMMENDATIONS

Optimum lengths of mooring lines are in the range of 35m to 50m
 Mooring lines in tension have a maximum restraining effect when horizontal



STERN SECTION

BOW SECTION

ELEVATION ON MSC MARINA

FENDERS (PHYSICAL MODEL TESTS)	FENDERS (PORT OF NGQURA)	MOORING LINES (MSC MARINA)	MOORING LINES (PHYSICAL MODEL TESTS)
TRELLEX 4 MV 1600 X 1000 RATED ENERGY ABSORPTION = 1680 kN/m RATED REACTION FORCE = 2280 kN/m FENDER STIFFNESS = 8550 kN/m	MARTIME INTERNATIONAL ME 1250 H X 2000 L RATED ENERGY ABSORPTION = 1100 kN/m RATED REACTION FORCE = 1913 kN/m FENDER STIFFNESS = 8550 kN/m	ATLAS 44mm ; mbl = 304 kN ATLAS 76mm ; mbl = 1069 kN (ASSUMED)	ULTRALINED NYEEMA 44mm ; mbl = 1398 kN

AFT MOORING ARRANGEMENT
 4 STERNLINES
 2 BREASTLINES
 3 SPRINGS

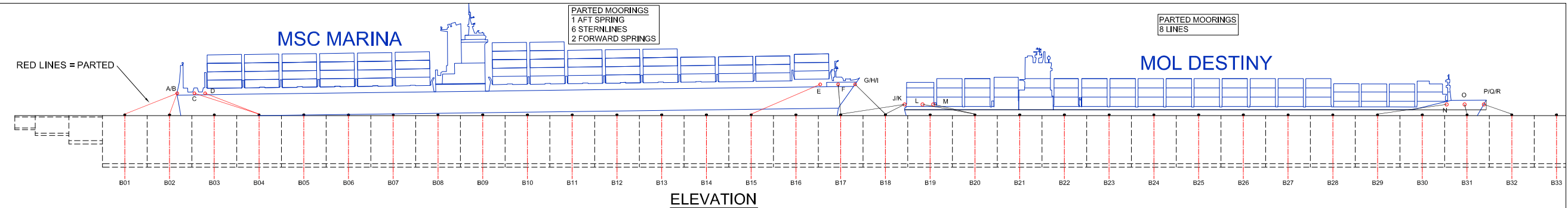
FORWARD MOORING ARRANGEMENT
 4 STERNLINES
 2 BREASTLINES
 3 SPRINGS

AFT MOORING ARRANGEMENT
 3 STERNLINES
 2 BREASTLINES
 3 SPRINGS

FORWARD MOORING ARRANGEMENT
 3 HEADLINES
 2 BREASTLINES
 3 SPRINGS

MOORING LAYOUT

ELEVATION



DRAWING NO. REFERENCE	NOTES:	CONSULTANT: PRESTEDGE RETIEF DRESNER WINBERG (PTY) LTD	EPCM CONSULTANT: TRANSNET PROJECTS				ORIGINATOR: PRDW																																																											
		<p>CONSULTING PORT AND COASTAL ENGINEERS CAPE TOWN TEL: (021) 418-3830 FAX: (021) 418-3834 E-MAIL: info@cpce.co.za</p>	<table border="1"> <thead> <tr> <th>TITLE</th> <th>NAME</th> <th>SIGNATURE</th> <th>DATE</th> </tr> </thead> <tbody> <tr><td>LEAD DES. ENG.</td><td></td><td></td><td></td></tr> <tr><td>ENG. COORD.</td><td></td><td></td><td></td></tr> <tr><td>ENG. MANAGER</td><td></td><td></td><td></td></tr> <tr><td>AREA MANAGER</td><td></td><td></td><td></td></tr> <tr><td>PROJECT MGR.</td><td></td><td></td><td></td></tr> <tr><td>DIVISION</td><td></td><td></td><td></td></tr> </tbody> </table>				TITLE	NAME	SIGNATURE	DATE	LEAD DES. ENG.				ENG. COORD.				ENG. MANAGER				AREA MANAGER				PROJECT MGR.				DIVISION				<table border="1"> <thead> <tr> <th>TITLE</th> <th>NAME</th> <th>SIGNATURE</th> <th>DATE</th> </tr> </thead> <tbody> <tr><td>DRAWN</td><td></td><td></td><td></td></tr> <tr><td>CHECKED</td><td></td><td></td><td></td></tr> <tr><td>ENG. COORD.</td><td></td><td></td><td></td></tr> <tr><td>DISCIP. ENG.</td><td></td><td></td><td></td></tr> <tr><td>ENG. MANAGER</td><td></td><td></td><td></td></tr> <tr><td>AREA MANAGER</td><td></td><td></td><td></td></tr> </tbody> </table>				TITLE	NAME	SIGNATURE	DATE	DRAWN				CHECKED				ENG. COORD.				DISCIP. ENG.				ENG. MANAGER				AREA MANAGER			
			TITLE	NAME	SIGNATURE	DATE																																																												
			LEAD DES. ENG.																																																															
ENG. COORD.																																																																		
ENG. MANAGER																																																																		
AREA MANAGER																																																																		
PROJECT MGR.																																																																		
DIVISION																																																																		
TITLE	NAME	SIGNATURE	DATE																																																															
DRAWN																																																																		
CHECKED																																																																		
ENG. COORD.																																																																		
DISCIP. ENG.																																																																		
ENG. MANAGER																																																																		
AREA MANAGER																																																																		
DRAWING NO: 0/620/1002 REV AA	<table border="1"> <thead> <tr> <th>NO.</th> <th>DESCRIPTION</th> <th>BY</th> <th>CHKD</th> <th>APPD</th> <th>DATE</th> </tr> </thead> <tbody> <tr> <td>AA</td> <td>ISSUED FOR INFORMATION</td> <td></td> <td></td> <td></td> <td></td> </tr> </tbody> </table>				NO.	DESCRIPTION	BY	CHKD	APPD	DATE	AA	ISSUED FOR INFORMATION					<table border="1"> <thead> <tr> <th>PR. ENG. / PR. TECH.</th> <th>NAME</th> <th>J. DRESNER</th> <th>DATE</th> </tr> </thead> <tbody> <tr> <td>SIGNATURE</td> <td></td> <td></td> <td></td> </tr> <tr> <td>REG. NUMBER</td> <td>790005</td> <td></td> <td></td> </tr> <tr> <td>SCALE:</td> <td>AS SHOWN</td> <td></td> <td></td> </tr> </tbody> </table>				PR. ENG. / PR. TECH.	NAME	J. DRESNER	DATE	SIGNATURE				REG. NUMBER	790005			SCALE:	AS SHOWN																																
NO.	DESCRIPTION	BY	CHKD	APPD	DATE																																																													
AA	ISSUED FOR INFORMATION																																																																	
PR. ENG. / PR. TECH.	NAME	J. DRESNER	DATE																																																															
SIGNATURE																																																																		
REG. NUMBER	790005																																																																	
SCALE:	AS SHOWN																																																																	
REFERENCE DRAWINGS		<p>THIS DOCUMENT INCLUDING ALL DESIGN AND INFORMATION IS THE CONFIDENTIAL INTELLECTUAL PROPERTY OF TRANSNET AND/OR PRDW/COPYRIGHT AND ALL OTHER RIGHTS ARE RESERVED BY TRANSNET AND/OR PRDW. THIS DOCUMENT MAY ONLY BE USED FOR THE INTENDED PURPOSE.</p>				<p>PORT OF NGQURA PARTED MOORINGS</p> <p>MOORING LAYOUT</p> <table border="1"> <thead> <tr> <th>PROJECT NUMBER</th> <th>DIV.</th> <th>FBS</th> <th>DIS</th> <th>TYPE</th> <th>DRG. NO.</th> <th>SHT.</th> <th>REV.</th> <th>ID</th> </tr> </thead> <tbody> <tr> <td></td> <td></td> <td></td> <td></td> <td></td> <td></td> <td></td> <td></td> <td></td> </tr> </tbody> </table>				PROJECT NUMBER	DIV.	FBS	DIS	TYPE	DRG. NO.	SHT.	REV.	ID																																																
PROJECT NUMBER	DIV.	FBS	DIS	TYPE	DRG. NO.	SHT.	REV.	ID																																																										